Response to Anonymous Referee #1.

We thank the reviewer for providing suggestions to improve the manuscript. Our responses to their comments are shown in blue. Added text is shown in italics.

In this work, measurements of OH and OH reactivity (OHR) from two Atom field deployments were used to evaluate the oxidation capacity over the remote oceans and its representation in the GEOS-Chem model. Good model-measurement agreement was obtained for OH and its precursors with over estimation of NOy to be attributed to insufficient or missing loss processes. The measured OHR below 3 km is greater than the sum OHR calculated from the measured OH reactants and the OHR in GEOS-Chem. The underestimate of acetaldehyde and peroxyacetic acid in GEOS-Chem and the reconcile of model-measurement agreement call for further work on the OH loss and production processes over land. In general, the paper is well written and within the scope of ACP. Evaluation of a transport chemical model against observations in a global scale are important and rare. I would recommend accepting it for publication after the authors address the following special comments in their revision.

Special Comments
P.2, L.1, maybe change "Organic aerosol is …" to "The production of organic aerosols is …" or something like that.
Done.

P.2, L.21-22: I would suggest adding "In the remote atmosphere" before "OH is primarily produced by the photolysis of ozone (O3) in the presence of water vapor." as in polluted environments other OH sources like the photolysis of HONO could be dominant at certain times of day.
We agree with the reviewer that other sources of OH can dominate in polluted environment, however this is not precluded by our statement that "OH is primarily produced by the photolysis of O3" which is an accurate reflection of global OH production. To address the reviewer's comment, we have revised the text on P8, L4 to read *"In the remote troposphere, OH…"* to address this comment.

In Section 2.1: a brief discussion of the GEOS-Chem model uncertainties in simulating OHR and OH as well other important species like acetaldehyde and PAA and should be included. Coupled with the measurement uncertainties in Table 2, the combined measurement-model uncertainties can help to understand if the discrepancies in the model-measurement comparisons (Figures 3-8 & 10-14) are significant or not.
The reviewer raises an interesting point. Quantifying how the uncertainty associated with the myriad processes (i.e. emissions, transport, removal, chemistry for each species…) integrated within a CTM propagates to simulated concentrations (or reactivity) would be a study (or career!) unto itself. We note that the uncertainties on many of these underlying processes are not well characterized themselves (e.g. how uncertain is the wet removal of nitric acid?). Thus, while we agree that in general, model uncertainty quantification could provide insight into model-observation comparisons, it is not straight-forward to estimate these uncertainties. Furthermore, and perhaps more importantly, here we intend to use the model as a tool to evaluate systematic biases that could be the cause of the global mean OH bias across models, as well as the remote nitric acid and acetaldehyde bias across models. Therefore, we do not believe that an assessment of specific model uncertainties is necessary. We clarify this point in the introduction, P3, line 28. *"We simulate the first two deployments (ATom-1: July-August 2016, ATom-2: January-February 2017) using the GEOS-Chem chemical transport model (CTM) as our tool to explore potential sources of systematic errors that could explain the community-wide model overestimate in global mean OH and underestimate of the methane lifetime."*

4. P.5, L.13 and Figure 1(a): define the altitude range of the surface layer.
We added the following to P4, L8 to address this point: *"The midpoint of the first model layer is 58 m."*

5. P.5, L.14-15: How are three quarters and 40% calculated? Are they numerical ratios or somehow weighted? In my opinion, spatially integrated and maybe air mass weighted cOHR values (over oceans versus over land and below 3 km versus above 3 km) should be considered in terms of global oxidation capacity.
Thank you for this suggestion. We now calculate $cOHR_{mod}$ below 3 km as an air-mass weighted quantity (P6, L5). *"Approximately 80 % of air-mass weighted $cOHR_{mod}$ resides below 3 km (Fig. 1b)."*

6. P.5, L.24: Noticed both Fig. and Figure are used. Not sure which one is required by ACP to use, but please be consistent.
Figure is only used when beginning a sentence. Fig. is used otherwise.

7. P.6, L.11: "accuracy of 1.35" is given for OH measurement: what are the units for 1.35? In Table 2, "factor of 1.35" is given for OH and HO2 detection limit and precision but no accuracy is given. Please clarify it.
Changed factor of 1.35 to "*74 % to 135%*" on P6, L29 and in Table 2.

8. P.6, L.14: the minimal bias of <1% seems too good to be true considering the spatiotemporal variabilities in both model and measurements (see e.g., Figures 3 and S1) as well as uncertainties and discrepancies (e.g., Fig. 6-7) in the measurement and model.
We agree that this was confusing. We have removed "minimal bias <1%" and added the following statement on P7, L21: *"As discussed above, model OH is overestimated in the lowest two kilometers during this period but this bias is minimized in the column average."*

9. P.6, L.15-16: please include standard deviations for these concentrations.
These are median values, and thus standard deviations are not appropriate metrics. We have clarified this in the text on P7, L3: "*We calculate the **median** air-mass weighted column average OH (OH_{col}) from Fig. 3 …. " and L9 "*Median model OH_{col} is within…"

10. Fig. 3-7: not sure if it's going to be too messy, but it is also important to see the percentiles in the model predictions. Maybe use whiskers to show the percentiles with different altitude bins for the measurement and model so that the whiskers will not be overlapped?
Thank you for the suggestion. We have added the 25th – 75th percentiles to the model as well for Fig. 3-7.

11. P.7 L.2: change VOC to VOCs
Changed.

12. P.7, L.15-16 and Fig. 5: the units for i(O3) should be 10-5 s-1. Also please point out this is for the photolysis reaction of O3 + hv → _O(1D) + O2 (sometimes it's called jO(1D), not the other one: O3 + hv → _O(3P) + O2. I pointed this out in the initial review before the ACPD publication, but it seemed the message didn't get through to the authors.
Changed jO3 to "$jO(^1D)$" in the text and the figure and fixed the units.

13. P.7, L.17-26: there is a discrepancy as large as 30 ppb at high altitudes for winter in ATom-1 and for winter and summer in Atom-2. A discrepancy of 20-30 ppb doesn't seem "unbiased" to me. Any explanation of this overestimate at high altitudes should be briefly discussed here. This also makes me believe the above <1% bias likely to be coincident or the right answers for the wrong reasons.
There is a nice analysis on the contribution of O1D + H_2O to PHO_x from Brune et al., 2020. We revised this sentence to read P8, L28: "*Upper tropospheric ozone is overestimated in all cases but Northern Hemisphere summer, but this would not have a large influence on primary OH production (or the methane lifetime) at these altitudes (Brune et al., 2020).*"

14. P.9, L.28-29: note in Table 2 an accuracy of 0.8 s-1 and a detection limit/precision of 0.3 s-1, which are comparable to the overall differences here. The authors should mention this to remind readers the uncertainty in the measure.
Thames et al. 2020 (just published in ACP) provide statistical tests of the missing reactivity discussed in this work. We add the following description of their findings on P11, L26. "*Thames et al. (2020) showed that median missing reactivity (between OHR and an observationally-constrained box model) below 4 km during the ATom-1, ATom-2, and ATom-3 deployments was between 0.2 and 0.8 s-1. They provided statistical evidence that while near the level of the instrument accuracy, missing OHR in the marine boundary layer was statistically significant.*"

15. P.9 bottom and P.10 top: both r and r2 are used for correlation. Please be consistent. In my opinion, r2 should be used. A scatter plot of the missing OH reactivity against acetaldehyde should be included in the SI to support the strongest relationship.
Only r^2 is now used, and a scatter plot of the missing OH reactivity against acetaldehyde is now Figure S3.

16. P.10, L.4: …oxygenated VOCs (OVOCs)
Replaced.

17. P.10, L.11: VOCs. There are many cases where "VOC" should be really "VOCs" and "aerosol" should be really 'aerosols". Please check this out through the manuscript.
Now using "VOCs" and "aerosols".

18. P.10: Fig. S3 and 9: any explanation why there is a belt of enhancement over the ocean in the mid-latitude of southern hemisphere?
This is due to setting a minimum seawater concentration for acetaldehyde. This was perhaps not clear because this adjustment is described later in the manuscript. We add the following clarification to P12, line 22, *"Figure 10 shows the annual mean impact of all ocean emissions described in Tables 3 and 4 (including an adjustment to the acetaldehyde seawater concentration described below in 5.1) on $cOHR_{mod}$…"*

And to P12, line 25, *"The largest increases occur in regions of higher biogenic activity along coastlines and in the Southern Ocean due to the adjustment to acetaldehyde emissions discussed in Section 5.1…"*

19. P.11, L. 24: change OF to of.
Fixed.

20. Table 2: in the reference for CH4, remove AMT
Fixed.

21. Note 1 of Table 2: H2 was measured but was set to 0.5 ppm. How does this value compare to the observations? If the difference is large, maybe use the measured value (e.g., mean) to constrain the model. From Figures 10 & 11, H2 contributed about 5-8% of observed and modeled OHR, which is not very small.
We added the following sentence to the model description on Page 5, L14: *"The model concentration of H_2 is fixed at 500 ppt, consistent with observed H_2 from ATom-1 and ATom-2 (520 ppt)."*

22. In Supplemental Information: both ethane and propane are underestimated in GEOS-Chem (Figures S6 and S7). Is this because of unaccounted emission sources like fracking?
We added the following citation to P16, L2: *"The model underestimates average ethane and propane below 10 km by 100 % and 40 %, respectively during ATom-2 (Figs. S8 and S9) which could be due to underestimated natural geologic and fossil fuel emissions (Dalsøren et al., 2018).*

Response to Anonymous Referee #2.

We thank the reviewer for providing suggestions to improve the manuscript. Our responses to their comments are shown in blue. Added text is shown in italics.

The Introduction does not acknowledge the Thames et al. (ACPD, 2019) manuscript, cited later on Pg. 11, which has a likelihood of being published prior to the finalization of this submission. That paper also discusses the ATom OHR measurements, albeit with a focus on the MBL instead of global oxidation capacity. Since the Thames et al. paper will be so closely related to this one by Travis et al., a discussion of its findings and how Travis et al. will complement Thames et al. is warranted here.

We agree with the reviewer – Thames et al. was very recently published in final peer reviewed form on ACP, and we now comment further on this paper in our own manuscript. Page 3, L14 - We add a citation for Thames et al, 2020 to the Introduction. We add additional discussion of Thames et al, 2020 in the following places:

P3, L19: *"Thames et al. (2020) found evidence of missing OHR between measurements an observationally-constrained box model during the first three ATom deployments."*

P11, L16: *"During ATom, Thames et al. (2020) measured OHR over the Atlantic and Pacific oceans in all four seasons and determined that missing OHR correlated with oxygenated VOCs suggesting the presence of unknown ocean emissions."*

P11, L16: "Thames et al. (2020) showed that median missing reactivity (between OHR and an observationally-constrained box model) below 4 km during the ATom-1, ATom-2, and ATom-3 deployments was between 0.2 and 0.8 s^{-1} and provided statistical evidence that while near the level of the instrument accuracy, missing OHR in the marine boundary layer is statistically significant."

Pg. 2 L. 29: The authors acknowledge "the persistent CO underestimate in models" yet do not go on to evaluate this large sink of OH. A figure analogous to Fig. 3, showing CO comparisons between model and observations should be included and discussed. Does the reasonably accurate OH field within this GEOS-Chem simulation translate to similarly well-simulated fields of CO over the oceans? Or does longer-lived CO have the imprint of biased continental OH, to which the authors refer?
We evaluate model CO in Fig. 11 and Fig. 12. We add the following statement to P13, L29: "*There is no systematic underestimate in CO as might be expected from the general model underestimate of CO described by Shindell et al. (2006) with the exception of a 10 % underestimate during Northern Hemisphere winter when the lifetime of CO is longer and biases in continental sources could have a larger impact."*

Pg. 4 L. 3: Could you specify whether the methane concentration boundary condition varies with latitude and/or longitude? And, since they derive from monthly observations, is it correct to assume that the boundary condition changes from month to month?
We revised the description on P4, L16 to read *"Surface methane concentrations are prescribed monthly using spatially interpolated observations from the NOAA GMD flask network."*

Pg. 4 L. 30: Please describe how exactly the tropospheric mean OH is being calculated. As Lawrence et al., 2001 explain, there are multiple ways to weight this calculation, and, for the purposes of facilitating comparisons of these values between studies, an explicit definition of this metric should be included in each paper that discusses it.
Thank you for this suggestion, we have added a link to the GEOS-Chem calculation of tropospheric mean OH on P5, L16 *"(see http://wiki.seas.harvard.edu/geos-chem/index.php/Mean_OH_concentration for the detailed calculation)."*

Figures 3-8, 12-14: Please consider trying to visualize not only the 25th/75th percentiles for the observed median profiles, but also for the modeled profiles. How well the spread of each of these quantities agrees can be instructive as well.
All figures now include the 25^{th}/75^{th} percentiles for the model as well.

On organization: I found, reading through the paper, that the topics of various results/discussion sections (Sections 3-6) jumped around quite a bit. For instance:

-Some discussion of the literature on acetaldehyde is initiated in Section 5 (mention of Read et al., 2012 on Pg. 10, L.4), mentioned again farther down on the page (Pg. 10, L. 29), and continued throughout Section 6. I would suggest consolidating the discussion of the acetaldehyde literature in one place, and perhaps making Section 6 a subsection of Section 5.

We appreciate the reviewer's suggestion to clarify the text. We have changed Section 6 to Section 5.1. We moved all discussion of acetaldehyde in the literature to the first paragraph of Section 5.1.

-Similarly, the discussion of NOy as a proxy for OH secondary source NOx is understandable, given the issues with measured NO2, but the discussion necessarily turns to HNO3 evaluation, all under Section 4: Constraints on the remote source of OH. Generally, HNO3 is viewed as a sink for OH, so this further contributes to the feeling of "jumping around" between topics. Additional subsections and improvements in framing the discussion should help to give a more logical structure to these sections .
We added a subsection for the discussion of HNO_3 evaluation: *"4.1 Causes of the remote model bias in HNO3"*

Technical Corrections

Pg. 2 L. 1: The sentence starting "Comparisons" is a run-on; either include a comma between "aerosol but" or separate into two sentences
We separated into two sentences.

Pg. 2 L. 5: Run-on sentence; place comma between "sources and" or split to two Sentences
Split into two sentences.

Pg. 2 L. 20: Run-on sentence; place comma between "atmosphere and" or split.
Placed a comma.

Pg. 4 L. 1: Place comma after "Sherwen et al."
Placed a comma.

Pg. 4 L. 25: MCM v3.3.1 has an additional reference, regarding the update from v3.2: Jenkin et al., 2015
Added.

Pg. 4 L. 29: Figures should generally be numbered in the order that they appear in the text, even Supplemental figures. Fig. S8 should be moved to S1. Same with Tables (S4 and S5 appear before S1), and Fig. S9 (appears before S5).
The supplement has been re-ordered to follow the order in the text.

Pg. 5 L. 13: Could the authors please state the number of species that are listed in Table S1?
We added the following to P6, L4 *"ninety simulated constituents…"*

Pg. 6 L. 6: "attitude" should be "altitude"
Changed.

Pg. 6 L. 11: Should there be units for the accuracy value provided here (molec cm–3)?
Clarified value as 74% to 135%, 2σ confidence level.

Pg. 6 L. 17: Please specify if Fig. S1 shows in situ OH concentrations of column averaged. If it is column averaged, please use the OHcol notation in the text at this location and in the figure.
Changed "OH" to *"OH concentrations".*

Pg. 6 L. 22: Instead of "successful" and "success" here, simulation should be described as having "good agreement" or similar wording.
We removed this sentence and rephrased our statement on P6, L30. "*This result from a global CTM is consistent with good agreement between OH measurements and a box model during NASA's Pacific Exploratory Mission-Tropics (PEM-Tropic B) campaign in the clean remote Pacific (Tan et al., 2001) and a similar analysis by Brune et al. (2020) for ATom 1 through 4."*

Pg. 7 L. 10 & 15: Replace “successfully”
Replaced “successfully” with *“reproduces”*

Pg. 7 L. 30: Run-on sentence; place comma between “2018) and”
Added this comma.

Pg. 8 L. 10: Anderson et al. 2014 also indicated a bias in the anthropogenic NOx inventory; please cite that paper here as well.
Added this citation.

Pg. 8 L. 18: “higher larger ozone” seems redundant
We have removed this text and incorporated the simulation of Wang et al., 2019 into our simulation.

Pg. 8 L. 21: “free tropospheric” should be “free tropospheric bias”?
Changed “free tropospheric” to *“free tropospheric bias”.*

Pg. 9 L. 21: “We compare OHR: : :” I would suggest explicitly stating here that “OHR” refers to directly measured OHR, to avoid confusion.
We changed “We compare OHR” to *“We compare directly measured OHR”.*

Pg. 11 L. 4: Thames et al. (2019) does not appear in the reference list.
Thames et al. (2020) has been added to the reference list.

Pg. 11 L. 17: “: : :when the lifetime of CO is long.” I would consider this circular reasoning; the reason the lifetime of CO is long in the wintertime is because OH concentrations are low.
We have revised the text to read on P13, L28: *“CO and methane make up half or greater of both cOHRobs and cOHRmod”.*

Pg. 11 L. 24: “OF” should be “of”
Fixed.

Pg. 11 L. 30: Nicely et al. (2016) also recognized the importance of acetaldehyde in explaining model vs. measurement-constrained OH differences, could be cited here.
We added this citation.

Pg. 12 L. 23: It would be helpful to state, quantitatively, how large the model bias in PAA is.
We changed the sentence on P15, L17 to read “*Figure 14 shows the average model underestimate of below 3 km of 70 to 90 % (60 to 250 ppt).”*

Pg. 13 L. 9: It is unclear what the percentage values provided in parentheses refer to– are they percent increases in acetaldehyde from corrections to model ethane/propane, or are they percent yields of acetaldehyde per molecule of ethane/propane oxidized?
Changed “currently…” to *“model yields are..”*

Table 2: Please number the superscripts in the order they appear in the table.
The subscripts have been re-ordered.

Figure 5: Units for jO3 should be 10–5 s–1 instead of 105. Would also be helpful to specify whether this is j(O3 –> O1D + O2) or j(O3 –> O3P + O2).
Fixed the units and changed jO_3 to jO^1D.

Fig. 11: I appreciate the difficulty of finding unique color choices for a figure like this, but I find the two shades of green, representing MHP and HCHO, practically indistinguishable on my computer screen (so the problem is likely worse in hard copy). Please adjust one of the two.
The color of HCHO has been adjusted to a darker green.

Constraining remote oxidation capacity with ATom observations

Katherine R. Travis[1a], Colette L. Heald[1,2], Hannah M. Allen[3], Eric C. Apel[4], Stephen R. Arnold[5], Donald R. Blake[6], William H. Brune[7], Xin Chen[8], Róisín Commane[9], John D. Crounse[10], Bruce C. Daube[11], Glenn S. Diskin[12], James W. Elkins[13], Mathew J. Evans[14,15], Samuel R. Hall[4], Eric J. Hintsa[13,16], Rebecca S. Hornbrook[4], Prasad S. Kasibhatla[17], Michelle J. Kim[10,18], Gan Luo[19], Kathryn McKain[20], Dylan B. Millet[8], Fred L. Moore[13,16], Jeffrey Peischl[16,20], Thomas B. Ryerson[20], Tomás Sherwen[14,15], Alexander B. Thames[7], Kirk Ullmann[4], Xuan Wang[11,21], Paul O. Wennberg[3,18], Glenn M. Wolfe[22], Fangqun Yu[19]

[1]Department of Civil and Environmental Engineering, Massachusetts Institute of Technology, Cambridge, MA, USA
[2]Department of Earth, Atmospheric and Planetary Sciences, Massachusetts Institute of Technology, Cambridge, MA, USA
[3]Division of Chemistry and Chemical Engineering, California Institute of Technology, Pasadena, CA
[4]Atmospheric Chemistry Observations & Modeling Laboratory, National Center for Atmospheric Research, Boulder, Colorado, USA
[5]Institute for Climate and Atmospheric Science, School of Earth and Environment, University of Leeds, Leeds, UK
[6]Department of Chemistry, University of California Irvine, Irvine, CA, USA
[7]Department of Meteorology, Pennsylvania State University, University Park, PA, USA
[8]University of Minnesota, Department of Soil, Water and Climate, St. Paul, Minnesota, USA
[9]Dept. of Earth & Environmental Sciences of Lamont-Doherty Earth Observatory and Columbia University, Palisades, NY
[10]Division of Geological and Planetary Sciences, California Institute of Technology, Pasadena, CA, USA
[11]Harvard John A. Paulson School of Engineering and Applied Sciences, Harvard University, Cambridge, MA, USA
[12]NASA Langley Research Center, Hampton, Virginia, USA
[13]Global Monitoring Division, NOAA Earth System Research Laboratory, Boulder, CO, USA
[14]Wolfson Atmospheric Chemistry Laboratories (WACL), Department of Chemistry, University of York, York, UK
[15]National Centre for Atmospheric Science (NCAS), University of York, York, UK
[16]Cooperative Institute for Research in Environmental Science, University of Colorado, USA
[17]Nicholas School of the Environment, Duke University, Durham, NC, USA
[18]Division of Engineering and Applied Science, California Institute of Technology, Pasadena, CA, USA
[19]Atmospheric Sciences Research Center, University of Albany, Albany, New York, USA
[20]Chemical Sciences Division, NOAA Earth System Research Laboratory, Boulder, CO, USA
[21]School of Energy and Environment, City University of Hong Kong, Hong Kong, China
[22]Atmospheric Chemistry and Dynamics Laboratory, NASA Goddard Space Flight Center, Greenbelt, MD, USA
[a]Now at NASA Langley Research Center, Hampton, Virginia, USA

Correspondence to: K. R. Travis (katherine.travis@nasa.gov) and C. L. Heald (heald@mit.edu)

Abstract. The global oxidation capacity, defined as the tropospheric mean concentration of the hydroxyl radical (OH), controls the lifetime of reactive trace gases in the atmosphere such as methane and carbon monoxide (CO). Models tend to underestimate the methane lifetime and CO concentrations throughout the troposphere, which is consistent with excessive OH. Approximately half of the oxidation of methane and non-methane volatile organic compounds (VOCs) is thought to occur over the oceans where oxidant chemistry has received little validation due to a lack of observational constraints. We use observations from the first two deployments of the NASA ATom aircraft campaign during July-August 2016 and January-February 2017 to evaluate the oxidation capacity over the remote oceans and its representation ~~in~~ by the GEOS-Chem chemical transport model. The model successfully simulates the magnitude and vertical profile of remote OH within the measurement

uncertainties. Comparisons against the drivers of OH production (water vapor, ozone, and NO_y concentrations, ozone photolysis frequencies) also show minimal bias with the exception of wintertime NO_y~~, for which a m~~The severe model overestimate of NO_y during this period~~odel overestimate~~ may indicate insufficient wet scavenging and/or missing loss on seasalt aerosol~~s~~-. L~~but l~~arge uncertainties in these processes ~~remain that~~ require further study to improve simulated~~ies of~~ NO_y partitioning and removal in the troposphere but preliminary tests suggest that their overall impact could be a partial resolution of the model bias in tropospheric OH. During the ATom-1 deployment, OH reactivity (OHR) below 3 km is significantly enhanced, and this is not captured by the sum of its measured components ($cOHR_{obs}$) or by the model ($cOHR_{mod}$). This enhancement could suggest missing reactive VOCs but cannot be explained by a ~~new~~ comprehensive ~~estimates of~~ simulation of both biotic and abiotic ocean sources of VOC ~~source~~s. A~~and a~~dditional sources of VOC reactivity ~~itional modeled reactivity~~ in this region~~-~~ are ~~would be~~ difficult to reconcile with the full suite of ATom measurement constraints. The model generally reproduces the magnitude and seasonality of $cOHR_{obs}$ but underestimates the contribution of oxygenated VOCs, mainly acetaldehyde, which is severely underestimated throughout the troposphere despite its calculated lifetime of less than a day. Missing model acetaldehyde in previous studies was attributed to measurement uncertainties that have been largely resolved. Observations of peroxyacetic acid (PAA) provide new support for remote levels of acetaldehyde. The underestimate in both model~~ed~~ acetaldehyde and PAA is present throughout the year in both hemispheres and peaks during Northern Hemisphere summer. The addition of ocean ~~VOC~~ sources of VOCs in the model increases ~~annual surface~~ $cOHR_{mod}$ by ~~1~~3-14~~0~~ % and improves model-measurement agreement for acetaldehyde particularly in winter but cannot resolve the model summertime bias. Doing so would require ~~a~~ 100 Tg yr^{-1} ~~source~~ of a long-lived unknown precursor throughout the year with significant additional emissions in the Northern Hemisphere summer. Improving the model bias for remote acetaldehyde and PAA is unlikely to fully resolve previously reported model global biases in OH and methane lifetime~~,~~ suggesting that future work should examine the sources and sinks of OH over land.

1 Introduction

The hydroxyl radical (OH) is the main oxidant responsible for removing trace gases from the atmosphere, and its concentration defines the tropospheric oxidation capacity. OH is primarily produced by the photolysis of ozone ~~(O_3)~~ in the presence of water vapor. The lifetimes of key atmospheric trace gases are governed by how quickly they are removed by reaction with OH. Oxidation of volatile organic compounds (VOCs) by OH ~~is a key process for formation~~produces ~~of both~~ tropospheric ozone and fine particulate matter which are detrimental to human health and vegetation, and impact climate. The oxidation of VOCs, ~~in addition to~~ carbon monoxide (CO), and methane~~,~~ provide~~s~~ the main sink of OH in the troposphere. Oxidation of methane

and VOCs accounts for ~~Over~~ over half of the global CO production ~~of CO results from the oxidation of methane and other VOCs by OH~~ (Duncan et al., 2007; Safieddine et al., 2017) resulting in a tight coupling of these compounds.

Models ~~tend to~~generally overestimate global mean tropospheric OH and its ~~the r~~ratio ~~of~~ in the Northern to Southern Hemisphere ~~mean OH~~ (Naik et al., 2013; Patra et al., 2014). These biases may be linked to the persistent CO underestimate in models (Shindell et al., 2006) as prescribing OH from observations improves ~~the~~ simulated CO ~~simulation~~ (Müller et al., 2018). However, ~~recent efforts to~~ constraining models with observations of ozone and water vapor cannot ~~could not completely resolve excessive model~~ resolve biases in model OH (Strode et al., 2015) which is~~. Estimates of OH across models vary due to~~ impacted by ~~-~~additional complex factors~~, including~~ such as ~~differing~~ the chemical mechanisms and ~~methods for calculating~~ the ozone photolysis frequency (Nicely et al., 2017) ~~which are more difficult to isolate~~. ~~Improving~~ Constraining the performance of model chemical mechanisms has largely focused ~~over~~ on regions of strong biogenic and anthropogenic activity (Emmerson and Evans, 2009; Yu et al., 2010; ~~e.g.~~ Marvin et al., 2017) but ~~over~~ at least half of the oxidation of methane occurs over the ocean where models have received little evaluation due to a lack of observational constraints.

The ~~advent~~introduction of airborne measurements of OH reactivity (OHR) provides a method to evaluate the ~~total~~ sink of OH across a range of altitudes and a variety of locations and chemical environments (Mao et al., 2009; Thames et al., ~~2019~~2020). Previous work compared surface observations of OHR at a single site to the sum of individually calculated OHR components from measurements (Di Carlo, 2004; Yoshino et al., 2006; Sinha et al., 2008, 2010; Mao et al., 2010; Dolgorouky et al., 2012; Hansen et al., 2014; Nakashima et al., 2014; Nölscher et al., 2012, 2016; Ramasamy et al., 2016; Zannoni et al., 2016, 2017) or from simple models (Ren et al., 2006; Lee et al., 2009; Lou et al., 2010; Mogensen et al., 2011; Mao et al., 2012; Edwards et al., 2013; Kaiser et al., 2016; Whalley et al., 2016). Thames et al. (2020) found evidence of missing OHR between measurements and an observationally-constrained box model during the first three ATom deployments. Chen et al. (2019) compared calculated OHR from a global model to OHR determined from a suite of VOCs but did not have measurements of OHR itself. Ferracci et al. (2018) ~~explored the~~found that ~~impact of~~ missing OHR estimated from surface observations could result in a small increase in the ~~on~~ modeled ~~global OH levels.~~methane lifetime. Safieddine et al. (2017) and Lelieveld et al. (2016) presented the first global model simulations of OHR but with ~~minimal~~ only ~~and~~ qualitative comparison to observations~~observational evaluation~~. No study has quantitatively compared simulated and observed ~~remote~~ OHR in a global model in an effort to constrain the OH sink.

The ATom campaign (Wofsy et al., 2018) provides an unprecedented opportunity to ~~evaluate~~test models~~OH~~ in the remote atmosphere with a detailed suite of chemical observations. We simulate the first two deployments (ATom-1: July-August 2016, ATom-2: January-February 2017) using ~~use~~ the GEOS-Chem chemical transport model (CTM) ~~to simulate the first two deployments (ATom-1: July-August 2016, ATom-2: January-February 2017) with the goal of reducing~~as our tool to explore potential sources of systematic errors that could explain the community-wide model overestimate in global mean ~~the uncertainty in simulating remote tropospheric~~ OH and underestimate of the methane lifetime. We ~~specifically focus on~~include

model ~~validation~~ evaluation with measurements of OHR, a relatively new constraint available for assessing ~~total~~ atmospheric oxidation capacity. To our knowledge, this is the first quantitative use of this measurement to evaluate a CTM.

2 Description of Model and Observations

2.1 The GEOS-Chem model

We use the GEOS-Chem global 3-D CTM in v12.3.0 (doi:10.5281/zenodo.2620535) driven by assimilated meteorological data from the Goddard Earth Observing System Modern-Era Retrospective analysis for Research and Applications, Version 2 (MERRA-2; Gelaro et al., 2017). The native MERRA-2 model has a horizontal resolution of 0.5° ~~×x~~ 0.625° and 72 vertical levels which we degrade to 2° ~~×x~~ 2.5° and 47 vertical levels for use in GEOS-Chem. The midpoint of the first model layer is 58 m. We use timesteps of 20 min for chemistry and 10 min ~~for chemistry and~~for transport~~, respectively,~~ as recommended by Philip et al. (2016). GEOS-Chem includes detailed treatment of HO_x-NO_x-VOC-halogen-aerosol chemistry with recent improvements for isoprene (Chan Miller et al., 2017; Fisher et al., 2016; Marais et al., 2016; Travis et al., 2016), peroxyacetyl nitrate (PAN) (Fischer et al., 2014) and halogen chemistry (Sherwen et al., 2016). The production of ~~Organic~~ organic aerosols is ~~parameterized~~ calculated using fixed yields from isoprene, monoterpenes, biomass burning, and anthropogenic fuel combustion (Pai et al., 2020~~19~~). Aerosol uptake of HO_2 is parameterized with a reactive uptake coefficient (γ) of 0.2 (Jacob, 2000) to produce H_2O (Mao et al., 2013). Aerosol thermodynamic equilibrium is calculated by ISORROPIA II version 2.0 (Pye et al., 2009). Surface ~~Methane~~ methane concentrations are prescribed monthly ~~e calculated~~ using ~~prescribed surfaces~~spatially interpolated ~~concentrations derived from monthly~~ observations from the NOAA GMD flask network. We simulate the 2016-2017 period with an 18-month ~~spin up~~initialization ~~period~~.

Global fire emissions ~~for 2016 and 2017,~~ at 3-hourly resolution (Mu et al., 2011)~~,~~ for 2016 and 2017 are from the Global Fire Emissions Database (GFED4s; van der Werf et al., 2017). The GFED4s burned area (Giglio et al., 2013) includes a parameterization of small fires (Randerson et al., 2012). Biogenic ~~VOC~~ emissions of VOCs are from MEGANv2.1 (Guenther et al., 2012; Hu et al., 2015). Global anthropogenic emissions are from the Community Emissions Data System (CEDS) inventory (Hoesly et al., 2018), overwritten by ethanol from the POET inventory (Olivier et al., 2003; Granier et al., 2005), ethane from Tzompa~~- -~~Sosa et al. (2017), and regional inventories for the United States (NEI11v1, Travis et al., 2016), Canada (CAC, https://www.canada.ca/en/services/environment/pollution-waste-management/national-pollutant-release-inventory.html), Mexico (BRAVO, Kuhns et al., 2003), Europe (EMEP, http://www.emep.int/index.html), Asia (MIX, Li et al., 2017), and Africa (DICE, Marais and Wiedinmyer, 2016). Lightning emissions are constrained with satellite data according to Murray et al. (2012) with a ~~revised~~ global flash rate of 280 mol NO flash^{-1} (Marais et al., 2018) ~~for a source strength of 6.0 Tg N yr^{-1}~~. Air-sea exchange is calculated for ~~We emit~~ acetaldehyde (Millet et al., 2010), acetone (Fischer et al., 2012), and dimethyl sulfide (Breider et al., 2017) ~~from air-sea exchange of VOCs produced from biogenic activity in the oceans~~. All

emissions are processed using the Harvard Emissions Component (HEMCO, Keller et al., 2014). Table 1 provides the 2016 emission budget for CO and NO_x.

~~We expand the~~The standard simulation ~~(which includes~~includes ~~only background~~prescribed methanol concentrations. We expand this simulation~~),~~ to include methanol emissions and chemistry~~, as well as~~ and emissions and chemistry of unsaturated C_2 compounds. Air-sea exchange of methanol is specified using the methodology of Millet et al. (2008) with a constant seawater concentration of 142 nM. Terrestrial biogenic methanol emissions are from MEGANv2.1 and anthropogenic and biomass burning emissions are from the inventories described above. We likewise include biomass burning and anthropogenic emissions of ethyne (C_2H_2) and ethene (C_2H_4) along with terrestrial biogenic emissions of C_2H_4 ~~as above~~. Oxidation of C_2H_2 by OH proceeds according to the Master Chemical Mechanism (MCM) v3.3.1 (Jenkin et al., 1997; Saunders et al., 2003; Jenkin et al., 2015), via: http://mcm.leeds.ac.uk/MCM. Simplified C_2H_4 chemistry is included based on Lamarque et al. (2012) with an updated OH rate constant from the MCM v3.3.1. Table ~~S4~~ S1 shows the reactions and species included for unsaturated C_2 compounds. The standard model does not consider the OH reactivity of a subset of organic acids (RCOOH) from the oxidation of VOCs ~~oxidation~~. We implement oxidation of RCOOH and evaluate the impact of excluding this species, which is minor, in Table ~~S5~~ S2 and Fig. ~~S8~~S1. The model concentration of H_2 is fixed at 500 ppt, consistent with observed H_2 from ATom-1 and ATom-2 (520 ppt).

The GEOS-Chem global mean ~~simulated~~ tropospheric OH ($[OH]_{GM}$) is calculated as an air-mass weighted quantity below the model tropopause (see http://wiki.seas.harvard.edu/geos-chem/index.php/Mean_OH_concentration for the calculation methodology). The $[OH]_{GM}$ for 2016 is 11.9 ~~x~~ 10^5 molecules cm^{-3} and the corresponding methane lifetime (τ_{CH_4}) is 9.0 years. This result is comparable to the multi-model $[OH]_{GM}$ ~~mean OH~~ of 11.1 ~~x~~ 10^5 molecules cm^{-3} and τ_{CH_4} of 9.7 years from Naik et al. (2013). The best ~~observationally derived~~observationally derived estimate of τ_{CH_4} is 11.2 ± 1.3 years (Prather et al., 2012), suggesting a model bias here of 20 %. We calculate the ratio of total 2016 airmass-weighted OH in the Northern(>0°N) to Southern Hemisphere(<0°S). The ratio calculated in this manner of 1.14 ~~The ratio of tropospheric mean OH in the Northern to Southern Hemisphere is 1.12, which~~ exceeds ~~observationally derived~~observationally derived ratios of 0.85 to 0.97 (Montzka et al., 2000; Patra et al., 2014) ~~but is improved~~and is at the low end ~~over~~ of previous model estimates ranging from 1.13 to 1.42 (Naik et al., 2013).

2.2 Calculated OH reactivity

The atmosphere contains thousands of reactive organic compounds (Goldstein and Galbally, 2007). Transforming the concentrations of these compounds ~~(as well as those for~~and reactive inorganics ~~that react with OH)~~ to calculated OH reactivity (cOHR) ranks them in order of their importance as OH sinks. The cOHR from a model ($cOHR_{mod}$) can then be compared to cOHR from a suite of measurements ($cOHR_{obs}$), where cOHR is defined by Eq. (1). ~~Recent work from Chen et al. (2019) used~~

~~this framework to compare the reactivity of a suite of VOCs from a model to observations and found that biogenic species dominate emitted VOC reactivity over North America.~~

$$cOHR(s^{-1}) = k_{OH,CH_4}[CH_4] + k_{OH,CO}[CO] + k_{OH,NO_2}[NO_2] + \sum k_{OH,VOC}[VOC] + \cdots, \quad (1)$$

Figure 1a shows ~~the simulated~~ annual surface $cOHR_{mod}$ for the year 2016 based on the ninety ~~simulated constituents~~components listed in Table ~~S1~~S3. Approximately 80 % of air-mass weighted ~~Three-quarters of~~ $cOHR_{mod}$ resides below 3 km (Fig. 1b). The average annual surface $cOHR_{mod}$ is 1.8 s^{-1} with~~with approximately~~ 40 %~~-~~ present ~~present~~ over the ocean (average of 1.0 s^{-1}). Higher $cOHR_{mod}$ occurs in coastal outflow regions and the lowest $cOHR_{mod}$ is present over the Southern Ocean. The maximum $cOHR_{mod}$ (48 s^{-1}) ~~appears~~ over northern China is due to high concentrations of SO_2, NO_x, and CO. In the tropics, elevated $cOHR_{mod}$ is mainly ~~due to~~from isoprene, other biogenic species, and CO.

2.3 ATom observations

The NASA ATom field campaign (Wofsy et al., 2018) sampled the remote troposphere with the DC-8 aircraft over the Atlantic and Pacific Oceans from approximately 200 m to 12 km altitude ~~over the Atlantic and Pacific Oceans~~ in four seasons from 2016 to 2018 with a~~the~~ goal~~s~~ of improving the representation of trace gases and short-lived greenhouse-gases in models of atmospheric chemistry and climate. We use data here from the first two deployments (ATom-1 and ATom-2) which sampled winter and summer conditions in each hemisphere. We consider only observations over the ocean (72 % of measurements). Flight tracks for ATom-1 with land-crossings removed are shown in Fig. 2; ATom-2 flight tracks are nearly identical. We sample ~~The~~ model ~~is sampled~~ along the flight tracks and both the model and observations are averaged to the model grid and timestep for all following comparisons. The aircraft carried an extensive chemical payload including observations of water vapor, methane, CO, OH, NO_x, VOCs, photolysis frequencies, and OHR. Table 2 describes the observations used in this work.

3 Comparison of simulated and measured OH

We compare observed and simulated OH concentrations to evaluate whether differences are consistent with the bias in τ_{CH_4} discussed in Section 2.1. Figure 3 shows modeled OH sampled along the flight tracks and compared to observed OH (Table 2) for ATom-1 (boreal summer 2016) and ATom-2 (boreal winter 2017) in each hemisphere from the lowest sampled al~~t~~titude (~200 m) to 10 km. There is no evidence of a systematic overestimate in modeled OH throughout the troposphere. Figure S2 shows similarly good agreement across the observed frequency distributions of OH concentration. A model OH overestimate is apparent in the lowest two kilometers in the Northern Hemisphere summer~~, which~~ that could indicate excessive OH production or an underestimated sink from emissions of ocean ~~VOC emissions~~VOCs. Global models tend to overestimate OH against constraints from methyl chloroform observations (Shindell et al., 2006; Naik et al., 2013; Nicely et al., 2017) but we find here that tropospheric OH is successfully simulated within observational uncertainty (~~accuracy of~~ 74% to 1~~.~~35%, 2σ confidence level). This result from a global CTM is consistent with good agreement between OH measurements and a box

model during NASA's Pacific Exploratory Mission - Tropics (PEM-Tropic B) campaign in the clean remote Pacific (Tan et al., 2001) and a similar analysis by Brune et al. (2020) for ATom 1 through 4.

We calculate the air-mass weighted column average OH (OH_{col}) from the median OH concentrations in Fig. 3 and the total tropospheric air mass over the ocean~~as a metric of the performance of total tropospheric model oxidation~~. ~~The model OH_{col} concentration is within approximately 20 % of observations during both deployments, with minimal bias (<1 %) during Northern Hemisphere summer when OH is at a maximum.~~ During ATom-1, ~~Modeled~~ modeled OH_{col} in the Northern (Southern) Hemisphere is 44.5~~.40~~ (1~~1~~.430)$\times10^6$ ~~)~~ molecules cm^{-3} compared against the observations of 44.439 (~~1.06~~1.1)~~-~~$\times10^6$ molecules cm^{-3} during ATom-1. Similarly, during ATom-2, OH_{col} is ~~and 0.~~0.994 (~~22~~.6~~.75~~) $\times10^6$ molecules cm^{-3} in the model and ~~compared against observations of~~ 0.~~89~~ 8(2~~2~~.468)~~-~~$\times10^6$ molecules cm^{-3} ~~during ATom-2~~in the observations. Model OH_{col} is within 30 % of observations during both deployments, with the smallest bias in the total column during Northern Hemisphere summer when OH is at a maximum. As discussed above, model OH is overestimated in the lowest two kilometers during this period but this bias is minimized in the column average. ~~Figure S1 shows the observed frequency distributions of OH which are well captured by the model.~~ The observed airmass-weighted ratio ~~-~~of Northern to Southern hemispheric OH, calculated in the same manner as described in Section 2, is ~~over the ocean of~~ 4~~2~~.~~1~~ 8 during ATom-1 and 0.~~36~~ 5 during ATom-2 ~~indicates~~ indicating a strong seasonality that the model ~~successfully captures (ratios of 3.4 and 0.34)~~largely reproduces (ratio of 2.3 and 0.4). This ratio is less than the ratio of OH_{col} because there is approximately 30 % less air mass over the ocean in the Northern Hemisphere ocean than over the Southern Hemisphere. This seasonality~~,~~ ~~and which~~ is masked by calculations performed on an annual mean basis. ~~(as given in Section 2.1).~~ The seasonality in this ratio reported by Wolfe et al. (2019) for satellite-derived OH during ATom-1 and ATom-2 ~~is more modest~~is more modest because they calculate a daily average OH that extends to the tropopause while here we use largely daytime aircraft observations below 10 km. ~~because they account for seasonal differences in remote tropospheric air mass between each hemisphere. The successful simulation shown here is consistent with previous success in representing remote OH measurements with simple models during NASA's Pacific Exploratory Mission - Tropics (PEM-Tropics) B campaign in the clean remote Pacific (Tan et al., 2001).~~

~~While the~~The model is in good agreement with OH measurements during ATom but~~,~~ the uncertainty in the observations is similar to a recent estimate of the GEOS-Chem model uncertainty for OH of 25 to 40 % (Christian et al., 2018). ~~-~~In addition, the lifetime of OH is short (seconds) and ~~thus~~ atmospheric concentrations are highly variable, thus ~~. As a result, the comparison in Fig. 3 is~~direct model comparison to measured OH is insufficient to demonstrate model skill in capturing the broader remote oxidation capacity. ~~Good a~~Agreement between the model and observations could also result from compensating errors in the

OH source and sink. We support the model comparison in Fig. 3 with an evaluation of the key factors governing OH production and loss measured by ATom and investigate potential missing sources of VOCs from the ocean during summertime.

4 Constraints on the remote source of OH

~~Tropospheric~~ In the remote troposphere, OH is primarily produced from the photolysis of ozone in the presence of water vapor (Monks, 2005) and is enhanced ~~over the ocean~~ by nitrogen oxides (NO_x) from lightning and transport from continental sources. Methane, CO, and VOCs provide the main OH sinks (Murray et al., 2014). We compare the model to ATom-1 and ATom-2 observations of the drivers of the tropospheric OH source (water vapor, ozone, ozone photolysis frequency, NO_x) to determine possible broader sources of model bias.

Figure 4 compares observations of water vapor mixing ratios to the NASA MERRA-2 reanalysis product used ~~used to drive~~by the model ~~GEOS-Chem~~. MERRA-2 ~~was~~ is generally successful at reproducing ~~successfully evaluated against recent~~ observed~~ations of~~ tropospheric water vapor (Gelaro et al., 2017) and we ~~find~~ also find~~similar good model-measurement agreement here for ATom-1 and ATom-2 with no apparent biases~~good agreement compared with ATom-1 and ATom-2 observations throughout the troposphere. We evaluate the model treatment of the incoming actinic flux and the resulting ozone photolysis frequency ($j(O^1D)$) in Figure ~~5 compares median ozone photolysis frequencies to~~5 ~~evaluate the model treatment of the incoming actinic flux based on MERRA-2 cloud fractions and optical depths~~. Hall et al. (2018) showed that GEOS-Chem actinic fluxes in both cloudy and clear skies were well simulated during the ATom-1 deployment. ~~The simulations shown in~~ Figure~~.~~ 5 ~~also show~~confirms the minimal model bias in $j(O^1D)$ and ~~successfully represents~~successful representation of the observed seasonality with average summertime values below 3 km (~3~~.4~~×10^{-5} s^{-1}) approximately ~~2.5~~4 times higher than in winter (~0.7~~1.3~~×10^{-5} s^{-1}).

The GEOS-Chem ozone simulation has been extensively tested against ozonesondes, aircraft, and satellite observations ~~and is largely~~and shows no systematic overestimates ~~unbiased~~ (Hu et al., 2017) with the exception of continental surface concentrations (Fiore et al., 2009; Travis et al., 2016). Figure 6 shows that the highest (54-63 ppb) and lowest (14 ppb) tropospheric ozone observed during ATom-1 and ATom-2 occur during summer in the mid to upper troposphere and marine boundary layer, respectively. Ozone is less variable in wintertime with values between 30-50 ppb. The model generally reproduces the magnitude and shape of the tropospheric ozone profiles as well as the seasonality observed during both deployments. There is no evidence of the systematic Northern Hemisphere ozone bias previously seen in global model evaluations (Young et al., 2013) that was suggested as a cause of excessive OH (Naik et al., 2013). This may be reflected in the improved model interhemispheric OH ratio (Section 2.1) seen here over previous studies. Upper tropospheric ozone is

overestimated in ~~winte~~all cases but Northern Hemisphere summer~~r~~, but this would not have a large influence on primary OH production (or the methane lifetime) at these altitudes (Brune et al., 2020).

OH is enhanced in the presence of NO_x (≡NO + NO_2). We use NO_y here (Fig. 7(a)) as our~~a~~ constraint as observed NO_2 was generally near the detection limit in both deployments. We also show NO (Fig. 7(b)) given its ~~key~~ role in secondary OH production. The model ~~represents~~~~captures~~reproduces the maximum in ~~Maximum~~ NO_y ~~occurs in~~ that occurs in the Northern Hemisphere upper troposphere in summertime due to lightning (Marais et al., 2018~~)) and the model captures this enhancement~~. Observations show little variability between summer and winter NO_y in the lower troposphere. Southern Hemisphere NO_y is underestimated in the lowest few kilometers in both seasons which could be due to missing ocean production of methyl nitrate (Fisher et al., 2018). The largest model discrepancy is an overestimate of approximately ~~50~~ 70 % in the Northern Hemisphere wintertime. Observations of NO reflect the structure of NO_y, with the exception of ~~in~~ Northern Hemisphere winter. ~~Figure S2 shows that the model NO_y overestimate in this period is driven by a high bias for nitric acid (HNO_3).~~

4.1 Causes of the remote model bias in NO_y

Figure 8 shows that the model NO_y overestimate in ~~this period~~winter is primarily caused by nitric acid (HNO_3). Excessive remote HNO_3 is a long-standing model deficiency (Bey et al., 2001; Staudt et al., 2003; Brunner et al., 2003, 2005). The model bias identified here is unlikely to result from overestimated continental emissions due to the short lifetime of NO_y against deposition (~3 days in the Northern Hemisphere winter). Models suggest that less than 40 % of emitted NO_x in the U.S. is exported downwind (Dentener et al., 2006; Zhang et al., 2012). However ~~The~~ the standard model configuration here does not address the large possible bias in the U.S. anthropogenic NO_x inventory of ~40 % (Anderson et al., 2014; Travis et al., 2016) or the downward trend in NO_x emissions from Asia of ~30 % since 2011 (Krotkov et al., 2016). As expected, ~~Scaling~~ scaling Asia and U.S. NO_x emissions by these percentages improves the model bias in winter by only 15 % below 3 km (Fig. 8~~S2~~). Recent improvements to the simulation of continental wintertime HNO_3 (Jaeglé et al., 2018) would similarly be expected to have a marginal effect in our study region.

Kasibhatla et al. (2018) showed that acid displacement of chloride (Cl^-) by HNO_3 on seasalt aerosol~~s~~ (SSA) could resolve model overestimates of gas-phase HNO_3 in the marine boundary layer using the GEOS-Chem model. A more comprehensive simulation of this process was developed by Wang ~~X~~. et al. (2019). Figure 8~~S2~~ shows sensitivity tests ~~with the mechanism from Wang X. et al. (2019) incorporated into our simulation of this mechanism over~~in the Northern Hemisphere ~~in~~ winter ~~using the mechanism from Wang X. et al. (2019). Their model configuration exhibits a higher larger ozone and smaller NO_y bias when compared to our simulation of the wintertime ATom 2 measurements shown in Figs. 6 and 7; we focus here on relative changes associated with the acid displacement of chloride. Remote~~Model HNO_3 decreases by ~~approximately 50~~approximately 100 ppt below ~~1~~ 3 km which, combined with reduced emissions, would significantly improve the wintertime NO_y bias in this region ~~but~~ although the free tropospheric bias remains. The displacement of Cl^- described above generates

photolysis of particulate nitrate on coarse-mode SSA (NITs). Photolysis of nitrate resulting from the acid displacement of Cl^- by HNO_3 described above has been proposed as a source of NO_x to the marine boundary layer (Ye et al., 2016; Romer et al., 2018) which could counteract the reductions from acid displacment of Cl^- by HNO_3might increase HNO_3. Kasibhatla et al. (2018) implemented photolysis of NITs produced from this mechanism to generate NO and HONO in the marine boundary layer. We include NITs photolysis add this process to the simulation of Wang X. et al. (2019) at a photolysis ffrequency of 50 times that of HNO_3 (Kasibhatla et al., 2018). As shown in FFigure. 8S2 shows that, this mechanism is consistent with observations of NO and ozone below 1-3 km and does not further biasincrease HNO_3 but results in increasedincreases the free tropospheric NO_y bias due to PAN formation and exacerbates the overestimate in upper tropospheric ozone during this season.

The difficulty in resolving the bias in wintertime model NO_y appears to bemay be due to an to an overestimate of the in the overall NO_y lifetime as demonstrated by our sensitivities discussed above. Luo et al. (2019) proposed a new treatment of model wet scavenging using MERRA2 spatially and temporally varying cloud condensation water content and an empirical description of tracer HNO_3 wet removal. This scheme, as a mechanism to drastically reduced reduce persistent model biases in model surface nitric acid and nitrate at the surface in the over the United States (Zhang et al., 2012; Heald et al., 2012). Preliminary tests (Fig. S2) showAs shown in Fig. 8, that the revised wet scavenging according to Luo et al. (2019) scheme could fully resolve the remote bias in HNO_3 throughout the troposphere. However, this parameterization has only received only limited testing over the surface of the continental U.S. and more testing evaluation is needed before it can be adopted widely in models.

The effect of increased scavenging could have complex effects on global OH due to reduced oxidant loss from heterogeneous chemistryWe find that scaling NO_x, implementing chlorine chemistry, and revised wet scavenging during both deployments (with the exception of Northern Hemisphere winter) have negative impacts on the modeled OH_{col} along the flight tracks of -1 %, -7 %, and -4 %, respectively. The addition of NITs photolysis to the chlorine chemistry simulation increases OH_{col} by 10% over the base model. In Northern Hemisphere winter only, revised wet scavenging increases OH_{col} by 16 % possibly due to the effect of reduced heterogeneous chemistry. Overall, the annual mean impact of revised wet scavenging from our preliminary sensitivity tests is a -3 % reduction in global mean airmass-weighted OH and a +2 % increase in the model methane lifetime. , another area of intensive current research. For example, recent improvements to N_2O_5 hydrolysis in cloud water (Holmes et al., 2019) would further increase tropospheric levels of HNO_3 over the current simulation shown here, complicating the results from Luo et al. (2019). Future work should further assess both the validity of the MERRA-2 cloud water product and the robustness of the scavenging mechanism from Luo et al. (2019), combined with improvements to cloud heterogeneous chemistry (Holmes et al., 2019), in the context of all components of NO_y and particulate nitrate throughout the troposphereThese preliminary sensitivities suggest that resolving before any conclusions can be reached about the impact of resolving the model wintertime Northern Hemisphere NO_y bias in the Northern Hemisphere could partially resolve overestimates of on global mean OH on an annual basis if the photolysis frequency of NITs is smaller than 50 times the rate

of HNO_3 photolysis. Recent~~.~~ work from the NASA KORUS-AQ field campaign found that a rate of 1 to 30 might be more consistent with observational constraints (Romer et al., 2018).

Overall, the main drivers of remote tropospheric OH production ~~are well-simulated~~ in our base-case simulation are in good agreement~~against the~~ with observations from the first two ATom deployments with the exception of an NO_y overestimate in the Northern Hemisphere wintertime. Acid displacement of Cl^- by HNO_3 on SSA (Kasibhatla et al., 2018; Wang X. et al., 2019) may somewhat improve remote HNO_3 below 3 km, but if the resulting ~~nitrate~~NITs undergoes photolysis at a rate of 50 times that of HNO_3 (Kasibhatla et al., 2018) the impact on remote NO_y may be ~~negligible~~lessened due to the formation of PAN. ~~However, b~~Both mechanisms require significant further study as tropospheric halogen sources and chemistry and the ~~rate and products of the photolysis of~~ photolysis frequency of NITs are highly uncertain. A new parameterization of ~~model~~ wet scavenging (Luo et al., 2019) would greatly improve modeled remote HNO_3 and NO_y but ~~also requires substantial further testing against observations of both cloud water and chemical tracers, in combination with recent work on in-cloud hydrolysis of N_2O_5 (Holmes et al., 2019)~~requires further testing and evaluation of its broader impacts on atmospheric chemistry.

5 Constraints on the remote sink of OH

The primary sinks of tropospheric OH are CO, methane, and VOCs; OHR measurements represent the sum effect of these species. Previous aircraft measurements of OHR provided evidence of missing reactivity in the remote atmosphere linked to unknown highly reactive VOCs (Mao et al., 2009). During ATom, Thames et al. (2020) measured OHR over the Atlantic and Pacific oceans and determined that missing OHR also correlated with oxygenated VOCs, suggesting the presence of unknown ocean emissions. We compare directly measured OHR during the ATom-1 and ATom-2 deployments to calculated OHR ($cOHR_{obs}$) according to Eq. 1 from the full ATom measurement suite and from the model ($cOHR_{mod}$) sampled along the flight path. Table 2 describes the observations used to calculate cOHR.

Figure ~~8~~ 9 shows the comparison of OHR and cOHR from the model and observations. The observed cOHR is typically less than observed OHR. Along the flight tracks, $cOHR_{obs}$ and $cOHR_{mod}$ show good agreement and ~~high~~ strong correlation (r^2=0.~~97~~ 95 for ATom-1 and ATom-2). The model underestimates $cOHR_{obs}$ by up to ~~up to 15~~ 12 % in the lowest 3 km; we discuss this difference ~~further~~ below. The measured relationship between OHR and $cOHR_{obs}$ is weaker (r^2=0.~~72~~ 53 for ATom-1, r^2=0.~~75~~ 56 for ATom-2) and $cOHR_{obs}$~~.~~ is less than OHR below 3 km ~~There is an enhancement in OHR near the surface not present in $cOHR_{obs}$ of~~by ~~approximate~~0.2 to ~~y~~ 0~~.~~.~~46~~ s^{-1} ~~in the Northern Hemisphere and 0.4 s^{-1} in the Southern Hemisphere.~~. Thames et al. (2020) showed that median missing reactivity (between OHR and an observationally-constrained box model) below 4 km during the ATom-1, ATom-2, and ATom-3 deployments was between 0.2 and 0.8 s^{-1}. They provided statistical evidence that while near the level of the instrument accuracy, missing OHR in the marine boundary layer was statistically significant. We find that ~~Th~~the missing OHR ~~is ~30 % discrepancy~~ is not associated with acetonitrile or CO (r^2~~r~~<0.~~03~~2) indicating that biomass

burning is not the cause. Acetaldehyde in Northern Hemisphere summer has the strongest relationship with ~~the~~ missing ~~reactivity~~ OHR (r^2 ~~r~~=0.~~42~~19, *p-value* << 0.01, Fig. S3) which suggests a potential role for unmeasured reactive VOCs or their oxidation products from the ocean, as also suggested by Read et al. (2012) and Thames et al. (2020).

Ocean emissions of ~~a variety of~~ VOCs have been suggested as a source ~~may be a source~~ of remote secondary organic aerosols (Gantt et al., 2010; Kim et al., 2017; Mungall et al., 2017) but their impact on remote reactivity has not been quantified. ~~Read et al. (2012) found that missing model oxygenated VOC (OVOC) in the remote marine tropical atmosphere (mainly acetaldehyde) may cause up to an 8% underestimation of the model global methane lifetime due to missing cOHR$_{mod}$.~~ Our base simulation, described in Section 2.1, only includes air-sea exchange of acetone, acetaldehyde, methanol, and dimethyl sulfide~~sulfide and methanol~~. We ~~test~~ determine whether additional compounds emitted from the ocean, but not generally included in models, could increase cOHR$_{mod}$ and ~~improve~~ reconcile the observed discrepancy described above. We follow the standard methodology for air-sea exchange described in Millet et al. (2008) to include emission of the species listed in Table 3 using ~~available~~ available ~~measurements~~ measured seawater concentrations, ~~of each species in seawater,~~ with the addition of isoprene implemented as a direct emission according to Arnold et al. (2009). As shown in Table 3, air-sea exchange represents a net sink of VOCs on an annual basis (-68 Tg C yr^{-1}) but this is ~~largely driven~~ mainly due to ~~by~~ ocean uptake of acetone which is ~~not~~ a ~~significant~~ negligible component of cOHR.

Interfacial photochemistry may provide an additional abiotic source of ~~abiotic~~ VOCs from the ocean. ~~This source is treated separately from air-sea exchange as described above but ocean uptake may still act on these emissions.~~ We model abiotic ocean ~~VOC~~ emissions of VOCs according to Brüggemann et al. (2018) by applying species-specific emission factors to the monthly ocean photochemical potential derived in their study. We use the emission factor appropriate for the upper bound of this source according to Brüggemann et al. (2017) (Table ~~S2~~S4). Table 4 provides a breakdown of these additional VOCs with a total annual emission of 28 Tg C yr^{-1}.

Figure ~~9~~ 10 shows the annual mean impact of all ocean emissions described in Tables 3 and 4 (including an adjustment to the acetaldehyde seawater concentration described below in Section 5.1) on cOHR$_{mod}$ by turning off those ocean sources in a one-year simulation. Average annual surface cOHR$_{mod}$ over the ocean increases by 10 % over the base simulation and 15 % over the simulation with no ocean emissions. The largest increases occur in regions of higher biogenic activity along coastlines and in the Southern Ocean due to the adjustment to acetaldehyde emissions discussed in Section 5.1. The incremental impact of the additional ocean emissions over the base simulation is shown in Fig. S~~4~~3. Without any ocean emissions, global mean OH would be 3 % greater than in the case with comprehensive treatment of ocean VOC ~~treatment~~. Figure ~~8~~ 9 shows that along the flight tracks, cOHR$_{mod}$ increases below 3 km by ~~approximately~~ 3-14 %~~0.1 s^{-1} in summer and 0.2 s^{-1} in winter~~ which reduces

the model bias against $cOHR_{obs}$. However ~~The~~ the majority of the added species (Table 3 and 4) were measured during ATom and would therefore contribute to $cOHR_{obs}$ and cannot explain the gap in OHR.

We evaluate the impact of further expanding the oceanic source of reactive VOCs to reconcile the discrepancy between $cOHR_{obs}$ and OHR in a similar manner to Mao et al. (2009). Here, we test a source of alkanes as previously suggested by ~~(~~Read et al. ~~(~~, 2012), using the model species ALK4 ($\geq C_4$ alkanes) that ~~which~~ has a calculated lifetime of less than two days in the Northern Hemisphere summer ($k_{OH} = 2.3 \times 10^{-12}$ cm^3 $molecules^{-1}$ s^{-1} at 298 K). Known alkanes have been measured in seawater (Plass - Dülmer et al., 1993) but the implied source is small. Consequently, we use ~~the~~ ALK4 ~~species~~ for testing ~~purposes~~ only. Generating the missing OHR in this way requires an implausibly large oceanic ALK4 source of 340 Tg C yr^{-1} compared against all other sources of VOCs in the model (Tables 3 and 4). A sensitivity test with this source, shown in Fig. ~~8~~9, largely closes the gap between $cOHR_{mod}$ and OHR but would result in a 20 to ~~-~~50 % reduction in OH ~~along the flight tracks~~below 3 km, biasing the model OH simulation (Fig. 3) and degrading model NO_y (Fig. 7) due to increased PAN formation.

Thames et al. (~~2019~~2020) found that a partial recycling of OH would be required to maintain consistency with observed OH and HO_2 during ATom when adding an unknown source of reactivity. If the unknown VOC we suggest includes some OH recycling in its oxidation mechanism, and does not produce PAN, the model bias in OH could be mitigated. We use isoprene as our test of a more reactive VOC that includes OH recycling ~~test an~~ by ~~additional source of more reactive VOC including OH recycling using isoprene as the new test species by~~ scaling the ALK4 emission source by the reaction rate of isoprene with OH to obtain a more reasonable~~n~~ emission source of approximately ~~11~~ 9 Tg C yr^{-1}. Figure ~~7~~ 9 shows that this source actually has a minimal impact on $cOHR_{mod}$ of no more than 0.1 s^{-1}. Only one third of the additional ~~This is due to the increased reactivity~~ $cOHR_{mod}$ from our ocean source of ALK4 is attributable to~~of~~ ALK4, the rest is due to CO, acetaldehyde, and other aldehydes ~~in our test with ALK4 that contribute over half of the increase in $cOHR_{mod}$~~ from both increased chemical~~increased~~ production and longer lifetimes from suppressed OH. Therefore a larger source of even a reactive VOC like isoprene is required to close the gap in missing OHR. Reconciling $cOHR_{mod}$ and OHR is therefore difficult using the existing suite of ATom measurement constraints and possible known precursors~~VOC precursors~~; further investigation of the accuracy of the OHR measurements in challenging remote conditions may be needed.

We also ~~examine~~assess whether the model ~~is able to capture~~accurately represents the components of $cOHR_{obs}$ and explore potential additional sources of missing $cOHR_{mod}$. Figures ~~10~~ 11 and ~~11~~ 12 show the components of median cOHR in the base simulation below 3 km for each deployment. The composition of $cOHR_{mod}$~~obs~~ is ~~is well-represented by the model~~generally consistent with $cOHR_{obs}$. CO and methane make up half or greater of both $cOHR_{obs}$ and $cOHR_{mod}$ ~~with a larger contribution in winter when the lifetime of CO is long~~. There is no systematic underestimate in CO as might be expected from the general model bias described by Shindell et al. (2006), with the exception of a 10 % underestimate during Northern Hemisphere winter when the lifetime of CO is longer and biases in continental sources could have a larger impact~~-~~. During the ATom-1 deployment, $cOHR_{obs}$ is 50 % higher in the Northern Hemisphere (summer) than in the Southern Hemisphere (winter)

primarily~~largely~~ due to the increase in methyl hydroperoxide (MHP) concentrations~~ and the higher reactivity of methane~~. During the ATom-2 deployment, $cOHR_{obs}$ is 60% higher in the Northern Hemisphere (winter) than in the Southern Hemisphere (summer) due to the large contribution of CO in Northern Hemisphere wintertime. The model successfully represents the observed seasonality during both deployments but underestimates $cOHR_{obs}$ by 12 % in the Northern Hemisphere and 9 % in the Southern Hemisphere.

The difference between measured and simulated cOHR is ~~largely~~mainly due to difference between measured and simulated ~~concentrations of~~ OVOCs.~~ ~~These compounds contribute on average ~~26~~ 25 % to $cOHR_{obs}$ but ~~only~~ 17 % to~~OF~~ $cOHR_{mod}$. The largest difference in reactivity is ~~due to the large enhancement in measured acetaldehyde compared with model simulat~~caused ~~by underestimated model~~ from acetaldehyde~~ions~~. Differences between simulated and measured MHP (Fig. ~~S9~~S5) are also important and could ~~and may~~ reflect an error in the ~~calculated~~ MHP lifetime (Müller et al. 2016). However,~~)s(CLH1). The differences could however reflect bias~~ interferences in the MHP measurement~~s~~ in the boundary layer (Supplement, Section ~~9~~6) have yet to be resolved and therefore~~.~~ ~~Due to the measurement uncertainty~~ we do not ~~explore~~ further evaluate causes of underestimated MHP here. ~~However, inability to reconcile remote acetaldehyde observations with models is a long-standing problem and has been previously observed over the remote ocean (Singh et al., 2001; Singh et al., 2003; Millet et al., 2010). Singh et al. (2001) proposed that a large, diffuse, and as-yet unknown source of oxygenated compounds such as acetaldehyde must exist in the troposphere. Using observations from Cape Verde, Read et al. (2012) speculated that underestimated model acetaldehyde could be due to alkanes from terrestrial or ocean biogenic sources.~~ We do consider potential missing sources of model acetaldehyde constrained by the ATom measurements over the ocean and assess their ~~potential~~ impact on simulated OH and CO in Section ~~6~~5.1.

~~6~~ 5.1 Evaluation of the remote sources of acetaldehyde

Inability to reconcile remote acetaldehyde observations with models is a long-standing problem (Singh et al., 2001; Singh et al., 2003; Millet et al., 2010; Nicely et al., 2016). Singh et al. (2001) proposed that a large, diffuse, and as-yet unknown source of OVOCs such as acetaldehyde must exist in the troposphere to solve this discrepancy. Read et al. (2012) determined that missing $cOHR_{mod}$ from OVOCs in the marine tropical atmosphere (mainly acetaldehyde), possibly from terrestrial or ocean sources of alkanes, could cause up to an 8% underestimation of the methane lifetime. Nicely et al. (2016) showed that constraining a box model with observed acetaldehyde reduced tropospheric column OH by 9% and that this acetaldehyde bias was present across eight different CTMs. Therefore, understanding the source of missing acetaldehyde may be part of the cause of the multi-model bias in the methane lifetime and global mean OH.

Figure ~~12~~ 13 compares the model simulation of acetaldehyde against observations. Average observed concentrations peak in the Northern Hemisphere during ATom-1 with an average mixing ratio of ~~250~~ 230 ppt below 3 km and 100 ppt above 3 km despite a lifetime of only several hours in summer. The maximum model underestimate occurs during this period. Observed

concentrations are at a minimum during the ATom-2 deployment indicating a strong seasonality in the source. In each deployment, concentrations remain as high as 70~~-~~ to 100 ppt as far south as 60ºS (Fig. S64) which the model does not reproduce. There is no apparent difference in model bias between observations over the Atlantic or Pacific Ocean (Fig. ~~S5~~S7). The model underestimates acetaldehyde on average by ~~more than a factor of two~~60 to 90 % (~~-~~50 to 200 ppt) below 3 km and does not capture the observed elevated levels throughout the troposphere~~, which could support the hypothesis of a missing long-lived precursor suggested by Singh et al. (2001)~~.

In earlier studies, measurement ~~artifacts~~ uncertainties prevented interpretation of model-measurement disagreements in the remote atmosphere~~,. Previous measurements of acetaldehyde had biases due~~ including ~~to~~ difficulties in background subtraction (Apel et al., 2008) with uncertainties as high as 70 ppt (Apel et al., 2003) which hindered analysis of clean conditions. The ATom measurement uncertainty is reduced to 10 ppt/20 % (Table 2) and does not have the biases present in previous campaigns (Wang S. et al., 2019). ~~Previous work~~Studies have also disputed whether observed acetaldehyde was compatible with observed PAN due to the significant role of acetaldehyde as a PAN precursor through production of the peroxyacetyl (PA) radical (Singh et al., 2001; Singh et al., 2003; Millet et al., 2010). Global simulations estimate that acetaldehyde is responsible for approximately 40 % of ~~the production of the~~ PA radical production (Fischer et al., 2014)~~,~~ which would be even larger if acetaldehyde is ~~underestimated as suggested above~~severely underestimated by models. Reaction of the PA radical with HO_2 is more prevalent in remote environments and produces peroxyacetic acid (PAA) preferentially over PAN, making PAA a more useful constraint for the conditions sampled by ATom. Figure ~~13~~ 14 shows the average model underestimate ~~model simulation~~ of PAA ~~against observations for each deployment. PAA is underestimated by the model~~below 3 km of 70 to 90 % (60 to 250 ppt)~~.~~ ~~with t~~The model biases for PAA and acetaldehyde both peak with similar magnitude ~~largest model bias~~ during Northern Hemisphere summer~~, consistent with the model bias in acetaldehyde~~. Fig. ~~14~~ 15 shows the model comparison with PAN, which is generally well simulated during this period.

Wang S. et al. (2019) ~~find using~~used an observationally-constrained box-model to show that the levels of acetaldehyde observed during ATom are required to explain the observed PAA~~,~~ ~~although the~~ The reaction rate of PAA + OH may be three times~~has an uncertainty of approximately a factor of three~~ larger (Wu et al., 2017) than the maximum value used by Wang S. et al. (2019) which could result in even better agreement between PAA and acetaldehyde in the marine boundary layer. We evaluate the standard GEOS-Chem acetaldehyde budget, described in detail by Millet et al. (2010), against available ATom observations. The 2016 model budget for the base simulation is provided in Table 5. Acetaldehyde is ~~mainly~~ produced from ~~VOC~~ oxidation of VOCs (ethane, propane, $\geq C_4$ alkanes, $\geq C_3$ alkenes, isoprene, ethanol) and is ~~also~~ directly emitted from the ocean, terrestrial plant growth, biomass burning, and anthropogenic activities. The model parameterization of acetaldehyde ocean emissions is dependent on satellite-based observations of colored dissolved organic matter (CDOM) (Millet et al., 2010).

The model free tropospheric bias suggests that long-lived oxidation of VOCs ~~oxidation~~ must be underestimated due to the short lifetime of acetaldehyde (< 1 day). The longest-lived precursor VOCs in the model are ethane (two months) and propane

(two weeks). Ethane has the highest concentration of any measured non-methane VOC during ATom with an average of 1.5 ppb below 3 km during the Northern Hemisphere winter. The model underestimates average ethane and propane below 10 km by ~~up to 30 % during ATom-1 and 80%~~100 % and 40 %, respectively ~~during ATom-2~~ (Figs. S~~8~~6 and S~~9~~7, ~~respectively~~) which could be due to underestimated natural geologic and fossil fuel emissions (Dalsøren et al., 2018). However, the oxidation of these species is too slow to provide the missing model acetaldehyde and would only marginally increase remote background levels even if it was produced at higher yield at low-NO_x (~~currently~~ model yields are ~50 % for ethane, ~20 % for propane, Millet et al., 2010). The ~~model c~~chemical mechanism used for these species is provided in Table ~~S3~~S5. One or more precursors able to resolve the model acetaldehyde bias must therefore be present at higher cumulative concentrations than ethane or propane. Modeled ALK4, parameterized as a butane/pentane mixture, maintains a high acetaldehyde yield at low-NO_x and has a shorter lifetime (~5 days), contributing to a larger perturbation to atmospheric acetaldehyde levels than ethane or propane for a given concentration change. The sensitivity test adding substantial ALK4 emissions from the ocean described in Section 4 would not resolve the free tropospheric bias in the Northern Hemisphere~~result in only small improvement in the free troposphere~~ but would result in a ~~50~~40 % overestimate below 1 km. Furthermore, ALK4 is ~~also~~ too short-lived to substantially perturb the remote atmosphere from a continental source, thus the potential missing acetaldehyde precursors (from either a marine or terrestrial source) must have a longer lifetime.

As shown in Table 5, primary ocean emissions of acetaldehyde in the base simulation (22 Tg yr^{-1}) are lower than previous work (57 Tg yr^{-1}) due to updates to the model parameterization of the water transfer velocity (Johnson, 2010). Additional independent estimates of the ocean source are also much larger (34 to ~~-~~42 Tg yr^{-1}, Read et al., 2012; Wang S. ~~et al,~~et al., 2019). However, an increased primary ocean source would not address the bias in the free troposphere or in winter when biogenic activity from CDOM is zero in the model at high latitudes. Ship-borne measurements generally measure non-zero acetaldehyde seawater concentrations of approximately 5 nM (Read et al., 2012) and a recent trans-Atlantic campaign found that acetaldehyde concentrations from 47°S to 50°N did not always correlate with levels of CDOM (Yang et al., 2014). Therefore, we set a minimum seawater concentration of 5 nM in the model parameterization regardless of CDOM level. This change adds 2 Tg C yr^{-1} in emissions and increases concentrations over the remote ocean in winter by up to 50 ppt.

Figure ~~12~~ 13 shows the combined effect of adding new ocean VOCs in Section ~~4~~ 5 and improving the seawater parameterization described above on modeled acetaldehyde (labelled as “Improve Ocean VOCs”). Although the direct ocean source in this work is lower than previous estimates as described above, the secondary source from precursor VOCs is enhanced. Of the additional marine VOCs described in Section ~~4~~5, 25 Tg C yr^{-1} produce acetaldehyde as an oxidation product (Tables 3 and 4). This is compared to 12 Tg C yr^{-1} of direct emissions in the base model. These sources substantially increase average ~~near-surface simulated~~modeled acetaldehyde below 3 km, with the largest improvement during winter (~~40~~60 to ~~-97~~0 ppt) when atmospheric lifetimes are longer and the influence of the ocean can extend aloft. In summer, the average model increase below 3 km ~~impacts of 10-60~~is less than 20 ppt ~~are limited to the lowest model layer~~ due to higher OH concentrations.

Recent work over North America suggested that free tropospheric VOCs may be underestimated due to errors in model vertical mixing (Chen et al. 2019), but in Northern Hemisphere summer slower mixing would not be expected to compensate for the short lifetime of acetaldehyde in this region (~4 hours). Thus the pervasive model bias in the free troposphere cannot be explained by an increase in known direct or indirect ocean sources.

Photodegradation of organic aerosols (OA) is another potential source of oxygenated VOCs such as acetaldehyde to the troposphere (Kwan et al., 2006; Epstein et al., 2014; Wong et al., 2015; Wang S. et al., 2019). The source of secondary organic aerosols (SOA) is uncertain and ~~it~~ has been suggested ~~that it~~ to be up to four times larger than current estimates given an implied underestimate of the photochemical loss term (Hodzic et al., 2016). We test the potential impact of ~~such a source~~the maximum possible source ~~on~~ of acetaldehyde from photochemical loss of OA ~~using the model simulation of OA described in Section 2.1 and~~by increasinge the overall model production of SOA by a factor of four to maximize the impact of R2 below. We apply a photolysis frequency for OA of $4 \times 10^{-4} J_{NO_2}$ (Hodzic et al., 2015) to the reactions R1 and R2 as an upper limit and describe the formulation of R1 and R2 below.

$$\mathrm{OCPI} + h\upsilon = 0.5\ \mathrm{ALD2} \quad \text{(R1)}$$

$$\mathrm{SOAS} + h\upsilon = 0.66\ \mathrm{SOAS} + \mathrm{ALD2} \quad \text{(R2)}$$

The model species OCPI and SOAS represent the majority of ~~modeled~~ simulated OA in the remote atmosphere. ~~.~~ OCPI is aged (hydrophilic) organic carbon (12 g C mol^{-1}) and SOAS is SOA from all emission categories (150 g mol^{-1}). Both are assumed for the purposes of the sensitivity tests here to have an OA/OC ratio of 2.1. In R1, one molecule of carbon (0.5 ALD2) is produced per reaction. ~~and i~~In R2, one acetaldehyde molecule (ALD2) is produced per reaction. The resulting impact on ~~modeled~~ acetaldehyde is only appreciable in the Northern Hemisphere winter (Fig. ~~12~~13) when modeled aerosol amounts are highest and the lifetime of acetaldehyde is long. Given that this test represents an upper limit, we conclude that photolysis of organic aerosols ~~photolysis~~ cannot provide a sufficient source of acetaldehyde to reconcile the model with observations.

We consider whether an entirely unknown VOC with moderate lifetime and a high yield of acetaldehyde at low NO_x could resolve the free-tropospheric model bias. We emit such a species with a lifetime of approximately one month against oxidation by OH, emissions of 100 Tg yr^{-1} from either anthropogenic, biomass burning, or ocean sources, and a yield of 1 acetaldehyde molecule per reaction with OH. We do not test a terrestrial biogenic source here but expect the results would be similar to the biomass ~~-~~burning case. These simulations result in average tropospheric concentrations of ~~1~~2 to ~~-~~4 ppb ~~of the precursor VOC throughout the troposphere~~. The effect of the unknown VOC is compatible with the model simulation of OH (unlike the addition of oceanic ALK4 needed to reconcile OHR observations as described in Section 5). ~~Summertime tropospheric OH below 3 km decreases by approximately 6 % against ATom observations over the case with improved ocean emissions, well within measurement and model uncertainty.~~ The maximum $cOHR_{mod}$ of this species is small (< 0.0~~3~~4 s^{-1}). The impact on

modeled acetaldehyde (Fig. ~~12~~13) is generally similar across all three source categories due to the long lifetime of this precursor. As shown in Fig. ~~12~~ 13 and ~~13~~ 14, the addition of this unknown VOC modestly improves the simulation of acetaldehyde and PAA everywhere but a large residual underestimate in Northern Hemisphere summer remains. The impact on PAN is minor with the exception of Northern Hemisphere winter (Fig. ~~14~~15), but this is likely driven by the model overestimate in NO_y (Fig. 7, Section 4.1).

~~VOC emissions~~Emission inventories of VOCs are known to be incomplete, ~~,~~ for example ~~missing~~neglecting emissions from volatile consumer products (McDonald et al., 2018) ~~and biomass burning~~or failing to identify as much as half of emitted VOCs from biomass burning (Akagi et al. 2011), both of which peak in summer. ~~In the case of fire emissions, half of VOC emissions are unidentified (Akagi et al., 2011) and t~~The average emission factor for ~~this u~~unidentified VOCs from biomass burning roughly corresponds to ~~76~~ 75 Tg yr^{-1}, ~~of unidentified VOC,~~ similar to our sensitivity tests of 100 Tg yr^{-1} described above. However, recent attempts to quantify these unidentified VOCs ~~from fire~~ (Stockwell et al., 2015; Koss et al., 2018) find that newly identified compounds tend to be too reactive to impact the remote atmosphere, as needed here; however, ~~, but~~ this work is ongoing and future efforts should investigate potential precursors of acetaldehyde that could be transported to the remote atmosphere. The missing source of precursor VOCs ~~must~~ would need to have substantial additional summertime emissions above and beyond the sensitivity tests shown in Fig. ~~12~~ 13 to address the Northern Hemisphere summertime bias. The required magnitude of this perturbation ~~will be~~is difficult to reconcile within known measurement and emission uncertainty constraints.

~~7~~ 6 Conclusions

The ~~rich~~ detailed set of chemical information available from the ATom field campaign provides the most comprehensive dataset ever collected to evaluate models in the remote atmosphere. The sampling strategy of collecting observations throughout the troposphere in multiple seasons is ideally suited for improving our understanding of tropospheric chemistry in a poorly observed region of the atmosphere. We use the first two deployments of the ATom field campaign during July-August 2016 and January-February 2017 to investigate sources of bias in model simulations of OH. Global models such as the GEOS-Chem CTM used here tend to overestimate the loss of methane by OH and underestimate CO which provides the main tropospheric sink of OH. Comparisons of the model with observations from the first two ATom deployments do not show systematic bias in the simulation of OH or the drivers of remote OH production (water vapor, photolysis of ozone, ozone and NO_y) with the exception of wintertime NO_y which is biased high by a factor two.

The model overestimate of wintertime NO_y is largely attributable to nitric acid. This bias is not due to an anthropogenic inventory overestimate but may reflect insufficient wet scavenging as well as loss to seasalt aerosols by nitric acid, although the former mechanism may be counteracted by photolysis of the resulting nitrate aerosols. The impact of resolving this wintertime NO_y bias ~~on remote OH~~ is uncertain but could partially improve the model overestimate of OH. Future work should

improve constraints on these mechanisms, which have all received only preliminary validation, and carefully examine their impact in the context of broader atmospheric chemistry, particularly NO_y partitioning throughout the troposphere.

We present the first comparison of measured OH reactivity (OHR) from aircraft with a global model to evaluate the tropospheric sink of OH. We calculate OH reactivity ($cOHR_{obs}$) from relevant species observed during ATom and compare this to cOHR from the model ($cOHR_{mod}$). Measured OHR is higher than $cOHR_{obs}$ by approximately ~~30 %~~0.2 to 0.4 s^{-1} below 3 km. This missing OHR correlates with acetaldehyde during summer indicating a potential source of missing reactive VOCs, similar to the findings of Mao et al. (2009) ~~for the NASA INTEX-B field campaign~~and Wang S. et al. (2020). The addition of a comprehensive set of ocean emissions of ~~VOC emissions~~VOCs increases global mean cOHR by 10 % but cannot reproduce the observed OHR enhancement during ATom-1. Adding sufficient alkanes to the model to resolve this bias requires an improbably large ocean ~~VOC~~ source ~~-~~(340 Tg C yr^{-1}) and would degrade the model simulation of OH and NO_y. Only one third of the increase in cOHR in this test is due to the alkanes, the rest is from oxidation products and changes in OH, therefore a more reactive VOC would still need to be emitted in large amounts.

The model successfully simulates the seasonality and hemispheric gradient in cOHR but has a persistent underestimate of up to ~~15~~ 12 % in the lowest 3 km, primarily due to ~~an~~ missing model acetaldehyde ~~underestimate~~. The model does not underestimate CO, with the exception of Northern Hemisphere winter which has been previously recognized by (Kopacz et al., 2010) and attributed to underestimated fossil fuel emissions. The inability to reproduce observations of remote acetaldehyde was first observed during the PEM-Tropics campaign (Singh et al., 2001; Singh et al., 2003; Millet et al., 2010) but the measurement was uncertain. Improvements in measurement precision and the accompanying measurement of PAA during Atom (Wang S. et al., 2019) strengthen the conclusion that there is a large amount of acetaldehyde present in the atmosphere that cannot be explained by current models. We investigate possible underestimates in known sources of acetaldehyde including ~~VOC~~ emissions of VOCs from anthropogenic, biomass, or oceanic sources or production from the photolysis of organic aerosols. No known source can fully resolve the bias in acetaldehyde throughout the troposphere, and particularly in the Northern Hemisphere summer. We consider the possibility that there is a large, diffuse source of unknown VOCs by implementing 100 Tg yr^{-1} of such a compound from ocean, biomass burning, or anthropogenic sources. This hypothetical source modestly reduces the model acetaldehyde bias and is compatible with the simulation of OH and cOHR; however, an additional source is required to resolve the largest bias in the Northern Hemisphere summer. Errors or omissions in the oxidation mechanism of known VOCs ~~may~~ could be another source ~~also contribute to~~of ~~this~~ bias. For example, significant uncertainties exist in peroxy radical (RO_2) chemistry for large RO_2 molecules (Praske et al., 2017), although the flux of carbon through a minor pathway would have to be large, restricting the possible known sources. Further laboratory and field observations are needed to understand which precursors and sources could lead to the sustained production of acetaldehyde observed during ATom and prior campaigns.

This study demonstrates that long-standing model biases in global mean OH are unlikely to be due to errors in simulating tropospheric chemistry over the ocean. This implies that a large bias must be present in OH production or loss over land and future work should focus on evaluating continental OH sources and sinks. Errors in modeled OH were recently investigated by Strode et al. (2015) and when overestimates related to production terms were corrected, model OH remained too high in the Northern Hemisphere, suggesting that future studies should focus on errors in OH loss.

Author Contributions. CLH and KRT designed the study and wrote the paper with input from the co-authors. KRT modified the code, performed the simulations and led the analysis. HMA, ECA, DRB, WHB, RC, JDC, BCD, GSD, JWE, SRH, EJH, SRH, MJK, KM, FLM, JP, TBR, ABT, KU, POW, GMW provided ATom measurements used in the analysis. XW provided the model code for the sensitivity runs including acid displacement of chloride on coarse-mode seasalt aerosols. TS, ME and PSK provided the model code for the photolysis of particulate nitrate. GL and FY were responsible for the code for the revised treatment of wet scavenging in the model. DBM and XC provided the methanol seawater concentration and assisted in the ocean budget analysis. SRA provided the biogenic ocean isoprene emissions. ~~KRT and CLH wrote the paper with input from the co-authors.~~

Competing interests. The authors declare that they have no conflict of interest.

*Funding***.** This study was supported by ~~CLH and KRT acknowledge from~~ the National Science Foundation (AGS-1564495) and the National Oceanic and Atmospheric Administration (NA18OAR4310110). DBM and XC acknowledge support from the National Aeronautics and Space Administration (NNX14AP89G). TBR was supported by the National Aeronautics and Space Administration (IAT NNH15AB12I) and by funding from the National Oceanic and Atmospheric Administration Climate Program Office and AC4 program. RH, EA, SRH, and KU were supported by the National Center for Atmospheric Research, which is a major facility sponsored by the National Science Foundation under Cooperative Agreement No. 1852977. SH and KU were supported by NASA (NNX15AG71A). GL and FY acknowledge support from the National Aeronautics and Space Administration (NNX17AG35G). Caltech authors acknowledge support from the National Aeronautics and Space Administration (NNX15AG61A).

Data Availability. The ATom-1 and ATom-2 data (Wofsy et al., 2018) are available here doi:10.3334/ORNLDAAC/1581.

Acknowledgements. We acknowledge helpful conversations and advice from Andrea Molod, Rachel Silvern, Eloïse Marais, Sarah Safieddine, Martin Brüggemann, Christian George and James Crawford. We acknowledge Tom Hanisco and Jason St. Clair for the use of ~~his~~ their formaldehyde observations from ATom and Barbara Barletta and Simone Meinardi for their contribution to the UCI WAS measurements.

References

Akagi, S. K., Yokelson, R. J., Wiedinmyer, C., Alvarado, M. J., Reid, J. S., Karl, T., Crounse, J. D. and Wennberg, P. O.: Emission factors for open and domestic biomass burning for use in atmospheric models, Atmos. Chem. Phys., 11(9), 4039–4072, doi:10.5194/acp-11-4039-2011, 2011.

Anderson, D. C., Loughner, C. P., Diskin, G., Weinheimer, A., Canty, T., P., Salawitch, R. J., Worden, H. M., Fried, A., Mikoviny, T., Wisthaler, A., and Dickerson, R. R.: Measured and modeled CO and NOy in DISCOVER-AQ: An evaluation of emissions and chemistry over the eastern US, Atmos. Environ., 96, 78–87, doi:10.1016/j.atmosenv.2014.07.004, 2014.

Apel, E. C., Hills, A. J., Lueb, R., Zindel, S., Eisele, S. and Riemer, D. D.: A fast-GC/MS system to measure C_2 to C_4 carbonyls and methanol aboard aircraft, J. Geophys. Res.: Atmospheres, 108(D20), doi:10.1029/2002JD003199, 2003.

Apel, E. C., Brauers, T., Koppmann, R., Bandowe, B., Boßmeyer, J., Holzke, C., Tillmann, R., Wahner, A., Wegener, R., Brunner, A., Jocher, M., Ruuskanen, T., Spirig, C., Steigner, D., Steinbrecher, R., Gomez Alvarez, E., Müller, K., Burrows, J. P., Schade, G., Solomon, S. J., Ladstätter-Weißenmayer, A., Simmonds, P., Young, D., Hopkins, J. R., Lewis, A. C., Legreid, G., Reimann, S., Hansel, A., Wisthaler, A., Blake, R. S., Ellis, A. M., Monks, P. S. and Wyche, K. P.: Intercomparison of oxygenated volatile organic compound measurements at the SAPHIR atmosphere simulation chamber, J. Geophys. Res.: Atmospheres, 113(D20), doi:10.1029/2008JD009865, 2008.

Apel, E. C., R. S. Hornbrook, A. J. Hills, N. J. Blake, M. C. Barth, A. Weinheimer, C. Cantrell, S. A. Rutledge, B. Basarab, J. Crawford, G. Diskin, C. R. Homeyer, T. Campos, F. Flocke, A. Fried, D. R. Blake, W. Brune, I. Pollack, J. Peischl, T. Ryerson, P. O. Wennberg, J. D. Crounse, A. Wisthaler, T. Mikoviny, G. Huey, B. Heikes, D. O'Sullivan, and D. D. Riemer: Upper tropospheric ozone production from lightning NO_x-impacted convection: Smoke ingestion case study from the DC3 campaign, Journal of Geophysical Research: Atmospheres, doi:10.1002/2014JD022121, 2015.

Arnold, S. R., Spracklen, D. V., Williams, J., Yassaa, N., Sciare, J., Bonsang, B., Gros, V., Peeken, I., Lewis, A. C., Alvain, S. and Moulin, C.: Evaluation of the global oceanic isoprene source and its impacts on marine organic carbon aerosol, Atmos. Chem. Phys., 10, 2009.

Bey, I., Jacob, D. J., Yantosca, R. M., Logan, J. A., Field, B. D., Fiore, A. M., Li, Q., Liu, H. Y., Mickley, L. J. and Schultz, M. G.: Global modeling of tropospheric chemistry with assimilated meteorology: Model description and evaluation, J. Geophys. Res., 106(D19), 23073–23095, doi:10.1029/2001JD000807, 2001.

Breider, T.J., L.J. Mickley, D.J. Jacob, C. Ge, J. Wang, M.P. Sulprizio, B. Croft, D.A. Ridley, J.R. McConnell, S. Sharma, L. Husain, V.A. Dutkiewicz, K. Eleftheriadis, H. Skov, and P.K. Hopke, Multi-decadal trends in aerosol radiative forcing over the Arctic: contribution of changes in anthropogenic aerosol to Arctic warming since 1980, J. Geophys. Res., 122(6), 3573â€“3594, doi:10.1002/2016JD025321, 2017.

Brüggemann, M., Hayeck, N., Bonnineau, C., Pesce, S., A. Alpert, P., Perrier, S., Zuth, C., Hoffmann, T., Chen, J. and George, C.: Interfacial photochemistry of biogenic surfactants: a major source of abiotic volatile organic compounds, Faraday Discussions, 200(0), 59–74, doi:10.1039/C7FD00022G, 2017.

Brüggemann, M., Hayeck, N. and George, C.: Interfacial photochemistry at the ocean surface is a global source of organic vapors and aerosols, Nature Communications, 9(1), doi:10.1038/s41467-018-04528-7, 2018.

Brune, W. H., Miller, D. O., Thames, A. B., Allen, H. M., Apel, E. C., Blake, D. R., Bui, T. P., Commane, R., Crounse, J. D., Daube, B. C., Diskin, G. S., DiGangi, J. P., Elkins, J. W., Hall, S. R., Hanisco, T. F., Hannun, R. A., Hintsa, E. J., Hornbrook, R. S., Kim, M. J., McKain, K., Moore, F. L., Neuman, J. A., Nicely, J. M., Peischl, J., Ryerson, T. B., St. Clair, J. M., Sweeney, C., Teng, A. P., Thompson, C., Ullmann, K., Veres, P. R., Wennberg, P. O. and Wolfe, G. M.: Exploring Oxidation in the Remote Free Troposphere: Insights From Atmospheric Tomography (ATom), J. Geophys. Res. Atmos., 125(1), doi:10.1029/2019JD031685, 2020.

Brunner, D., Staehelin, J., Rogers, H. L., Köhler, M. O., Pyle, J. A., Hauglustaine, D., Jourdain, L., Berntsen, T. K., Gauss, M., Isaksen, I. S. A., Meijer, E., Velthoven, P. V., Pitari, G., Mancini, E., Grewe, G. and Sausen, R.: An evaluation of the performance of chemistry transport models by comparison with research aircraft observations. Part 1: Concepts and overall model performance, Atmos. Chem. Phys., 24, 2003.

Brunner, D., Staehelin, J., Rogers, H. L., Kohler, M. O., Pyle, J. A., Hauglustaine, D. A., Jourdain, L., Berntsen, T. K., Gauss,

M., Isaksen, I. S. A., Meijer, E., van Velthoven, P., Pitari, G., Mancini, E., Grewe, V. and Sausen, R.: An evaluation of the performance of chemistry transport models – Part 2: Detailed comparison with two selected campaigns, Atmos. Chem. Phys., 23, 2005.

Chan Miller, C., Jacob, D. J., Marais, E. A., Yu, K., Travis, K. R., Kim, P. S., Fisher, J. A., Zhu, L., Wolfe, G. M., Hanisco, T. F., Keutsch, F. N., Kaiser, J., Min, K.-E., Brown, S. S., Washenfelder, R. A., González Abad, G. and Chance, K.: Glyoxal yield from isoprene oxidation and relation to formaldehyde: chemical mechanism, constraints from SENEX aircraft observations, and interpretation of OMI satellite data, Atmos. Chem. Phys., 17(14), 8725–8738, doi:10.5194/acp-17-8725-2017, doi:10.1021/ac0604235, 2017.

Chen, X., Millet, D. B., Singh, H. B., Wisthaler, A., Apel, E. C., Atlas, E. L., Blake, D. R., Bourgeois, I., Brown, S. S., Crounse, J. D., de Gouw, J. A., Flocke, F. M., Fried, A., Heikes, B. G., Hornbrook, R. S., Mikoviny, T., Min, K.-E., Müller, M., Neuman, J. A., O'Sullivan, D. W., Peischl, J., Pfister, G. G., Richter, D., Roberts, J. M., Ryerson, T. B., Shertz, S. R., Thompson, C. R., Treadaway, V., Veres, P. R., Walega, J., Warneke, C., Washenfelder, R. A., Weibring, P., and Yuan, B.: On the sources and sinks of atmospheric VOCs: an integrated analysis of recent aircraft campaigns over North America, Atmos. Chem. Phys., 19, 9097–9123, doi:10.5194/acp-19-9097-2019, 2019.

Christian, K. E., W. H. Brune, J. Q. Mao and Ren, X. R.: Global sensitivity analysis of GEOS-Chem modeled ozone and hydrogen oxides during the INTEX campaigns, Atmos. Chem. Phys., 18, 2443-2460, doi:10.5194/acp-18-2443-2018 2018.

Colman, J., Swanson, A., Meinardi, S., Sive B., Blake, D. R. and Rowland, F. S.: Description of the analysis of a wide range of volatile organic compounds in whole air samples collected during PEM-Tropics A and B, Anal. Chem., 73, 3723–3731, doi: 10.1021/ac010027g, 2001.

Crounse, J. D., McKinney, K. A., Kwan, A. J., and Wennberg, P. O.: Measurement of gas-phase hydroperoxides by chemical ionization mass spectrometry, Anal. Chem., 78(19), 6726-6732, 2006.

Dalsøren, S. B., Myhre, G., Hodnebrog, Ø., Myhre, C. L., Stohl, A., Pisso, I., Schwietzke, S., Höglund-Isaksson, L., Helmig, D., Reimann, S., Sauvage, S., Schmidbauer, N., Read, K. A., Carpenter, L. J., Lewis, A. C., Punjabi, S. and Wallasch, M.: Discrepancy between simulated and observed ethane and propane levels explained by underestimated fossil emissions, Nature Geoscience, 11(3), 178–184, doi:10.1038/s41561-018-0073-0, 2018.

Dentener, F., Drevet, J., Lamarque, J. F., Bey, I., Eickhout, B., Fiore, A. M., Hauglustaine, D., Horowitz, L. W., Krol, M., Kulshrestha, U. C., Lawrence, M., Galy‐Lacaux, C., Rast, S., Shindell, D., Stevenson, D., Noije, T. V., Atherton, C., Bell, N., Bergman, D., Butler, T., Cofala, J., Collins, B., Doherty, R., Ellingsen, K., Galloway, J., Gauss, M., Montanaro, V., Müller, J. F., Pitari, G., Rodriguez, J., Sanderson, M., Solmon, F., Strahan, S., Schultz, M., Sudo, K., Szopa, S. and Wild, O.: Nitrogen and sulfur deposition on regional and global scales: A multimodel evaluation, Global Biogeochemical Cycles, 20(4), doi:10.1029/2005GB002672, 2006.

Di Carlo, P.: Missing OH Reactivity in a Forest: Evidence for Unknown Reactive Biogenic VOCs, Science, 304(5671), 722–725, doi:10.1126/science.1094392, 2004.

Diskin, G.S.; Podolske, J.R.; Sachse, G.W.; and Slate, T.A.: "Open-Path Airborne Tunable Diode Laser Hygrometer," in Diode Lasers and Applications in Atmospheric Sensing, SPIE Proceedings 4817, A. Fried, editor, 196-204 (2002).

Dolgorouky, C., Gros, V., Sarda-Esteve, R., Sinha, V., Williams, J., Marchand, N., Sauvage, S., Poulain, L., Sciare, J. and Bonsang, B.: Total OH reactivity measurements in Paris during the 2010 MEGAPOLI winter campaign, Atmos. Chem. Phys., 12(20), 9593–9612, doi:10.5194/acp-12-9593-2012, 2012.

Duncan, B. N., Logan, J. A., Bey, I., Megretskaia, I. A., Yantosca, R. M., Novelli, P. C., Jones, N. B. and Rinsland, C. P.: Global budget of CO, 1988–1997: Source estimates and validation with a global model, J. Geophys. Res., 112(D22), D22301, doi:10.1029/2007JD008459, 2007.

Edwards, P. M., Evans, M. J., Furneaux, K. L., Hopkins, J., Ingham, T., Jones, C., Lee, J. D., Lewis, A. C., Moller, S. J., Stone, D., Whalley, L. K. and Heard, D. E.: OH reactivity in a South East Asian tropical rainforest during the Oxidant and Particle Photochemical Processes (OP3) project, Atmos. Chem. Phys., 13(18), 9497–9514, doi:10.5194/acp-13-9497-2013, 2013.

Elkins, J. W., F. Moore and E.S. Kline, Next Generation Airborne Gas chromatograph for NASA Airborne Platforms, Earth Science Technology Conference 2001, August 28-30, 2001, College Park, MD, 2001.

Emmerson, K. M. and Evans, M. J.: Comparison of tropospheric gas-phase chemistry schemes for use within global models, Atmos. Chem. Phys., 9, 1831-1845, doi: 10.5194/acp-9-1831-2009, 2009.

Epstein, S. A., Blair, S. L. and Nizkorodov, S. A.: Direct Photolysis of α-Pinene Ozonolysis Secondary Organic Aerosol: Effect on Particle Mass and Peroxide Content, Env. Sci. Tech., 48(19), 11251–11258, doi:10.1021/es502350u, 2014.

Ferracci, V., Heimann, I., Abraham, N. L., Pyle, J. A. and Archibald, A. T.: Global modelling of the total OH reactivity: investigations on the "missing" OH sink and its atmospheric implications, Atmos. Chem. Phys., 18(10), 7109–7129, doi:10.5194/acp-18-7109-2018, 2018.

Fiore, A. M., Dentener, F. J., Wild, O., Cuvelier, C., Schultz, M. G., Hess, P., Textor, C., Schulz, M., Doherty, R. M., Horowitz, L. W., MacKenzie, I. A., Sanderson, M. G., Shindell, D. T., Stevenson, D. S., Szopa, S., Van Dingenen, R., Zeng, G., Atherton, C., Bergmann, D., Bey, I., Carmichael, G., Collins, W. J., Duncan, B. N., Faluvegi, G., Folberth, G., Gauss, M., Gong, S., Hauglustaine, D., Holloway, T., Isaksen, I. S. A., Jacob, D. J., Jonson, J. E., Kaminski, J. W., Keating, T. J., Lupu, A., Marmer, E., Montanaro, V., Park, R. J., Pitari, G., Pringle, K. J., Pyle, J. A., Schroeder, S., Vivanco, M. G., Wind, P., Wojcik, G., Wu, S. and Zuber, A.: Multimodel estimates of intercontinental source-receptor relationships for ozone pollution, J. Geophys. Res., 114(D4), D04301, doi:10.1029/2008JD010816, 2009.

Fischer, E. V., Jacob D. J., Millet D. B., Yantosca R. M. and Mao J.: The role of the ocean in the global atmospheric budget of acetone, Geophys. Res. Lett., 39(1), doi:10.1029/2011GL050086, 2012.

Fischer, E. V., Jacob, D. J., Yantosca, R. M., Sulprizio, M. P., Millet, D. B., Mao, J., Paulot, F., Singh, H. B., Roiger, A., Ries, L., Talbot, R. W., Dzepina, K. and Pandey Deolal, S.: Atmospheric peroxyacetyl nitrate (PAN): a global budget and source attribution, Atmos. Chem. Phys., 14(5), 2679–2698, doi:10.5194/acp-14-2679-2014, 2014.

Fisher, J. A., Jacob, D. J., Travis, K. R., Kim, P. S., Marais, E. A., Chan Miller, C., Yu, K., Zhu, L., Yantosca, R. M., Sulprizio, M. P., Mao, J., Wennberg, P. O., Crounse, J. D., Teng, A. P., Nguyen, T. B., St. Clair, J. M., Cohen, R. C., Romer, P., Nault, B. A., Wooldridge, P. J., Jimenez, J. L., Campuzano-Jost, P., Day, D. A., Hu, W., Shepson, P. B., Xiong, F., Blake, D. R., Goldstein, A. H., Misztal, P. K., Hanisco, T. F., Wolfe, G. M., Ryerson, T. B., Wisthaler, A. and Mikoviny, T.: Organic nitrate chemistry and its implications for nitrogen budgets in an isoprene- and monoterpene-rich atmosphere: constraints from aircraft (SEAC^{4}RS) and ground-based (SOAS) observations in the Southeast US, Atmos. Chem. Phys., 16(9), 5969–5991, doi:10.5194/acp-16-5969-2016, 2016.

Fisher, J. A., Atlas, E. L., Barletta, B., Meinardi, S., Blake, D. R., Thompson, C. R., Ryerson, T. B., Peischl, J., Tzompa-Sosa, Z. A. and Murray, L. T.: Methyl, ethyl, and propyl nitrates: global distribution and impacts on reactive nitrogen in remote marine environments, J. Geophys. Res., 123, 25, doi:10.1029/2018JD029046, 2018.

Gantt, B., Meskhidze, N., Zhang, Y. and Xu, J.: The effect of marine isoprene emissions on secondary organic aerosol and ozone formation in the coastal United States, Atmos. Env., 44(1), 115–121, doi:10.1016/j.atmosenv.2009.08.027, 2010.

Gelaro, R., McCarty, W., Suárez, M. J., Todling, R., Molod, A., Takacs, L., Randles, C. A., Darmenov, A., Bosilovich, M. G., Reichle, R., Wargan, K., Coy, L., Cullather, R., Draper, C., Akella, S., Buchard, V., Conaty, A., da Silva, A. M., Gu, W., Kim, G.-K., Koster, R., Lucchesi, R., Merkova, D., Nielsen, J. E., Partyka, G., Pawson, S., Putman, W., Rienecker, M., Schubert, S. D., Sienkiewicz, M. and Zhao, B.: The Modern-Era Retrospective Analysis for Research and Applications, Version 2 (MERRA-2), J. Climate, 30(14), 5419–5454, doi:10.1175/JCLI-D-16-0758.1, 2017.

Giglio, L., Randerson, J. T. and van der Werf, G. R.: Analysis of daily, monthly, and annual burned area using the fourth-generation global fire emissions database (GFED4): ANALYSIS OF BURNED AREA, J. Geophys. Res.: Biogeosciences, 118(1), 317–328, doi:10.1002/jgrg.20042, 2013.

Goldstein, A. H. and Galbally, I. E.: Known and unexplored organic constituents in the Earth's Atmosphere, Env. Sci. Tech., 41(5), 1514–1521, doi:10.1021/es072476p, 2007.

Granier, C., Lamarque, J. F., Mieville, A., Muller, J. F., Olivier, J., Orlando, J., Peters, J., Petron, G., Tyndall, G. and Wallens, S.: POET, a database of surface emissions of ozone precursors, Jussieu, France. [online] Available from: http://www.aero.jussieu.fr/projet/ ACCENT/POET.php, 2005.

Hall, S. R., Ullmann, K., Prather, M. J., Flynn, C. M., Murray, L. T., Fiore, A. M., Correa, G., Strode, S. A., Steenrod, S. D., Lamarque, J.-F., Guth, J., Josse, B., Flemming, J., Huijnen, V., Abraham, N. L. and Archibald, A. T.: Cloud impacts on photochemistry: building a climatology of photolysis rates from the Atmospheric Tomography mission, Atmos. Chem. Phys., 18(22), 16809–16828, doi:10.5194/acp-18-16809-2018, 2018.

Hansen, R. F., Griffith, S. M., Dusanter, S., Rickly, P. S., Stevens, P. S., Bertman, S. B., Carroll, M. A., Erickson, M. H.,

Flynn, J. H., Grossberg, N., Jobson, B. T., Lefer, B. L. and Wallace, H. W.: Measurements of total hydroxyl radical reactivity during CABINEX 2009 – Part 1: field measurements, Atmos. Chem. Phys., 14(6), 2923–2937, doi:10.5194/acp-14-2923-2014, 2014.

Heald, C. L., Coe, H., Jimenez, J. L., Weber, R. J., Bahreini, R., Middlebrook, A. M., Russell, L. M., Jolleys, M., Fu, T.-M., Allan, J. D., Bower, K. N., Capes, G., Crosier, J., Morgan, W. T., Robinson, N. H., Williams, P. I., Cubison, M. J., DeCarlo, P. F. and Dunlea, E. J.: Exploring the vertical profile of atmospheric organic aerosol: comparing 17 aircraft field campaigns with a global model, Atmos. Chem. Phys., 11(24), 12673–12696, doi:10.5194/acp-11-12673-2011, 2011.

Heald, C. L., Collett Jr., J. L., Lee, T., Benedict, K. B., Schwandner,0 F. M., Li, Y., Clarisse, L., Hurtmans, D. R., Van Damme, M., Clerbaux, C., Coheur, P.-F., Philip, S., Martin, R. V., and Pye, H. O. T.: Atmospheric ammonia and particulate inorganic nitrogen over the United States, Atmos. Chem. Phys., 12, 10295–10312, doi:/10.5194/acp-12-10295-2012, 2012.

Hintsa,E. J., F. L. Moore, D. F. Hurst, G. S. Dutton, B. D. Hall, J. D. Nance, L. Patrick, A. McClure-Begley, J. W. Elkins, E. G. Hall, A. F. Jordan, R.-S. Gao, A. W. Rollins, T. D. Thornberry, L. A. Watts, C. Thompson, J. Peischl, I. Bourgeois, T. Ryerson, B. C. Daube, J. V. Pittman, S. C. Wofsy, G. Diskin, T. P. Bui, S. Montzka, and B. Miller, UAS Chromatograph for Atmospheric Trace Species (UCATS) – a versatile instrument for trace gas measurements on different airborne platforms, Atmospheric Measurement Techniques (in preparation, soon to be re-submitted)

Hodzic, A., Madronich, S., Kasibhatla, P. S., Tyndall, G., Aumont, B., Jimenez, J. L., Lee-Taylor, J. and Orlando, J.: Organic photolysis reactions in tropospheric aerosols: effect on secondary organic aerosol formation and lifetime, Atmos. Chem. Phys., 15(16), 9253–9269, doi:10.5194/acp-15-9253-2015, 2015.

Hodzic, A., Kasibhatla, P. S., Jo, D. S., Cappa, C. D., Jimenez, J. L., Madronich, S. and Park, R. J.: Rethinking the global secondary organic aerosol (SOA) budget: stronger production, faster removal, shorter lifetime, Atmos. Chem. Phys., 16(12), 7917–7941, doi:10.5194/acp-16-7917-2016, 2016.

Hoesly, R. M., Smith, S. J., Feng, L., Klimont, Z., Janssens-Maenhout, G., Pitkanen, T., Seibert, J. J., Vu, L., Andres, R. J., Bolt, R. M., Bond, T. C., Dawidowski, L., Kholod, N., Kurokawa, J.-I., Li, M., Liu, L., Lu, Z., Moura, M. C. P., O'Rourke, P. R. and Zhang, Q.: Historical (1750–2014) anthropogenic emissions of reactive gases and aerosols from the Community Emissions Data System (CEDS), Geosci. Model Dev., 11(1), 369–408, doi:10.5194/gmd-11-369-2018, 2018.

Hofzumahaus, A., Lefer, B. L., Monks, P. S., Hall, S. R., Kylling, A., Mayer, B., Shetter, R. E., Junkermann, W., Bais, A., Calvert, J. G., Cantrell, C. A., Madronich, S., Edwards, G. D., and Kraus, A.: Photolysis frequency of O_3 to O(1D): Measurements and modeling during the International Photolysis Frequency Measurement and Modeling Intercomparison (IPMMI), J. Geophys. Res.-Atmos., 109, D08S90, doi:10.1029/2003JD004333, 2004.

Holmes, C. D., Bertram, T. H., Confer, K. L., Graham, K. A., Ronan, A. C., Wirks, C. K., & Shah, V.: The role of clouds in the tropospheric NO_x cycle: A new modeling approach for cloud chemistry and its global implications, Geophysical Research Letters, 46(9), 4980–4990, doi:10.1029/2019GL081990, 2019.

Hu, L., Jacob, D. J., Liu, X., Zhang, Y., Zhang, L., Kim, P. S., Sulprizio, M. P. and Yantosca, R. M.: Global budget of tropospheric ozone: Evaluating recent model advances with satellite (OMI), aircraft (IAGOS), and ozonesonde observations, Atmos. Env., 167, 323–334, doi:10.1016/j.atmosenv.2017.08.036, 2017.

Jacob, D.J.: Heterogeneous chemistry and tropospheric ozone, Atmos. Environ., 34, 2131-2159, 2000.

Jaeglé, L., Shah, V., Thornton, J. A., Lopez-Hilfiker, F. D., Lee, B. H., McDuffie, E. E., Fibiger, D., Brown, S. S., Veres, P., Sparks, T. L., Ebben, C. J., Wooldridge, P. J., Kenagy, H. S., Cohen, R. C., Weinheimer, A. J., Campos, T. L., Montzka, D. D., Digangi, J. P., Wolfe, G. M., Hanisco, T., Schroder, J. C., Campuzano-Jost, P., Day, D. A., Jimenez, J. L., Sullivan, A. P., Guo, H. and Weber, R. J.: Nitrogen Oxides Emissions, Chemistry, Deposition, and Export Over the Northeast United States During the WINTER Aircraft Campaign, J. Geophys. Res.: Atmospheres, 0(0), doi:10.1029/2018JD029133, 2018.

Jenkin, M. E., Young, J. C., and Rickard, A. R.: The MCM v3.3.1 degradation scheme for isoprene, Atmos. Chem. Phys., 15, 11433–11459, doi:10.5194/acp-15- 11433-2015, 2015.

Johnson, M. T.: A numerical scheme to calculate temperature and salinity dependent air-water transfer velocities for any gas, Ocean Sci., 6(4), 913–932, doi:10.5194/os-6-913-2010, 2010.

Kaiser, J., Skog, K. M., Baumann, K., Bertman, S. B., Brown, S. B., Brune, W. H., Crounse, J. D., de Gouw, J. A., Edgerton, E. S., Feiner, P. A., Goldstein, A. H., Koss, A., Misztal, P. K., Nguyen, T. B., Olson, K. F., St. Clair, J. M., Teng, A. P., Toma, S., Wennberg, P. O., Wild, R. J., Zhang, L. and Keutsch, F. N.: Speciation of OH reactivity above the

canopy of an isoprene-dominated forest, Atmos. Chem. Phys., 16(14), 9349–9359, doi:10.5194/acp-16-9349-2016, 2016.

Karion, A., Sweeney, C., Wolter, S., Newberger, T., Chen, H., Andrews, A., Kofler, J., Neff, D. and Tans, P.: Long-term greenhouse gas measurements from aircraft, Atmos. Meas. Tech. 5, 511-526, doi:10.5194/amt-6-511-2013, 2013.

Kasibhatla, P., Sherwen, T., Evans, M. J., Carpenter, L. J., Reed, C., Alexander, B., Chen, Q., Sulprizio, M. P., Lee, J. D., Read, K. A., Bloss, W., Crilley, L. R., Keene, W. C., Pszenny, A. A. P. and Hodzic, A.: Global impact of nitrate photolysis in sea-salt aerosol on NO_x, OH, and O_3 in the marine boundary layer, Atmos. Chem. Phys., 18(15), 11185–11203, doi:10.5194/acp-18-11185-2018, 2018.

Kim, M. J., Novak, G. A., Zoerb, M. C., Yang, M., Blomquist, B. W., Huebert, B. J., Cappa, C. D. and Bertram, T. H.: Air-Sea exchange of biogenic volatile organic compounds and the impact on aerosol particle size distributions, Geophys. Res. Lett., 44(8), 3887–3896, doi:10.1002/2017GL072975, 2017.

Kopacz, M., Jacob, D. J., Fisher, J. A., Logan, J. A., Zhang, L., Megretskaia, I. A., Yantosca, R. M., Singh, K., Henze, D. K., Burrows, J. P., Buchwitz, M., Khlystova, I., McMillan, W. W., Gille, J. C., Edwards, D. P., Eldering, A., Thouret, V. and Nedelec, P.: Global estimates of CO sources with high resolution by adjoint inversion of multiple satellite datasets (MOPITT, AIRS, SCIAMACHY, TES), Atmos. Chem. Phys., 22, 2010.

Koss, A. R., Sekimoto, K., Gilman, J. B., Selimovic, V., Coggon, M. M., Zarzana, K. J., Yuan, B., Lerner, B. M., Brown, S. S., Jimenez, J. L., Krechmer, J., Roberts, J. M., Warneke, C., Yokelson, R. J. and de Gouw, J.: Non-methane organic gas emissions from biomass burning: identification, quantification, and emission factors from PTR-ToF during the FIREX 2016 laboratory experiment, Atmos. Chem. Phys., 18(5), 3299–3319, doi:10.5194/acp-18-3299-2018, 2018.

Krotkov, N. A., McLinden, C. A., Li, C., Lamsal, L. N., Celarier, E. A., Marchenko, S. V., Swartz, W. H., Bucsela, E. J., Joiner, J., Duncan, B. N., Boersma, K. F., Veefkind, J. P., Levelt, P. F., Fioletov, V. E., Dickerson, R. R., He, H., Lu, Z. and Streets, D. G.: Aura OMI observations of regional SO_2 and NO_2 pollution changes from 2005 to 2015, Atmos. Chem. Phys., 16(7), 4605–4629, doi:10.5194/acp-16-4605-2016, 2016.

Kuhns, H., Green, M. and Etyemezian, V.: Big Bend Regional Aerosol and Visibility Observational (BRAVO) Study Emissions Inventory, Desert Research Institute, Las Vegas, NV., 2003.

Kwan, A. J., Crounse, J. D., Clarke, A. D., Shinozuka, Y., Anderson, B. E., Crawford, J. H., Avery, M. A., McNaughton, C. S., Brune, W. H., Singh, H. B. and Wennberg, P. O.: On the flux of oxygenated volatile organic compounds from organic aerosol oxidation, Geophys. Res. Lett, 33(15), doi:10.1029/2006GL026144, 2006.

Lamarque, J.-F., Emmons, L. K., Hess, P. G., Kinnison, D. E., Tilmes, S., Vitt, F., Heald, C. L., Holland, E. A., Lauritzen, P. H., Neu, J., Orlando, J. J., Rasch, P. J. and Tyndall, G. K.: CAM-chem: description and evaluation of interactive atmospheric chemistry in the Community Earth System Model, Geosci. Mod. Dev., 5(2), 369–411, doi:10.5194/gmd-5-369-2012, 2012.

Lee, J. D., Young, J. C., Read, K. A., Hamilton, J. F., Hopkins, J. R., Lewis, A. C., Bandy, B. J., Davey, J., Edwards, P., Ingham, T., Self, D. E., Smith, S. C., Pilling, M. J. and Heard, D. E.: Measurement and calculation of OH reactivity at a United Kingdom coastal site, Journal of Atmospheric Chemistry, 64(1), 53–76, doi:10.1007/s10874-010-9171-0, 2009.

Lelieveld, J., Gromov, S., Pozzer, A. and Taraborrelli, D.: Global tropospheric hydroxyl distribution, budget and reactivity, Atmos. Chem. Phys., 16, 12477–12493, doi:10.5194/acp-16-12477-2016, 2016.

Li, M., Zhang, Q., Kurokawa, J., Woo, J.-H., He, K., Lu, Z., Ohara, T., Song, Y., Streets, D. G., Carmichael, G. R., Cheng, Y., Hong, C., Huo, H., Jiang, X., Kang, S., Liu, F., Su, H. and Zheng, B.: MIX: a mosaic Asian anthropogenic emission inventory under the international collaboration framework of the MICS-Asia and HTAP, Atmos. Chem. Phys., 17(2), 935–963, doi:10.5194/acp-17-935-2017, 2017.

Li, S. M., Leithead, A., Moussa, S. G., Liggio, J., Moran, M. D., Wang, D., Hayden, K., Darlington, A., Gordon, M., Staebler, R., Makar, P. A., Stroud, C. A., McLaren, R., Liu, P. S. K., O'Brien, J., Mittermeier, R. L., Zhang, J., Marson, G., Cober, S. G.,Wolde, M., andWentzell, J. J. B.: Differences between measured and reported volatile organic compound emissions from oil sands facilities in Alberta, Canada, P. Natl. Acad. Sci. USA, 114, E3756–E3765, doi:10.1073/pnas.1617862114, 2017.

Lou, S., Holland, F., Rohrer, F., Lu, K., Bohn, B., Brauers, T., Chang, C. C., Fuchs, H., Haseler, R., Kita, K., Kondo, Y., Li, X., Shao, M., Zeng, L., Wahner, A., Zhang, Y., Wang, W. and Hofzumahaus, A.: Atmospheric OH reactivities in the Pearl River Delta – China in summer 2006: measurement and model results, Atmos. Chem. Phys., 18, 2010.

Luo, G., Yu, F. and Schwab, J.: Revised treatment of wet scavenging processes dramatically improves GEOS-Chem 12.0.0 simulations of surface nitric acid, nitrate, and ammonium over the United States, Geosci. Model Dev., 12, 3439–3447, doi: 10.5194/gmd-12-3439-2019, 2019.

Mao, J., Ren, X., Brune, W. H., Olson, J. R., Crawford, J. H., Fried, A., Huey, L. G., Cohen, R. C., Heikes, B., Singh, H. B., Blake, D. R., Sachse, G. W., Diskin, G. S., Hall, S. R. and Shetter, R. E.: Airborne measurement of OH reactivity during INTEX-B, Atmos. Chem. Phys., 9(1), 163–173, doi:10.5194/acp-9-163-2009, 2009.

Mao, J., Ren, X., Chen, S., Brune, W. H., Chen, Z., Martinez, M., Harder, H., Lefer, B., Rappenglück, B., Flynn, J. and Leuchner, M.: Atmospheric oxidation capacity in the summer of Houston 2006: Comparison with summer measurements in other metropolitan studies, Atmos. Env., 44(33), 4107–4115, doi:10.1016/j.atmosenv.2009.01.013, 2010.

Mao, J., Ren, X., Zhang, L., Van Duin, D. M., Cohen, R. C., Park, J.-H., Goldstein, A. H., Paulot, F., Beaver, M. R., Crounse, J. D., Wennberg, P. O., DiGangi, J. P., Henry, S. B., Keutsch, F. N., Park, C., Schade, G. W., Wolfe, G. M., Thornton, J. A. and Brune, W. H.: Insights into hydroxyl measurements and atmospheric oxidation in a California forest, Atmos. Chem. Phys., 12(17), 8009–8020, doi:10.5194/acp-12-8009-2012, 2012.

Mao, J., Fan, S., Jacob, D. J., and Travis, K. R.: Radical loss in the atmosphere from Cu-Fe redox coupling in aerosols, Atmos. Chem. Phys., 13, 509-519, doi:10.5194/acp-13-509-2013, 2013.

Marais, E. A. and Wiedinmyer, C.: Air Quality Impact of Diffuse and Inefficient Combustion Emissions in Africa (DICE-Africa), Environ. Sci. Technol., 50(19), 10739–10745, doi:10.1021/acs.est.6b02602, 2016.

Marais, E. A., Jacob, D. J., Jimenez, J. L., Campuzano-Jost, P., Day, D. A., Hu, W., Krechmer, J., Zhu, L., Kim, P. S., Miller, C. C., Fisher, J. A., Travis, K., Yu, K., Hanisco, T. F., Wolfe, G. M., Arkinson, H. L., Pye, H. O. T., Froyd, K. D., Liao, J. and McNeill, V. F.: Aqueous-phase mechanism for secondary organic aerosol formation from isoprene: application to the southeast United States and co-benefit of SO_2 emission controls, Atmos. Chem. Phys., 16(3), 1603–1618, doi:10.5194/acp-16-1603-2016, 2016.

Marais, E. A., Jacob, D. J., Choi, S., Joiner, J., Belmonte-Rivas, M., Cohen, R. C., Beirle, S., Murray, L. T., Schiferl, L., Shah, V. and Jaeglé, L.: Nitrogen oxides in the global upper troposphere: interpreting cloud-sliced NO_2 observations from the OMI satellite instrument, Atmos. Chem. Phys. Discussions, 1–14, doi:10.5194/acp-2018-556, 2018.

Marvin, M. R., Wolfe, G. M., Salawitch, R. J., Canty, T. P., Roberts, S. J., Travis, K. R., Aikin, K. C., de Gouw, J. A., Graus, M., Hanisco, T. F., Holloway, J. S., Hübler, G., Kaiser, J., Keutsch, F. N., Peischl, J., Pollack, I. B., Roberts, J. M., Ryerson, T. B., Veres, P. R. and Warneke, C.: Impact of evolving isoprene mechanisms on simulated formaldehyde: An inter-comparison supported by in situ observations from SENEX, Atmos. Env., 164, 325–336, doi:10.1016/j.atmosenv.2017.05.049, 2017.

McDonald, B. C., Gouw, J. A. de, Gilman, J. B., Jathar, S. H., Akherati, A., Cappa, C. D., Jimenez, J. L., Lee-Taylor, J., Hayes, P. L., McKeen, S. A., Cui, Y. Y., Kim, S.-W., Gentner, D. R., Isaacman-VanWertz, G., Goldstein, A. H., Harley, R. A., Frost, G. J., Roberts, J. M., Ryerson, T. B. and Trainer, M.: Volatile chemical products emerging as largest petrochemical source of urban organic emissions, Science, 359(6377), 760–764, doi:10.1126/science.aaq0524, 2018.

Millet, D. B., Jacob, D. J., Custer, T. G., de Gouw, J. A., Goldstein, A. H., Karl, T., Singh, H. B., Sive, B. C., Talbot, R. W., Warneke, C. and Williams, J.: New constraints on terrestrial and oceanic sources of atmospheric methanol, Atmos. Chem. Phys., 8(23), 6887–6905, doi:10.5194/acp-8-6887-2008, 2008.

Millet, D. B., Guenther, A., Siegel, D. A., Nelson, N. B., Singh, H. B., de Gouw, J. A., Warneke, C., Williams, J., Eerdekens, G., Sinha, V., Karl, T., Flocke, F., Apel, E., Riemer, D. D., Palmer, P. I. and Barkley, M.: Global atmospheric budget of acetaldehyde: 3-D model analysis and constraints from in-situ and satellite observations, Atmos. Chem. Phys., 10(7), 3405–3425, doi:10.5194/acp-10-3405-2010, 2010.

Mogensen, D., Smolander, S., Sogachev, A., Zhou, L., Sinha, V., Guenther, A., Williams, J., Nieminen, T., Kajos, M. K., Rinne, J., Kulmala, M. and Boy, M.: Modelling atmospheric OH-reactivity in a boreal forest ecosystem, Atmos. Chem. Phys., 11(18), 9709–9719, doi:10.5194/acp-11-9709-2011, 2011.

Monks, P. S.: Gas-phase radical chemistry in the troposphere, Chemical Society Reviews, 34(5), 376, doi:10.1039/b307982c, 2005.

Montzka, S. A., Spivakovsky, C. M., Butler, J. H., Elkins, J. W., Lock, L. T., and Mondeel, D. J.: New observational constraints for atmospheric hydroxyl on global and hemispheric scales, Science, 288(5465), doi:10.1126/science.288.5465.500, 2000.

Mu, M., Randerson, J. T., van der Werf, G. R., Giglio, L., Kasibhatla, P., Morton, D., Collatz, G. J., DeFries, R. S., Hyer, E. J., Prins, E. M., Griffith, D. W. T., Wunch, D., Toon, G. C., Sherlock, V. and Wennberg, P. O.: Daily and 3-hourly variability in global fire emissions and consequences for atmospheric model predictions of carbon monoxide, J. Geophys. Res.: Atmospheres, 116(D24), doi:10.1029/2011JD016245, 2011.

Müller, J.-F., Liu, Z., Nguyen, V. S., Stavrakou, T., Harvey, J. N. and Peeters, J.: The reaction of methyl peroxy and hydroxyl radicals as a major source of atmospheric methanol, Nature Communications, 7, 13213, doi:10.1038/ncomms13213, 2016.

Müller, J.-F., Stavrakou, T., Bauwens, M., George, M., Hurtmans, D., Coheur, P.-F., Clerbaux, C. and Sweeney, C.: Top-Down CO Emissions Based On IASI Observations and Hemispheric Constraints on OH Levels, Geophys. Res. Lett., 45(3), 2017GL076697, doi:10.1002/2017GL076697, 2018.

Mungall, E. L., Abbatt, J. P. D., Wentzell, J. J. B., Lee, A. K. Y., Thomas, J. L., Blais, M., Gosselin, M., Miller, L. A., Papakyriakou, T., Willis, M. D. and Liggio, J.: Microlayer source of oxygenated volatile organic compounds in the summertime marine Arctic boundary layer, PNAS, 114(24), 6203–6208, doi:10.1073/pnas.1620571114, 2017.

Murray, L. T., Jacob, D. J., Logan, J. A., Hudman, R. C. and Koshak, W. J.: Optimized regional and interannual variability of lightning in a global chemical transport model constrained by LIS/OTD satellite data, J. Geophys. Res.: Atmospheres, 117(D20), doi:10.1029/2012JD017934, 2012.

Murray, L. T., Mickley, L. J., Kaplan, J. O., Sofen, E. D., Pfeiffer, M. and Alexander, B.: Factors controlling variability in the oxidative capacity of the troposphere since the Last Glacial Maximum, Atmos. Chem. Phys., 14(7), 3589–3622, doi:10.5194/acp-14-3589-2014, 2014.

Naik, V., Voulgarakis, A., Fiore, A. M., Horowitz, L. W., Lamarque, J.-F., Lin, M., Prather, M. J., Young, P. J., Bergmann, D., Cameron-Smith, P. J., Cionni, I., Collins, W. J., Dalsøren, S. B., Doherty, R., Eyring, V., Faluvegi, G., Folberth, G. A., Josse, B., Lee, Y. H., MacKenzie, I. A., Nagashima, T., van Noije, T. P. C., Plummer, D. A., Righi, M., Rumbold, S. T., Skeie, R., Shindell, D. T., Stevenson, D. S., Strode, S., Sudo, K., Szopa, S. and Zeng, G.: Preindustrial to present-day changes in tropospheric hydroxl radical and methane lifetime from the Atmospheric Chemistry and Climate Model Intercomparison Project (ACCMIP), Atmos. Chem. Phys., 13, 5277–5298, doi:10.5194/acp-13-5277-2013, 2013.

Nakashima, Y., Kato, S., Greenberg, J., Harley, P., Karl, T., Turnipseed, A., Apel, E., Guenther, A., Smith, J. and Kajii, Y.: Total OH reactivity measurements in ambient air in a southern Rocky mountain ponderosa pine forest during BEACHON-SRM08 summer campaign, Atmos. Env., 85, 1–8, doi:10.1016/j.atmosenv.2013.11.042, 2014.

Nicely, J. M., Anderson, D. C., Canty, T. P., Salawitch, R. J., Wolfe, G. M., Apel, E. C., Arnold, S. R., Atlas, E. L., Blake, N. J., Bresch, J. F., Campos, T. L., Dickerson, R. R., Duncan, B., Emmons, L. K., Evans, M. J., Fernandez, R. P., Flemming, J., Hall, S. R., Hanisco, T. F., Honomichl, S. B., Hornbrook, R. S., Huijnen, V., Kaser, L., Kinnison, D. E., Lamarque, J.-F., Mao, J., Monks, S. A., Montzka, D. D., Pan, L. L., Riemer, D. D., Saiz-Lopez, A., Steenrod, S. D., Stell, M. H., Tilmes, S., Turquety, S., Ullmann, K. and Weinheimer, A. J.: An observationally constrained evaluation of the oxidative capacity in the tropical western Pacific troposphere: Observationally Constrained OH in TWP, J. Geophys. Res. Atmos., 121(12), 7461–7488, doi:10.1002/2016JD025067, 2016.

Nicely, J. M., Salawitch, R. J., Canty, T., Anderson, D. C., Arnold, S. R., Chipperfield, M. P., Emmons, L. K., Flemming, J., Huijnen, V., Kinnison, D. E., Lamarque, J.-F., Mao, J., Monks, S. A., Steenrod, S. D., Tilmes, S. and Turquety, S.: Quantifying the causes of differences in tropospheric OH within global models, J. Geophys. Res.: Atmospheres, 122(3), 1983–2007, doi:10.1002/2016JD026239, 2017.

Nölscher, A. C., Williams, J., Sinha, V., Custer, T., Song, W., Johnson, A. M., Axinte, R., Bozem, H., Fischer, H., Pouvesle, N., Phillips, G., Crowley, J. N., Rantala, P., Rinne, J., Kulmala, M., Gonzales, D., Valverde-Canossa, J., Vogel, A., Hoffmann, T., Ouwersloot, H. G., Vilà-Guerau de Arellano, J. and Lelieveld, J.: Summertime total OH reactivity measurements from boreal forest during HUMPPA-COPEC 2010, Atmos. Chem. Phys., 12(17), 8257–8270, doi:10.5194/acp-12-8257-2012, 2012.

Nölscher, A. C., Yañez-Serrano, A. M., Wolff, S., de Araujo, A. C., Lavrič, J. V., Kesselmeier, J. and Williams, J.: Unexpected seasonality in quantity and composition of Amazon rainforest air reactivity, Nature Communications, 7(1), doi:10.1038/ncomms10383, 2016.

Olivier, J., Peters, J., Granier, C., Petron, G., Muller, J. F. and Wallens, S.: Present and future surface emissions of atmospheric compounds, Eur. Union, Brussels., 2003.

Pai, S. J., Heald, C. L., Pierce, J. R., Farina, S. C., Marais, E. A., Jimenez, J. L., Campuzano-Jost, P., Nault, B. A., Middlebrook, A. M., Coe, H., Shilling, J. E., Bahreini, R., Dingle, J. H. and Vu, K.: An evaluation of global organic aerosol schemes using airborne observations, Atmos. Chem. Phys. ~~Discussions~~, 20, 2637-2665, ~~1–39,~~ doi:10.5194/acp-20-2637~~19-331~~-2020, ~~2019~~2020.

Patra, P. K., Krol, M. C., Montzka, S. A., Arnold, T., Atlas, E. L., Lintner, B. R., Stephens, B. B., Xiang, B., Elkins, J. W., Fraser, P. J., Ghosh, A., Hintsa, E. J., Hurst, D. F., Ishijima, K., Krummel, P. B., Miller, B. R., Miyazaki, K., Moore, F. L., Mühle, J., O'Doherty, S., Prinn, R. G., Steele, L. P., Takigawa, M., Wang, H. J., Weiss, R. F., Wofsy, S. C. and Young, D.: Observational evidence for interhemispheric hydroxyl-radical parity, Nature, 513(7517), 219–223, doi:10.1038/nature13721, 2014.

Petropavlovskikh, I., Shetter, R., Hall, S., Ullmann, K., and Bhartia, P. K.: Algorithm for the charge-coupled-device scanning actinic flux spectroradiometer ozone retrieval in support of the Aura satellite validation, J. Appl. Remote Sens., 1, 013540, doi:10.1117/1.2802563, 2007.

Philip, S., Martin, R. V., and Keller, C. A.: Sensitivity of a chemistry-transport model simulations to the duration of chemical operators: a case study with GEOS-Chem v10-01, Geosci. Mod. Dev., 9, 1683-1695, doi: 10.5194/gmd-9-1683-2016, 2016.

Plass‐Dülmer C., Khedim A., Koppmann R., Johnen F. J., Rudolph J. and Kuosa H.: Emissions of light nonmethane hydrocarbons from the Atlantic into the atmosphere, Global Biogeochemical Cycles, 7(1), 211–228, doi:10.1029/92GB02361, 1993.

Podolske, J. R., G. W. Sachse, G. S. Diskin, Calibration and data retrieval algorithms for the NASA Langley/Ames Diode Laser Hygrometer for the NASA Transport and Chemical Evolution Over the Pacific (TRACE-P) mission, J. Geophys. Res., 108 (D20), 8792, doi:10.1029/2002JD003156, 2003

Praske, E., Otkjær, R. V., Crounse, J. D., Hethcox, J. C., Stoltz, B. M., Kjaergaard, H. G., and Wennberg, P. O.: Atmospheric autoxidation is increasingly important in urban and suburban North America, P. Natl. Acad. Sci. USA, 115, 64–69, doi:10.1073/pnas.1715540115, 2017.

Prather, M. J., Holmes, C. D. and Hsu, J.: Reactive greenhouse gas scenarios: Systematic exploration of uncertainties and the role of atmospheric chemistry, Geophys. Res. Lett., 39, *L09803*, doi:10.1029/2012GL051440, 2012.

Pye, H. O. T., Liao, H., Wu, S., Mickley, L. J., Jacob, D. J., Henze, D. K., and Seinfeld, J. H.: Effect of changes in climate and emissions on future sulfate-nitrate-ammonium aerosol levels in the United States, J. Geophys. Res., 114(D01205), doi: 10.1029/2008JD010701, 2009.

Ramasamy, S., Ida, A., Jones, C., Kato, S., Tsurumaru, H., Kishimoto, I., Kawasaki, S., Sadanaga, Y., Nakashima, Y., Nakayama, T., Matsumi, Y., Mochida, M., Kagami, S., Deng, Y., Ogawa, S., Kawana, K. and Kajii, Y.: Total OH reactivity measurement in a BVOC dominated temperate forest during a summer campaign, 2014, Atmos. Env., 131, 41–54, doi:10.1016/j.atmosenv.2016.01.039, 2016.

Randerson, J. T., Chen, Y., van der Werf, G. R., Rogers, B. M. and Morton, D. C.: Global burned area and biomass burning emissions from small fires, J. Geophys. Res.: Biogeosciences, 117(G4), doi:10.1029/2012JG002128, 2012.

Read, K. A., Carpenter, L. J., Arnold, S. R., Beale, R., Nightingale, P. D., Hopkins, J. R., Lewis, A. C., Lee, J. D., Mendes, L. and Pickering, S. J.: Multiannual Observations of Acetone, Methanol, and Acetaldehyde in Remote Tropical Atlantic Air: Implications for Atmospheric OVOC Budgets and Oxidative Capacity, Environ. Sci. Technol., 46(20), 11028–11039, doi:10.1021/es302082p, 2012.

Ren, X., Brune, W. H., Oliger, A., Metcalf, A. R., Simpas, J. B., Shirley, T., Schwab, J. J., Bai, C., Roychowdhury, U., Li, Y., Cai, C., Demerjian, K. L., He, Y., Zhou, X., Gao, H. and Hou, J.: OH, HO_2, and OH reactivity during the PMTACS–NY Whiteface Mountain 2002 campaign: Observations and model comparison, J. Geophys. Res.: Atmos., 111(D10), doi:10.1029/2005JD006126, 2006.

Romer, P. S., Wooldridge, P. J., Crounse, J. D., Kim, M. J., Wennberg, P. O., Dibb, J. E., Scheuer, E., Blake, D. R., Meinardi, S., Brosius, A. L., Thames, A. B., Miller, D. O., Brune, W. H., Hall, S. R., Ryerson, T. B. and Cohen, R. C.: Constraints on aerosol nitrate photolysis as a potential source of HONO and NO_x. Environ. Sci. Technol., 52, 13738–13746, doi:10.1021/acs.est.8b03861, 2018.

Safieddine, S. A., Heald, C. L. and Henderson, B. H.: The global nonmethane reactive organic carbon budget: A modeling perspective, Geophys. Res. Lett., 44(8), 3897–3906, doi:10.1002/2017GL072602, 2017.

Santoni, G. W.; Daube, B. C.; Kort, E. A.; Jimenez, R.; Park, S.; Pittman, J. V.; Gottlieb, E.; Xiang, B.; Zahniser, M. S.;

Nelson, D. D.; et al. Evaluation of the Airborne Quantum Cascade Laser Spectrometer (QCLS) Measurements of the Carbon and Greenhouse Gas Suite - CO_2, CH_4, N_2O, and CO - during the CalNex and HIPPO Campaigns. Atmospheric Measurement Techniques 2014, 7 (6), 1509–1526.

Sherwen, T., Schmidt, J. A., Evans, M. J., Carpenter, L. J., Großmann, K., Eastham, S. D., Jacob, D. J., Dix, B., Koenig, T. K., Sinreich, R., Ortega, I., Volkamer, R., Saiz-Lopez, A., Prados-Roman, C., Mahajan, A. S. and Ordóñez, C.: Global impacts of tropospheric halogens (Cl, Br, I) on oxidants and composition in GEOS-Chem, Atmos. Chem. Phys., 16(18), 12239–12271, doi:10.5194/acp-16-12239-2016, 2016.

Shetter, R. E. and Muller, M.: Photolysis frequency measurements using actinic flux spectroradiometry during PEM-Tropics Mission: Instrumentation description and some results, J. Geophys. Res.-Atmos., 104, 5647–5661, doi:10.1029/98JD01381, 1999.

Shindell, D. T., Faluvegi, G., Stevenson, D. S., Krol, M. C., Emmons, L. K., Lamarque, J.-F., Pétron, G., Dentener, F. J., Ellingsen, K., Schultz, M. G., Wild, O., Amann, M., Atherton, C. S., Bergmann, D. J., Bey, I., Butler, T., Cofala, J., Collins, W. J., Derwent, R. G., Doherty, R. M., Drevet, J., Eskes, H. J., Fiore, A. M., Gauss, M., Hauglustaine, D. A., Horowitz, L. W., Isaksen, I. S. A., Lawrence, M. G., Montanaro, V., Müller, J.-F., Pitari, G., Prather, M. J., Pyle, J. A., Rast, S., Rodriguez, J. M., Sanderson, M. G., Savage, N. H., Strahan, S. E., Sudo, K., Szopa, S., Unger, N., van Noije, T. P. C. and Zeng, G.: Multimodel simulations of carbon monoxide: Comparison with observations and projected near-future changes, J. Geophys. Res., 111(D19), D19306, doi:10.1029/2006JD007100, 2006.

Simpson, I. J., Blake, N. J., Barletta, B., Diskin, G. S., Fuelberg, H. E., Gorham, K., Huey, L. G., Meinardi, S., Rowland, F. S., Vay, S. A., Weinheimer, A. J., Yang, M., and Blake, D. R.: Characterization of trace gases measured over Alberta oil sands mining operations: 76 speciated C_2–C_{10} volatile organic compounds (VOCs), CO_2, CH_4, CO, NO, NO_2, NO_y, O_3 and SO_2, Atmos. Chem. Phys., 10, 11931-11954, doi:10.5194/acp-10-11931-2010, 2010.

Singh, H., Chen, Y., Staudt, A., Jacob, D., Blake, D., Heikes, B. and Snow, J.: Evidence from the Pacific troposphere for large global sources of oxygenated organic compounds, Nature, 410(6832), 1078, doi:10.1038/35074067, 2001.

Singh H. B., Tabazadeh A., Evans M. J., Field B. D., Jacob D. J., Sachse G., Crawford J. H., Shetter R. and Brune W. H.: Oxygenated volatile organic chemicals in the oceans: Inferences and implications based on atmospheric observations and air ‐ sea exchange models, Geophys. Res. Lett., 30(16), doi:10.1029/2003GL017933, 2003.

Sinha, V., Williams, J., Crowley, J. N. and Lelieveld, J.: The Comparative Reactivity Method – a new tool to measure total OH Reactivity in ambient air, Atmos. Chem. Phys., 15, 2008.

Sinha, V., Williams, J., Lelieveld, J., Ruuskanen, T. M., Kajos, M. K., Patokoski, J., Hellen, H., Hakola, H., Mogensen, D., Boy, M., Rinne, J. and Kulmala, M.: OH Reactivity Measurements within a Boreal Forest: Evidence for Unknown Reactive Emissions, Environ. Sci. Technol., 44(17), 6614–6620, doi:10.1021/es101780b, 2010.

Staudt, A. C., Jacob, D. J., Ravetta, F., Logan, J. A., Bachiochi, D., Krishnamurti, T. N., Sandholm, S., Ridley, B. and Singh, H. B.: Sources and chemistry of nitrogen oxides over the tropical Pacific, J. Geophys. Res., 108(D2), doi:10.1029/2002JD002139, 2003.

Stockwell, C. E., Veres, P. R., Williams, J. and Yokelson, R. J.: Characterization of biomass burning emissions from cooking fires, peat, crop residue, and other fuels with high-resolution proton-transfer-reaction time-of-flight mass spectrometry, Atmos. Chem. Phys., 15(2), 845–865, doi:10.5194/acp-15-845-2015, 2015.

Strode, S. A., Duncan, B. N., Yegorova, E. A., Kouatchou, J., Ziemke, J. R. and Douglass, A. R.: Implications of carbon monoxide bias for methane lifetime and atmospheric composition in chemistry climate models, Atmos. Chem. Phys., 15(20), 11789–11805, doi:10.5194/acp-15-11789-2015, 2015.

Tan, D., Faloona, I., Simpas, J. B., Brune, W., Olson, J., Crawford, J., Avery, M., Sachse, G., Vay, S., Sandholm, S., Guan, H.-W., Vaughn, T., Mastromarino, J., Heikes, B., Snow, J., Podolske, J. and Singh, H.: OH and HO_2 in the tropical Pacific: Results from PEM-Tropics B, J. Geophys. Res.: Atmospheres, 106(D23), 32667–32681, doi:10.1029/2001JD900002, 2001.

Thames, A. B., Brune, W. H., Miller, D. O., Allen, H. M., Apel, E. C., Blake, D. R., Bui, T. P., Commane, R., Crounse, J. D., Daube, B. C., Diskin, G. S., DiGangi, J. P., Elkins, J. W., Hall, S. R., Hanisco, T. F., Hannun, R. A., Hintsa, E., Hornbrook, R. S., Kim, M. J., McKain, K., Moore, F. L., Nicely, J. M., Peischl, J., Ryerson, T. B., St. Clair, J. M., Sweeney, C., Teng, A., Thompson, C. R., Ullmann, K., Wennberg, P. O., and Wolfe, G. M.: Missing OH Reactivity in the global marine boundary layer, Atmos. Chem. Phys., doi:10.5194/acp-20-4-13-2020, 2020.

Travis, K. R., Jacob, D. J., Fisher, J. A., Kim, P. S., Marais, E. A., Zhu, L., Yu, K., Miller, C. C., Yantosca, R. M., Sulprizio,

M. P., Thompson, A. M., Wennberg, P. O., Crounse, J. D., St. Clair, J. M., Cohen, R. C., Laughner, J. L., Dibb, J. E., Hall, S. R., Ullmann, K., Wolfe, G. M., Pollack, I. B., Peischl, J., Neuman, J. A. and Zhou, X.: Why do models overestimate surface ozone in the Southeast United States?, Atmos. Chem. Phys., 16(21), 13561–13577, doi:10.5194/acp-16-13561-2016, 2016.

Tzompa - Sosa Z. A., Mahieu E., Franco B., Keller C. A., Turner A. J., Helmig D., Fried A., Richter D., Weibring P., Walega J., Yacovitch T. I., Herndon S. C., Blake D. R., Hase F., Hannigan J. W., Conway S., Strong K., Schneider M. and Fischer E. V.: Revisiting global fossil fuel and biofuel emissions of ethane, J. Geophys. Res.: Atmospheres, 122(4), 2493–2512, doi:10.1002/2016JD025767, 2017.

van der Werf, G. R., Randerson, J. T., Giglio, L., van Leeuwen, T. T., Chen, Y., Rogers, B. M., Mu, M., Marle, M. J. E. van, Morton, D. C., Collatz, G. J., Yokelson, R. J. and Kasibhatla, P. S.: Global fire emissions estimates during 1997–2016, Earth System Science Data; Katlenburg-Lindau, 9(2), 697–720, doi:10.5194/essd-9-697-2017, 2017.

Wang, S., Hornbrook, R. S., Hills, A., Emmons, L. K., Tilmes, S., Lamarque, J.-F., Jimenez, J. L., Campuzano - Jost, P., Nault, B. A., Crounse, J. D., Wennberg, P. O., Kim, M., Allen, H., Ryerson, T. B., Thompson, C. R., Peischl, J., Moore, F., Nance, D., Hall, B., Elkins, J., Tanner, D., Huey, L. G., Hall, S. R., Ullmann, K., Orlando, J. J., Tyndall, G. S., Flocke, F. M., Ray, E., Hanisco, T. F., Wolfe, G. M., Clair, J. S., Commane, R., Daube, B., Barletta, B., Blake, D. R., Weinzierl, B., Dollner, M., Conley, A., Vitt, F., Wofsy, S. C., Riemer, D. D. and Apel, E. C.: Atmospheric Acetaldehyde: Importance of Air-Sea Exchange and a Missing Source in the Remote Troposphere, Geophys. Res. Lett., 0(0), doi:10.1029/2019GL082034, 2019.

Wang, X., Jacob, D. J., Eastham, S. D., Sulprizio, M. P., Zhu, L., Chen, Q., Alexander, B., Sherwen, T., Evans, M. J., Lee, B. H., Haskins, J. D., Lopez-Hilfiker, F. D., Thornton, J. A., Huey, G. L. and Liao, H.: The role of chlorine in tropospheric chemistry, Atmos. Chem. Phys., 19, 3981-4003, doi:10.5194/acp-19-3981-2019, 2019.

Whalley, L. K., Stone, D., Bandy, B., Dunmore, R., Hamilton, J. F., Hopkins, J., Lee, J. D., Lewis, A. C. and Heard, D. E.: Atmospheric OH reactivity in central London: observations, model predictions and estimates of in situ ozone production, Atmos. Chem. Phys., 16(4), 2109–2122, doi:10.5194/acp-16-2109-2016, 2016.

Wofsy, S.C., S. Afshar, H.M. Allen, E. Apel, E.C. Asher, B. Barletta, J. Bent, H. Bian, B.C. Biggs, D.R. Blake, N. Blake, I. Bourgeois, C.A. Brock, W.H. Brune, J.W. Budney, T.P. Bui, A. Butler, P. Campuzano-Jost, C.S. Chang, M. Chin, R. Commane, G. Correa, J.D. Crounse, P. D. Cullis, B.C. Daube, D.A. Day, J.M. Dean-Day, J.E. Dibb, J.P. DiGangi, G.S. Diskin, M. Dollner, J.W. Elkins, F. Erdesz, A.M. Fiore, C.M. Flynn, K. Froyd, D.W. Gesler, S.R. Hall, T.F. Hanisco, R.A. Hannun, A.J. Hills, E.J. Hintsa, A. Hoffman, R.S. Hornbrook, L.G. Huey, S. Hughes, J.L. Jimenez, B.J. Johnson, J.M. Katich, R.F. Keeling, M.J. Kim, A. Kupc, L.R. Lait, J.-F. Lamarque, J. Liu, K. McKain, R.J. Mclaughlin, S. Meinardi, D.O. Miller, S.A. Montzka, F.L. Moore, E.J. Morgan, D.M. Murphy, L.T. Murray, B.A. Nault, J.A. Neuman, P.A. Newman, J.M. Nicely, X. Pan, W. Paplawsky, J. Peischl, M.J. Prather, D.J. Price, E. Ray, J.M. Reeves, M. Richardson, A.W. Rollins, K.H. Rosenlof, T.B. Ryerson, E. Scheuer, G.P. Schill, J.C. Schroder, J.P. Schwarz, J.M. St.Clair, S.D. Steenrod, B.B. Stephens, S.A. Strode, C. Sweeney, D. Tanner, A.P. Teng, A.B. Thames, C.R. Thompson, K. Ullmann, P.R. Veres, N. Vieznor, N.L. Wagner, A. Watt, R. Weber, B. Weinzierl, P. Wennberg, C.J. Williamson, J.C. Wilson, G.M. Wolfe, C.T. Woods, and L.H. Zeng. 2018. ATom: Merged Atmospheric Chemistry, Trace Gases, and Aerosols. ORNL DAAC, Oak Ridge, Tennessee, USA. doi:10.3334/ORNLDAAC/1581.

Wofsy, S. C.: HIAPER Pole-to-Pole Observations (HIPPO): fine-grained, global-scale measurements of climatically important atmospheric gases and aerosols, Philos. T. Roy. Soc. A, 369, 2073–2086, doi:10.1098/rsta.2010.0313, 2011.

Wolfe, G. M., Nicely, J. M., St. Clair, J. M., Hanisco, T. F., Liao, J., Oman, L. D., Brune, W. B., Miller, D., Thames, A., González Abad, G., Ryerson, T. B., Thompson, C. R., Peischl, J., McCain, K., Sweeney, C., Wennberg, P. O., Kim, M., Crounse, J. D., Hall, S. R., Ullmann, K., Diskin, G., Bui, P., Chang, C. and Dean-Day, J.: Mapping hydroxyl variability throughout the global remote troposphere via synthesis of airborne and satellite formaldehyde observations, PNAS, 201821661, doi:10.1073/pnas.1821661116, 2019.

Wong, J. P. S., Zhou, S. and Abbatt, J. P. D.: Changes in Secondary Organic Aerosol Composition and Mass due to Photolysis: Relative Humidity Dependence, J. Phys. Chem. A, 119(19), 4309–4316, doi:10.1021/jp506898c, 2015.

Wu., H., Wang, Y., Li, H., Huang, L., Huang, D., Shen, H., Xing, Y., Chen, Z.: The OH-initiated oxidation of atmospheric

peroxyacetic acid: Experimental and model studies, Atmos. Env., 164, 61-70, doi: 10.1016/j.atmosenv.2017.05.038, 2017.

Yang, M., Beale, R., Liss, P., Johnson, M., Blomquist, B. and Nightingale, P.: Air–sea fluxes of oxygenated volatile organic compounds across the Atlantic Ocean, Atmos. Chem. Phys., 14(14), 7499–7517, doi:10.5194/acp-14-7499-2014, 2014.

Ye, C., Zhou, X., Pu, D., Stutz, J., Festa, J., Spolaor, M., Tsai, C., Cantrell, C., Mauldin, R. L., Campos, T., Weinheimer, A., Hornbrook, R. S., Apel, E. C., Guenther, A., Kaser, L., Yuan, B., Karl, T., Haggerty, J., Hall, S., Ullmann, K., Smith, J. N., Ortega, J. and Knote, C.: Rapid cycling of reactive nitrogen in the marine boundary layer, Nature, 532(7600), 489–491, doi:10.1038/nature17195, 2016.

Young, P. J., Archibald, A. T., Bowman, K. W., Lamarque, J.-F., Naik, V., Stevenson, D. S., Tilmes, S., Voulgarakis, A., Wild, O., Bergmann, D., Cameron-Smith, P., Cionni, I., Collins, W. J., Dalsøren, S. B., Doherty, R. M., Eyring, V., Faluvegi, G., Horowitz, L. W., Josse, B., Lee, Y. H., MacKenzie, I. A., Nagashima, T., Plummer, D. A., Righi, M., Rumbold, S. T., Skeie, R. B., Shindell, D. T., Strode, S. A., Sudo, K., Szopa, S., and Zeng, G.: Pre-industrial to end 21st century projections of tropospheric ozone from the Atmospheric Chemistry and Climate Model Intercomparison Project (ACCMIP), Atmos. Chem. Phys., 13, 2063–2090, doi:10.5194/acp-13-2063-2013, 2013.

Yoshino, A., Sadanaga, Y., Watanabe, K., Kato, S., Miyakawa, Y., Matsumoto, J. and Kajii, Y.: Measurement of total OH reactivity by laser-induced pump and probe technique—comprehensive observations in the urban atmosphere of Tokyo, Atmos. Env., 40(40), 7869–7881, doi:10.1016/j.atmosenv.2006.07.023, 2006.

Yu, S., Mathur, R., Sarwar, G., Kang, D., Tong, D., Pouliot, G. and Pleim, J.: Eta-CMAQ air quality forecasts for O_3 and related species using three different photochemical mechanisms (CB4, CB05, SAPRC-99): comparisons with measurements during the 2004 ICARTT study, Atmos. Chem. Phys., 25, 2010.

Zannoni, N., Gros, V., Lanza, M., Sarda, R., Bonsang, B., Kalogridis, C., Preunkert, S., Legrand, M., Jambert, C., Boissard, C. and Lathiere, J.: OH reactivity and concentrations of biogenic volatile organic compounds in a Mediterranean forest of downy oak trees, Atmos. Chem. Phys., 16(3), 1619–1636, doi:10.5194/acp-16-1619-2016, 2016.

Zannoni, N., Gros, V., Sarda Esteve, R., Kalogridis, C., Michoud, V., Dusanter, S., Sauvage, S., Locoge, N., Colomb, A. and Bonsang, B.: Summertime OH reactivity from a receptor coastal site in the Mediterranean Basin, Atmos. Chem. Phys., 17(20), 12645–12658, doi:10.5194/acp-17-12645-2017, 2017.

Zhang, L., Jacob, D. J., Knipping, E. M., Kumar, N., Munger, J. W., Carouge, C. C., van Donkelaar, A., Wang, Y. X. and Chen, D.: Nitrogen deposition to the United States: distribution, sources, and processes, Atmos. Chem. Phys.; Katlenburg-Lindau, 12(10), 4539, 2012.

Table 1. Annual emissions of CO and NO_x for 2016 used in the GEOS-Chem simulations.

Emissions category	**CO, Tg**	**Emissions category**	**NO_x, Tg N**
Fuel combustion[1]	590	Fuel combustion[1]	32.9
Biomass burning	311	Biomass Burning	6.0
NMVOC Oxidation	69~~88~~9	Soil Emissions	7.8
Methane Oxidation	93~~68~~	Lightning emissions	6.0
Total	25~~28~~16	Total	52.7
[1]Anthropogenic fossil fuel and biofuel combustion			

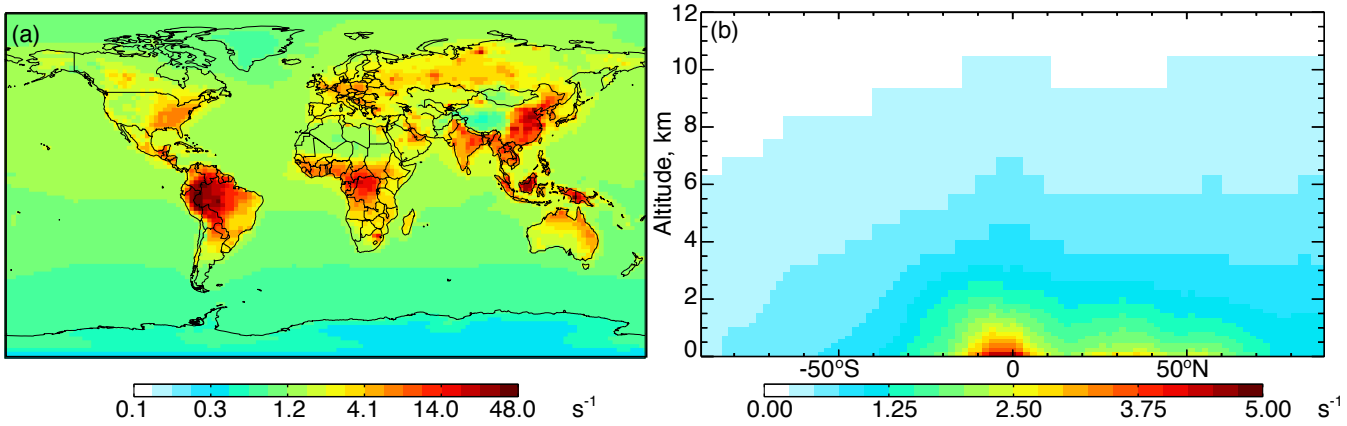

Figure 1. Annual mean 2016 a) surface (log scale) and b) zonal mean cOHR calculated from individual model species. The GEOS-Chem species included in the calculation of cOHR are listed in Table S1.

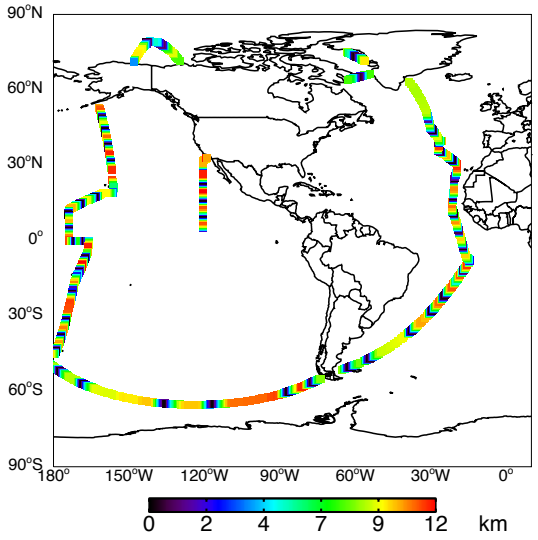

Figure 2. ATom-1 ocean-only flight tracks colored by altitude.

Table 2. Description of ATom measurements used to evaluate the model simulation.

Measurement	Instrument	Accuracy	Detection Limit/Precision	Reference
OHR	Airborne Tropospheric Hydrogen Oxides Sensor (ATHOS)	0.8 s^{-1}	± ±0.3 4 s^{-1}	Faloona et al., 2004; Mao et al., 2009
Water vapor	Diode laser hygrometer (DLH)	5%	0.1% or 50 ppb	Diskin et al., 2002 Podolske et al., 2003
NO_y[61]	NOAA Nitrogen oxides and ozone (NO_yO_3)		0.05 ppb[42]	Pollack et al., 2010; Ryerson et al., 1998, 2000
Photolysis frequencies via actinic flux	Charged-coupled device Actinic Flux Spectroradiometers (CAFS)	jO_3 20% jNO_2 12%	jO_3 10^{-7} /s s^{-1} jNO_2 10^{-6} s^{-1} /s	Shetter and Mueller, 1999, Petropavloskikh, 2007, Hofzumahaus et al., 2004
Peroxyacetyl nitrate (PAN)	PAN and Trace Hydrohalocarbon ExpeRiment (PANTHER)	10%	2 ppt ± ±10 %	Elkins et al., 2001; Wofsy et al., 2011
Components of OH reactivity[37]				
CH_4	NOAA Picarro	0.6 ppb	0.3 ppb	Karion et al., 2013 AMT
CO	Harvard Quantum Cascade Laser System (QCLS)	3.5 ppb	0.15 ppb	McManus et al., 2005; Santoni et al., 2014
H_2[41]	UAS Chromatograph for Atmospheric Trace Species (UCATS)/PANTHER		7.5 ppb[35]	Hintsa et al., 2019
NO, NO_2, O_3	NOAA NO_yO_3		0.006 ppb[42], 0.03 ppb[42], 1.7 ppb[42]	Pollack et al., 2010; Ryerson et al., 1998, 2000
Methyl hydroperoxide, nitric acid, hydrogen peroxide, peroxyacetic acid, peroxynitric acid	Caltech Chemical ionization mass spectrometer (CIMS)	± ±30 %, ± ±30 %, ± ±30 %, ± ±50 %, ± ±30 %	25 ppt, 50 ppt, 50 ppt, 30 ppt, 100 ppt	St. Clair et al., 2010; Crounse et al., 2006
Formaldehyde	NASA In Situ Airborne Formaldehyde (ISAF)	10%	10 ppt	Cazorla et al., 2015; DiGangi et al., 2011; Hottle et al., 2009
Methanol, acetaldehyde, propane, dimethyl sulfide, ethanol, acetone, methyl ethyl ketone, propanal[65], butanal[65], toluene, methyl vinyl ketone, methacrolein i-Butane + n-butane + i-pentane + n-pentane[72]	NCAR Trace Organic Gas Analyzer (TOGA)	30%, 20%, 30%, 15%, 30%, 20%, 20%, 20%, 30%, 15%, 20%, 20% 15%, 15%, 15%, 15%	10 ppt, 10 ppt, 20 ppt, 2 ppt, 30 ppt, 10 ppt, 2 ppt, 20 ppt, 2 ppt, 0.6 ppt, 4 ppt, 2 ppt 2 ppt, 2 ppt, 4 ppt, 4 ppt	Apel et al., 2015

OH, HO_2	ATHOS	74 % to 135%	0.018 ppt, 0.2 ppt ~~factor of 1.35~~	Faloona et al., 2004; Brune et al., 2020
Ethane, benzene	UCI Whole air sampler (WAS)	5%, 5%	3 ppt, 3 ppt	Colman et al., 2001; Simpson et al.; 2010

[1]Model NO_y is defined as NO + NO_2 + HONO + HNO_3 + HNO_4 + 2*N_2O_5 + $ClNO_2$ + ∑PNs + ∑ANs.

[2]Average of 2-sigma uncertainty for each individual 1 Hz measurement for ATom-1 and ATom-2.

[3]Included in cOHR are observations of species where at least 20% of the possible available measurements below 3 km are not missing.

[14]The GEOS-Chem concentration of H_2 is set to a constant value of ~~0.5 ppm~~500 ppt. ~~.~~

[5]Average of reported error for each individual measurement for ATom-1 and ATom-2.

[62]Lumped as >C_4 alkanes (ALK4) in GEOS-Chem.

~~[3]Average of reported error for each individual measurement for ATom-1 and ATom-2.~~

~~[4]Average of 2-sigma uncertainty for each individual 1 Hz measurement for ATom-1 and ATom-2.~~

[57]Lumped as >C_3 aldehydes (RCHO) in GEOS-Chem.

~~[6]Model NO_y is defined as NO + NO_2 + HONO + HNO_3 + HNO_4 + 2*N_2O_5 + $ClNO_2$ + ∑PNs + ∑ANs.~~

~~[7]Included in cOHR are observations of species where at least 20% of the possible available measurements below 3 km are not missing.~~

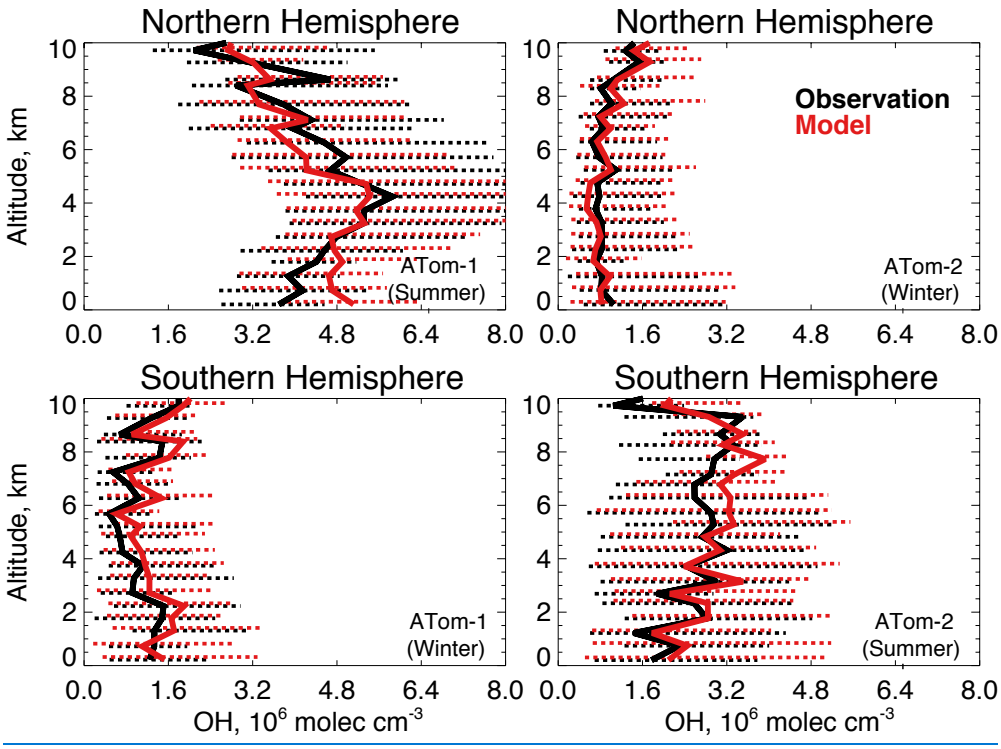

Figure 3. Median OH concentrations for the Northern hemisphere (>0°N) and Southern hemisphere (<0°S) from the ATHOS instrument described in Table 2 during ATom-1 (Jul-Aug, 2016) and ATom-2 (Jan-Feb, 2017) compared against the GEOS-

Chem model in 0.5 km altitude bins. The observations have been filtered to remove biomass burning (acetonitrile >200 ppt) and stratospheric (O_3/CO > 1.25) influence. The dashed lines show the observed 25th-75th percentiles.

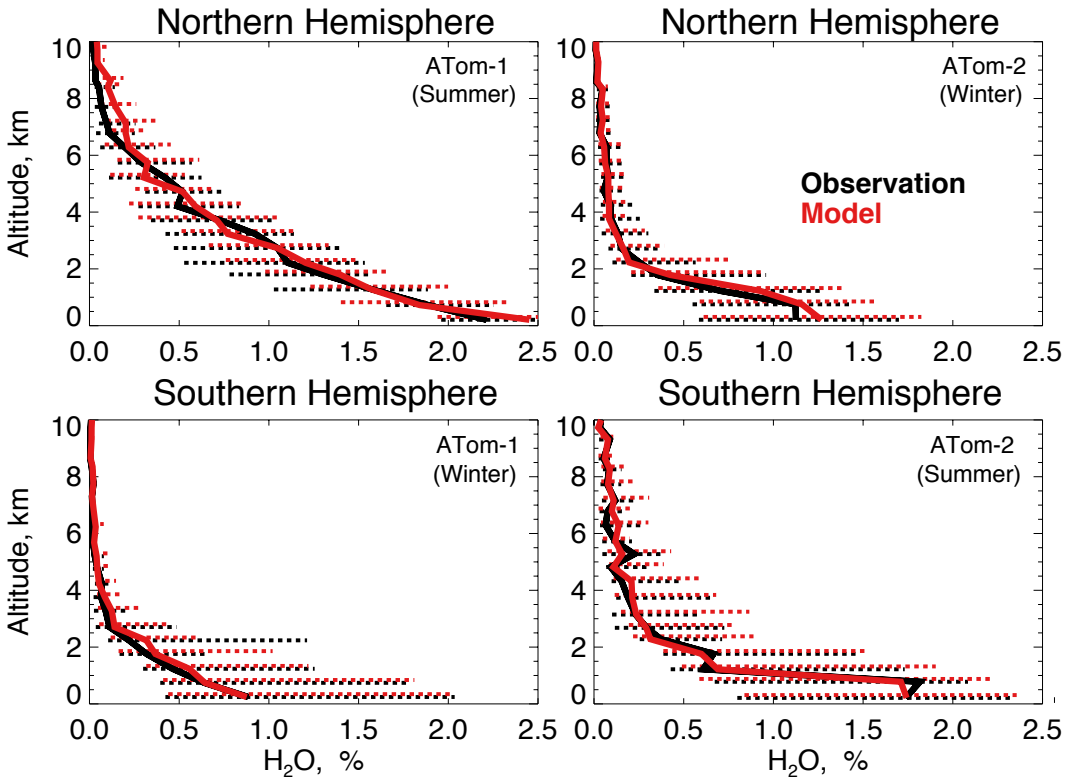

Figure 4. The same as Fig~~ure~~ 3 for median water vapor concentrations. Water vapor mixing ratio was measured by the DLH instrument as described in Table 2.

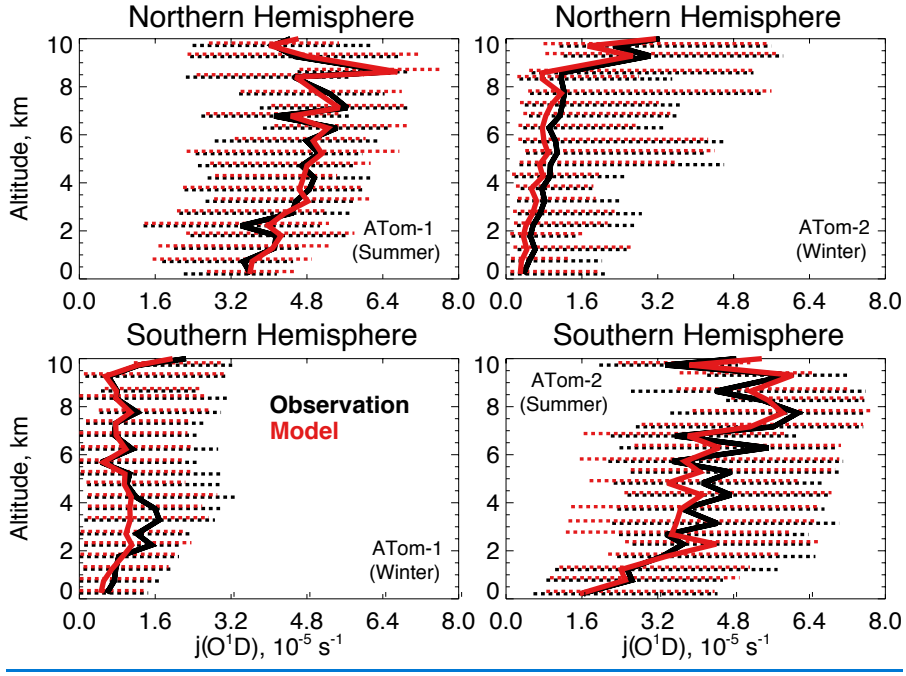

Figure 5. The same as ~~Figure~~ Fig. 3 for median photolysis frequencies for ozone (~~$jO_3 j(O^1D)$~~). ~~).~~ The ~~jO_3 was determined from~~ actinic flux measured by the CAFS instrument is used to calculate $j(O^1D)$ as described in Table 2.

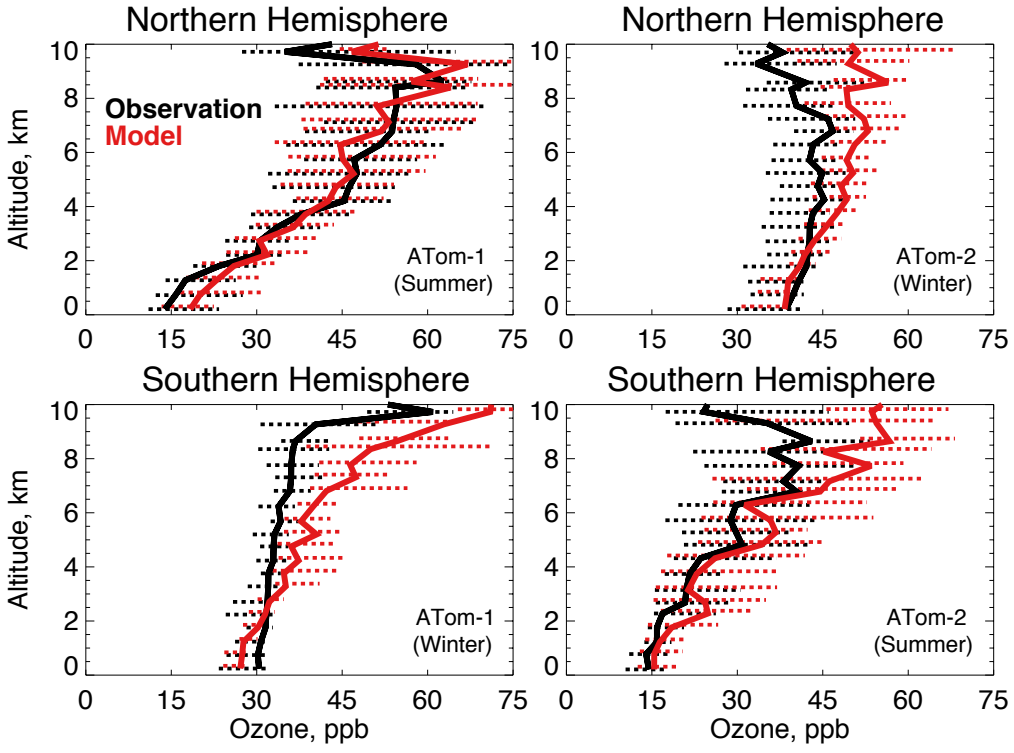

Figure 6. The same as ~~Figure~~ Fig. 3 for median ozone concentrations. Ozone was measured by the NOAA NO_yO_3 instrument as described in Table 2.

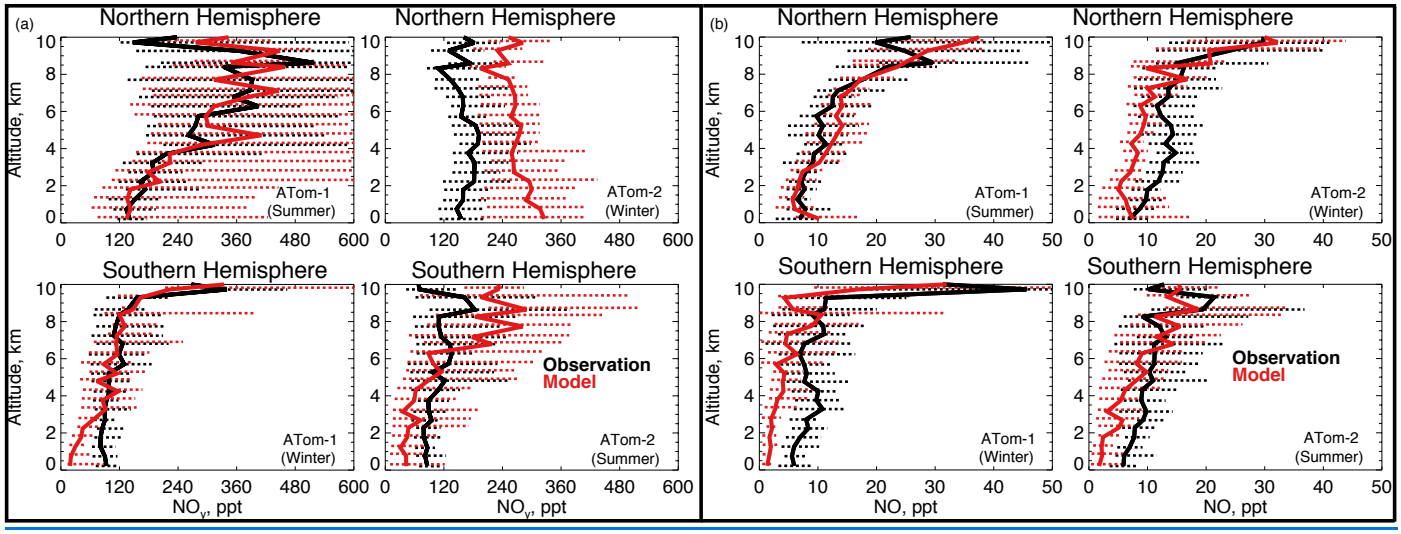

Figure 7. The same as ~~Figure~~ Fig. 3 for median NO_y (a) and NO (b) concentrations. NO_y and NO were measured by the NOAA NO_yO_3 instrument as described in Table 2.

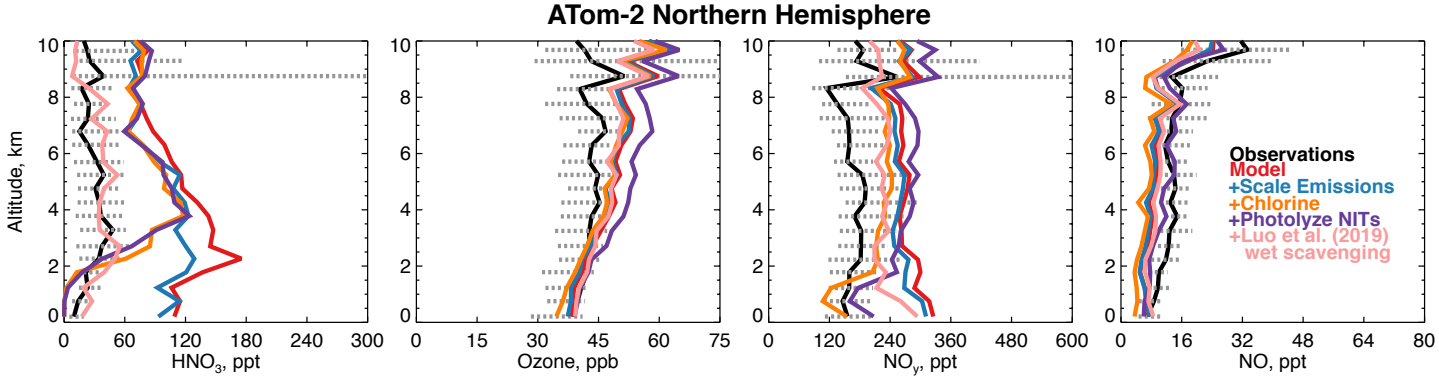

Figure 8. Comparison of modeled and observed HNO_3, ozone, NO_y and NO with sensitivity studies including scaling emissions from the U.S. and Asia, improved chlorine chemistry (Wang X. et al., 2019), and the photolysis of particulate nitrate

on coarse-mode seasalt aerosols (Kasibhatla et al., 2018) as described in Section 4. HNO_3 was measured by the Caltech CIMS, ozone, NO_y and NO were measured by the NOAA NO_yO_3 instrument (Table 2).

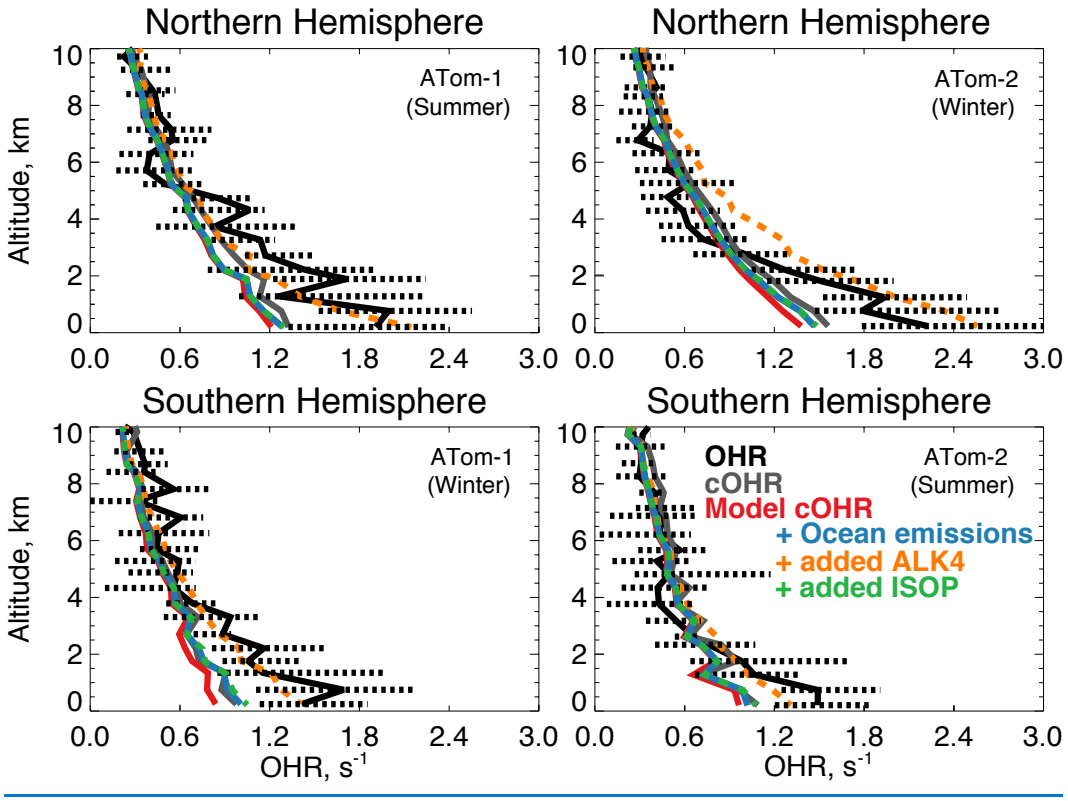

Figure 89. The same as ~~Figure~~ Fig. 3 for median OHR. OHR was measured by the ATHOS instrument as described in Table 2. The calculation of cOHR in the model and observations includes the species described in Table 2. In order to allow for a point-by-point comparison of cOHR in the model and observations, missing values are filled in the observational components of cOHR using linear interpolation. All calculated reactivity values are determined using the temperature and pressure of the ATHOS instrument inlet which differs from ambient values. The sensitivity tests are described in Section 5.

Table 3. Biogenic ocean ~~VOC~~ emissions of VOCs

GEOS-Chem species[2]	# lumped species	Produces acetaldehyde?	Annual Net Emissions (Tg C)	Reference for seawater concentration
ALD2	1	Yes	10.~~25~~15	Millet et al., 2010
MOH	1	No	-1.~~55~~56	Pers. comm. D. Millet
ACET	1	No	-75.70	Fischer et al., 2012
LIMO	1	Yes	0.04	Hackenberg et al., 2017
MTPA	3	Yes	0.05	Hackenberg et al., 2017
MTPO	2	Yes	0.06	Hackenberg et al., 2017
EOH	1	Yes	-5.60	Beale et al., 2010
C2H6	1	Yes	0.3~~43~~	Plass-Dülmer et al., 1993
C2H4	1	No	0.75	Plass-Dülmer C. et al., 1993
PRPE	2	Yes	0.9~~65~~	Plass-Dülmer C. et al., 1993

GEOS-Chem species[2]	# lumped species	Produces acetaldehyde?	Annual Net Emissions (Tg C)	Reference for seawater concentration
C3H8	1	Yes	0.176	Plass-Dülmer et al., 1993
ALK4	2	Yes	0.12	Plass-Dülmer et al., 1993
C2H2	1	No	0.052	Plass-Dülmer et al., 1993
ISOP	1	Yes	1.64	Arnold et al., 2009
RCHO	1	Yes	7.47	Singh et al., 2003
MEK	1	Yes	-7.243	Schlundt et al., 2017
Total net emission			-68.3225	
Total net emission producing acetaldehyde			8.1523	

[1]Net ocean emissions = upward flux out of the ocean - ocean uptake.
[2]More information on the GEOS-Chem species definitions can be found here: http://wiki.seas.harvard.edu/geos-chem/index.php/Species_in_GEOS-Chem.

Table 4. Abiotic ocean ~~VOC~~ emissions of VOCs according to Brüggemann et al. (2018)[1]

GEOS-Chem species[2]	# lumped species	Produces acetaldehyde?	Annual Emission (Tg C)
ACET	1	No	10.07
EOH	1	Yes	5.16
ALD2	1	Yes	2.26
MOH	2	No	0.79
RCHO	21	Yes	3.88
ISOP	1	Yes	1.04
PRPE	13	Yes	4.44
MACR	1	Yes	0.42
ACTA	1	Yes	0.10
CH2O	1	No	0.03
XYLE	1	No	0.05
TOLU	1	No	0.04
BENZ	1	No	0.02
Total net emission			28.30
Total net emission producing acetaldehyde			17.29

[1]Table S2 shows the emission factor assumed for each species and the lumping methodology for Table 4.
[2]More information on the GEOS-Chem species definitions can be found here: http://wiki.seas.harvard.edu/geos-chem/index.php/Species_in_GEOS-Chem.

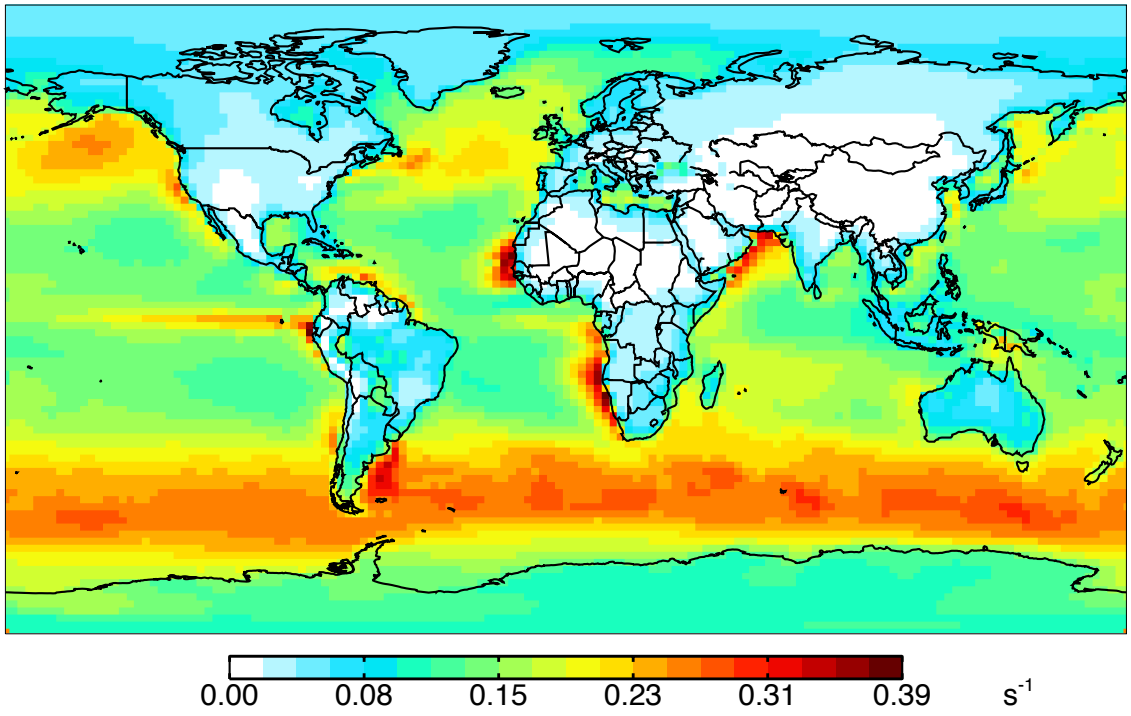

Figure ~~9~~10. Impact of all ocean emissions (Tables 3 and 4) on annual simulated 2016 surface cOHR as described in the text.

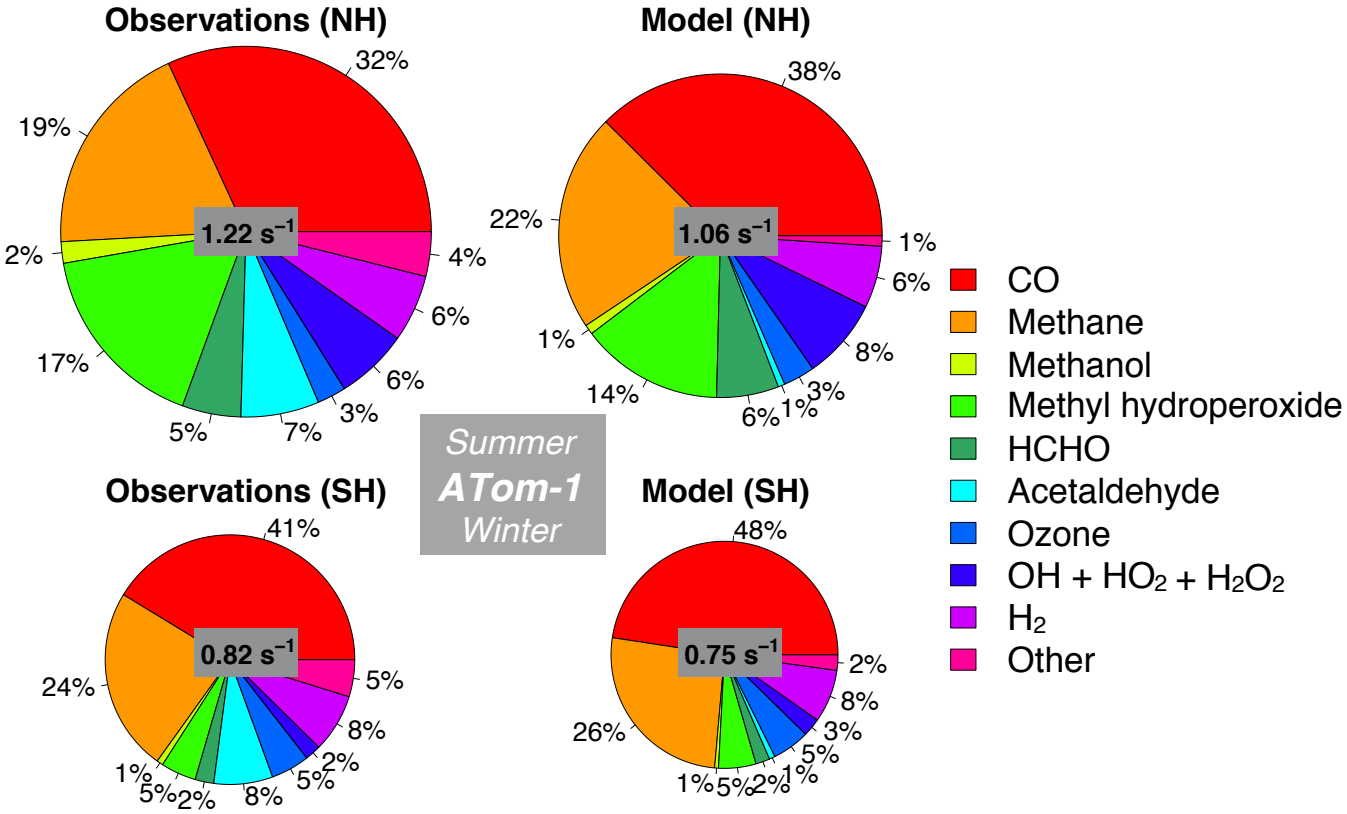

Figure ~~10~~11. Median observed and modeled OHR and cOHR (see text) below 3km in the Northern Hemisphere (>0°N) and Southern Hemisphere (<0°S) during ATom-1. The "Other" category the following species as described in Table 2: ethanol, propane, ethane, acetone, >C_3 aldehydes, methyl ethyl ketone, methyl vinyl ketone, methacrolein, benzene, toluene, >C_4 alkanes, peroxyacetic acid, peroxynitric acid, dimethyl sulfide, nitric acid, NO, and NO_2. The diameter of each pie chart is scaled relative to that with maximum cOHR for ATom-1.

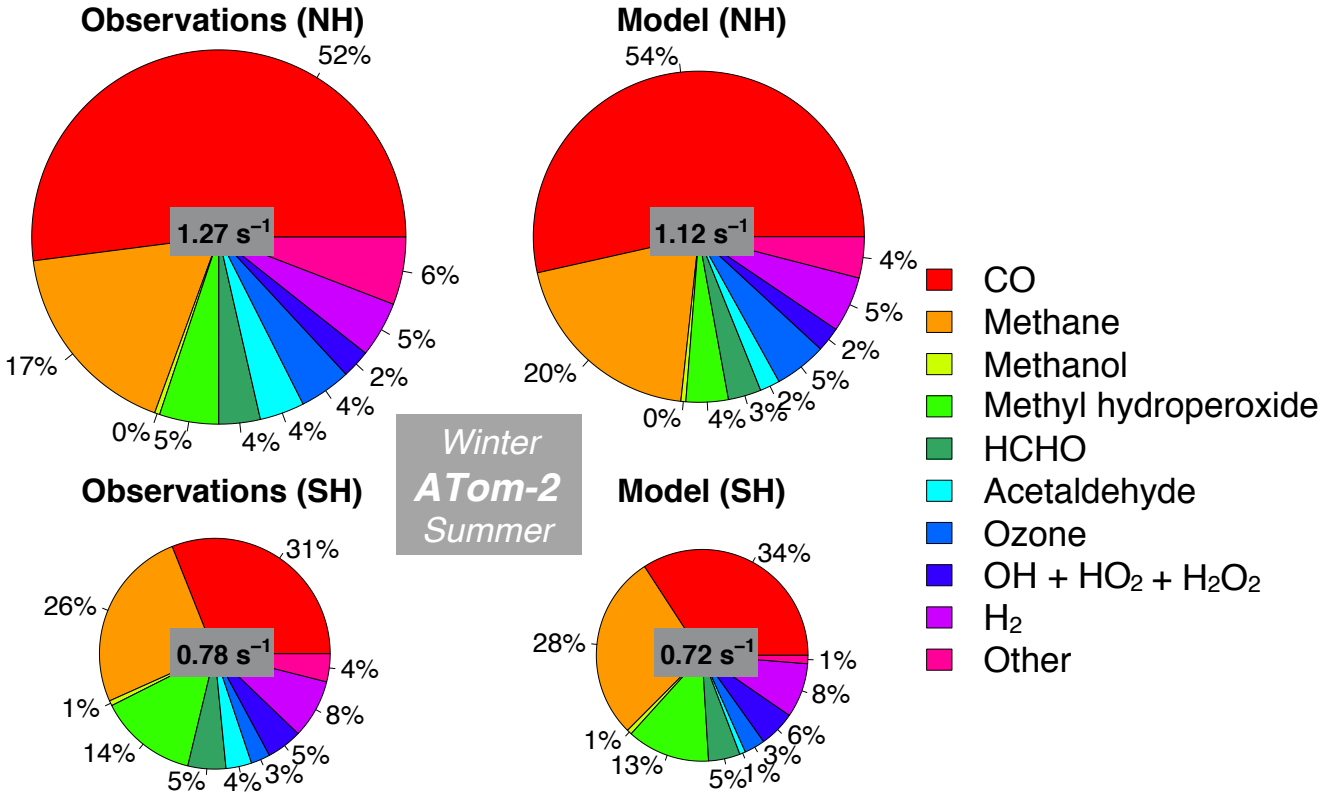

Figure ~~11~~12. Same as ~~Figure~~ Fig. 10 but for ATom-2. The diameter of each pie chart is scaled relative to that with maximum cOHR for ATom-2.

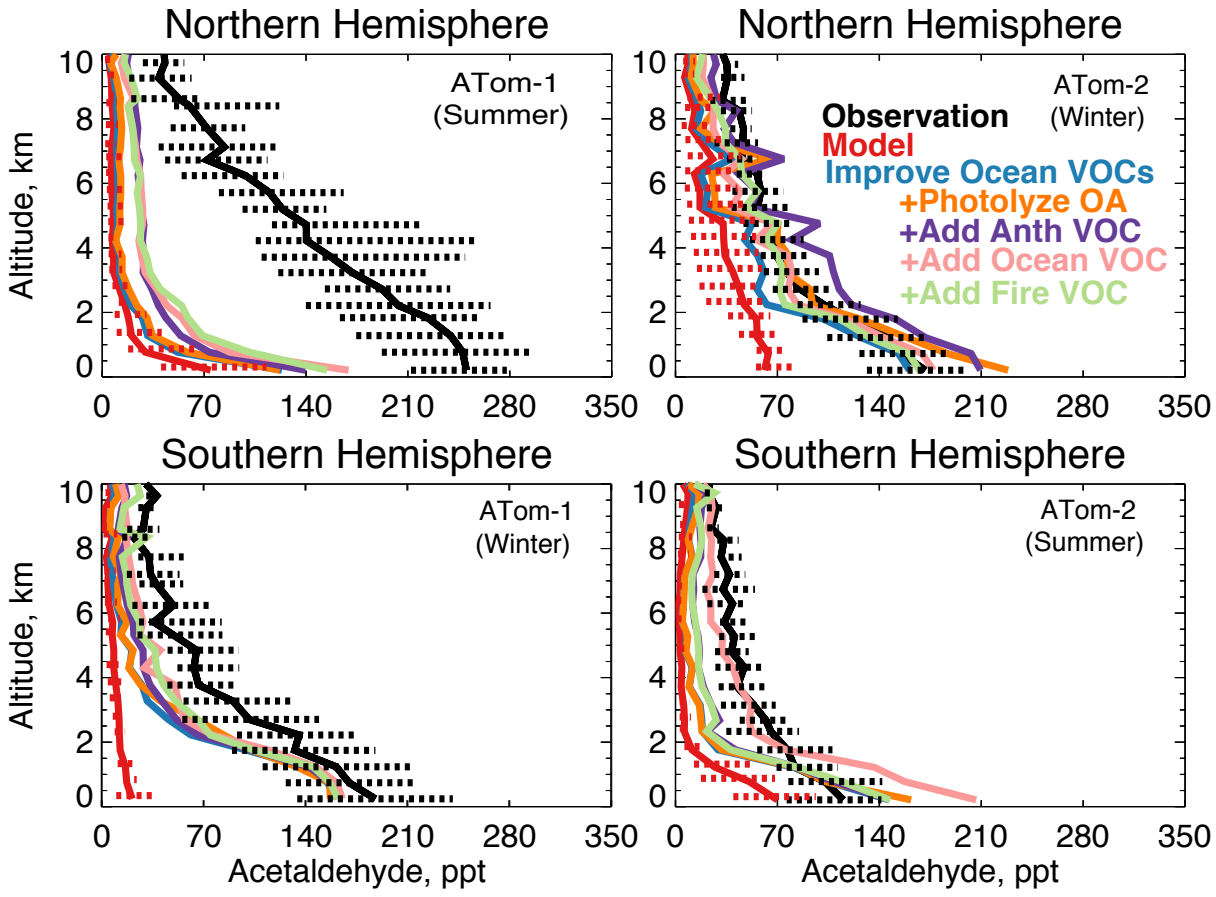

Figure 1~~3~~2. The same as ~~Figure~~ Fig. 3 for median acetaldehyde profiles. Acetaldehyde was measured by the TOGA instrument as described in Table 2. The sensitivity studies are described in the text.

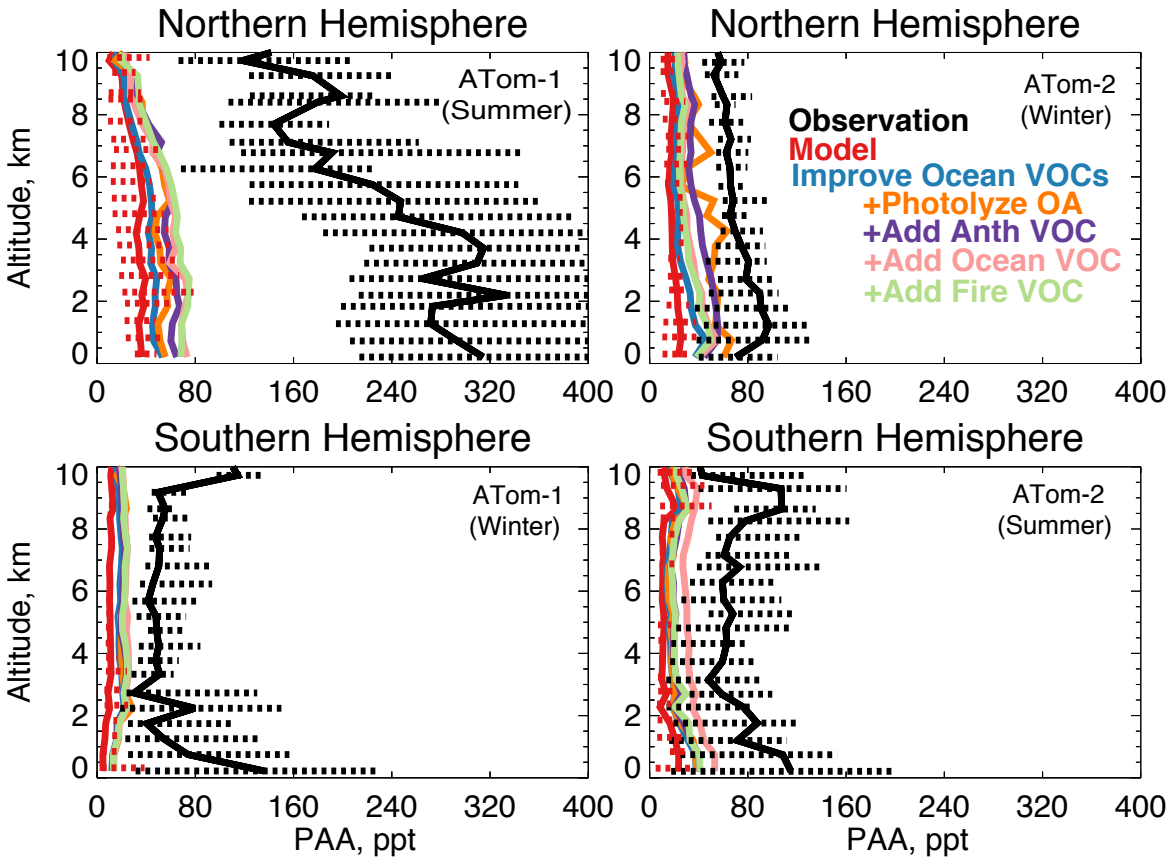

Figure 1~~4~~3. The same as ~~Figure~~ Fig. 3 for median peroxyacetic acid (PAA) profiles. PAA was measured by the Caltech CIMS instrument as described in Table 2. The sensitivity studies are described in the text.

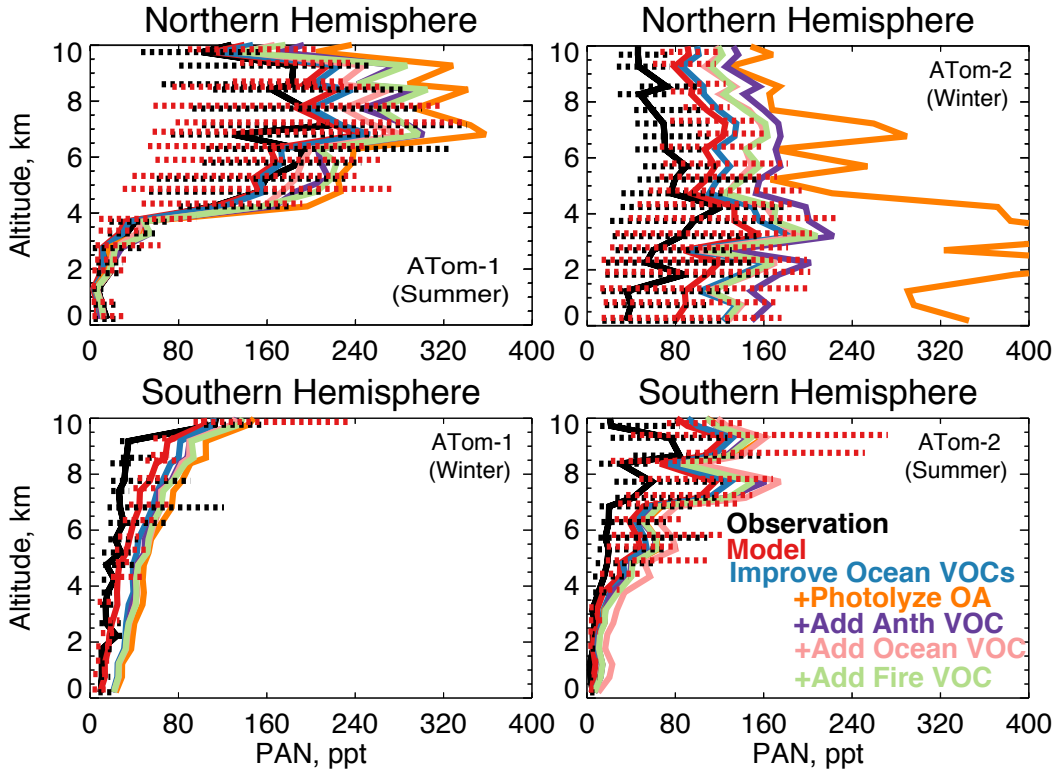

Figure 1~~5~~4. The same as ~~Figure~~ Fig. 3 for median peroxyacetyl nitrate (PAN) profiles. PAN was measured by the PANTHER instrument as described in Table 2. The sensitivity studies are described in the text.

5

Table 5. Model sources of acetaldehyde in 2016

Sources (Tg yr^{-1})[1]	Millet et al. (2010)	This Work
Photochemical production	128	~~160~~166
Net ocean emission	57	22
Terrestrial plant growth + decay	23	26
Biomass burning	3	3
Anthropogenic emission	2	2
Total source	213	~~213~~219

[1]Emissions are given in Tg of acetaldehyde per year for comparison to Millet et al. (2010). These totals are for the baseline model simulation described in Section 2.1.

Supplemental Information

Section 81. Description of chemistry added to GEOS-Chem for unsaturated C_2 compounds and organic acids.

Chemistry added to GEOS-Chem.

Table S1.

Species added	
C2H2 = IGNORE; {C2H2; Acetylene}	
C2H4 = IGNORE; {C2H4; Ethene}	
EO2 = IGNORE; {HOCH2CH2O2; Peroxy radical from C2H4}	
EO = IGNORE; {HOCH2CH2O; from C2H4}	
Chemistry added	
C2H2 + OH = GLYX + OH :	GCKMT17(0.636);
C2H2 + OH = HCOOH + CO + HO2 :	GCKMT17(0.364);
C2H4 + OH = 0.750EO2 + 0.500CH2O + 0.250HO2 :	GCKMT15();
EO2 + NO = EO + NO2:	GCARR(4.2E-12,0.0E+00,180.0);
EO + O2 = GLYC + HO2:	1.00E-14;
C2H4 + O3 = CH2O + 0.120HO2 + 0.500CO + 0.120OH + 0.500HCOOH:	GCARR(1.2E-14,0.0E+00, -2630.); {Lamarque et al., 2012}

In GEOS-Chem, RCOOH, or organic acids produced during VOC oxidation, do not themselves undergo further oxidation and thus are a loss of carbon in the model. We include oxidation of RCOOH parameterized as propionic acid from the MCMv3.3.1.

Table S2.

Species added	
RCOOH = IGNORE; {C2H5C(O)OH; > C2 organic acids}	
RCO2 = IGNORE; {Peroxy from RCOOH}	
Chemistry added	
RCOOH + OH = RCO2 :	GCARR(1.2E-12, 0.0E+00, 0.0) ;
RCO2 + HO2 = ETP :	GCARR(4.3E-12, 0.0E+00, 870.0) ;
RCO2 + NO = ALD2 + HO2 + NO2 :	GCARR(2.55E-12, 0.0E+00, 380.0) ;

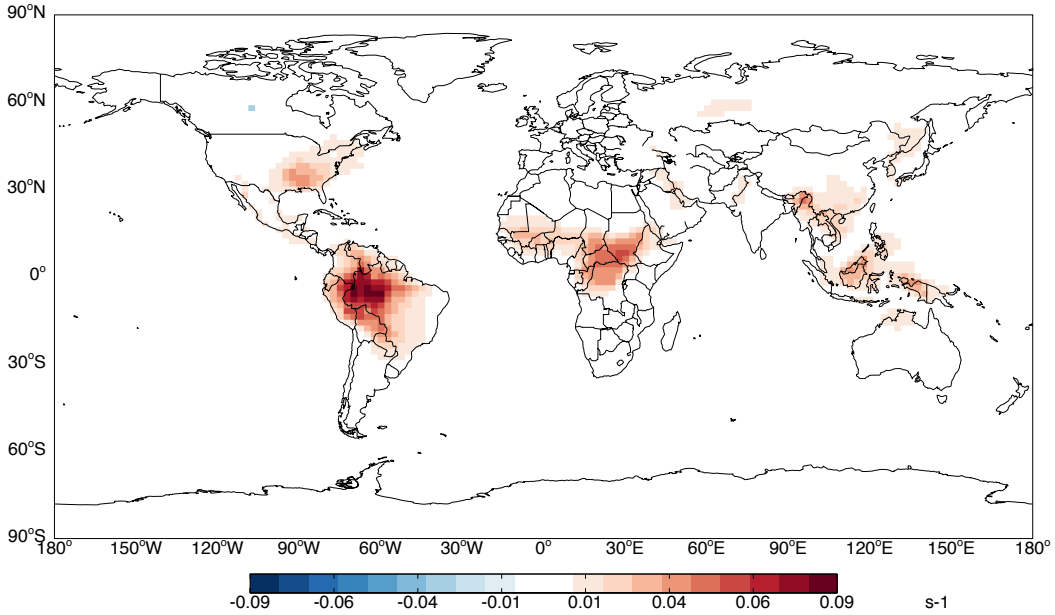

Figure S1. One-month test of the impact of RCOOH on surface cOHR, including the chemistry from Table S2.

Section ~~1~~2. Model variables included in the calculation of Figure. 1

Table ~~S1~~S3. Variables included in the calculated OH reactivity shown in Figure 1.

GEOS-Chem Species[1]	Species description
ACET	Acetone
ACTA	Acetic acid
ALD2	Acetaldehyde
ALK4	>C_4 alkanes
BENZ	Benzene
Br2	Molecular bromine
BrO	Bromine monoxide
C2H2	Ethyne (Acetylene)
C2H4	Ethylene
C2H6	Ethane
C3H8	Propane
CH2Br2	Dibromomethane
CH2Cl2	Dichloromethane
CH2O	Formaldehyde
CH3Br	Methyl bromide
CH3Cl	Methyl chloride
CH3I	Methyl iodide
CH4	Methane
CHBr3	Bromoform
CHCl3	Chloroform

GEOS-Chem Species[1]	Species description
Cl2	Molecular chlorine
ClNO2	Nitryl chloride
ClNO3	Chlorine nitrate
ClO	Chlorine monoxide
CO	Carbon monoxide
DMS	Dimethyl sulfide
EOH	Ethanol
ETHLN	Ethanal nitrate
GLYC	Glycoaldehyde
GLYX	Glyoxal
H2	Molecular hydrogen
H2O2	Hydrogen peroxide
HAC	Hydroxyacetone
HBr	Hydrobromic acid
HC187	Epoxide oxidation product m/z 187-189
HCl	Hydrochloric acid
HCOOH	Formic acid
HI	Hydrogen iodide
HNO2	Nitrous acid
HNO3	Nitric acid
HNO4	Peroxynitric acid
HO2	Hydroperoxy radical
HOCl	Hypochlorous acid
HOI	Hypoiodous acid
HONIT	2nd generation monoterpene organic nitrate
HPALD	Hydroperoxyaldehydes
I2	Molecular iodine
IEPOXA	trans-β isoprene epoxydiol
IEPOXB	cis-β isoprene epoxydiol
IEPOXD	δ isoprene epoxydiol
IMAE	C_4 epoxide from oxidation of PMN
IPMN	Peroxymethacryloyl nitrate (MPAN) from isoprene oxidation
ISN1	Nighttime isoprene nitrate
ISOP	Isoprene
ISOPNB	Isoprene nitrate Beta
ISOPND	Isoprene nitrate Delta
LIMO	Limonene
LVOC	Gas-phase low-volatility non-IEPOX product of ISOPOOH (RIP) oxidation

GEOS-Chem Species[1]	Species description
MACR	Methacrolein
MACRN	Nitrate from MACR
MAP	Peroxyacetic acid
MEK	Methyl ethyl ketone
MGLY	Methylglyoxal
MOBA	5C acid from isoprene
MOH	Methanol
MONITS	Saturated 1st generation monoterpene organic nitrate
MONITU	Unsaturated 1st generation monoterpene organic nitrate
MHP	Methylhydroperoxide
MTPA	Lumped monoterpenes (α-pinene, β-pinene, sabinene, carene)
MTPO	Terpinene, terpinolene, myrcene, ocimene, other monoterpenes
MVK	Methyl vinyl ketone
MVKN	Nitrate from MVK
NO	Nitric oxide
NO2	Nitrogen dioxide
NO3	Nitrate radical
NPMN	Non-isoprene peroxymethacryloyl nitrate (MPAN)
O3	Ozone
OClO	Chlorine dioxide
OH	Hydroxyl radical
PROPNN	Propanone nitrate
PRPE	≥C_3 alkenes
R4N2	≥C_4 alkylnitrates
RCHO	≥C_3 aldehydes
RCOOH	>C_2 organic acids
RIPA	1,2-ISOPOOH (Peroxide from RIO2)
RIPB	4,3-ISOPOOH (Peroxide from RIO2)
RIPD	δ(1,4 and 4,1)-ISOPOOH (Peroxide from RIO2)
SO2	Sulfur dioxide
TOLU	Toluene
XYLE	Xylene

[1] For more information, visit http://wiki.seas.harvard.edu/geos-chem/index.php/Species_in_GEOS-Chem

Section 3. Distributions of observed and modeled OH.

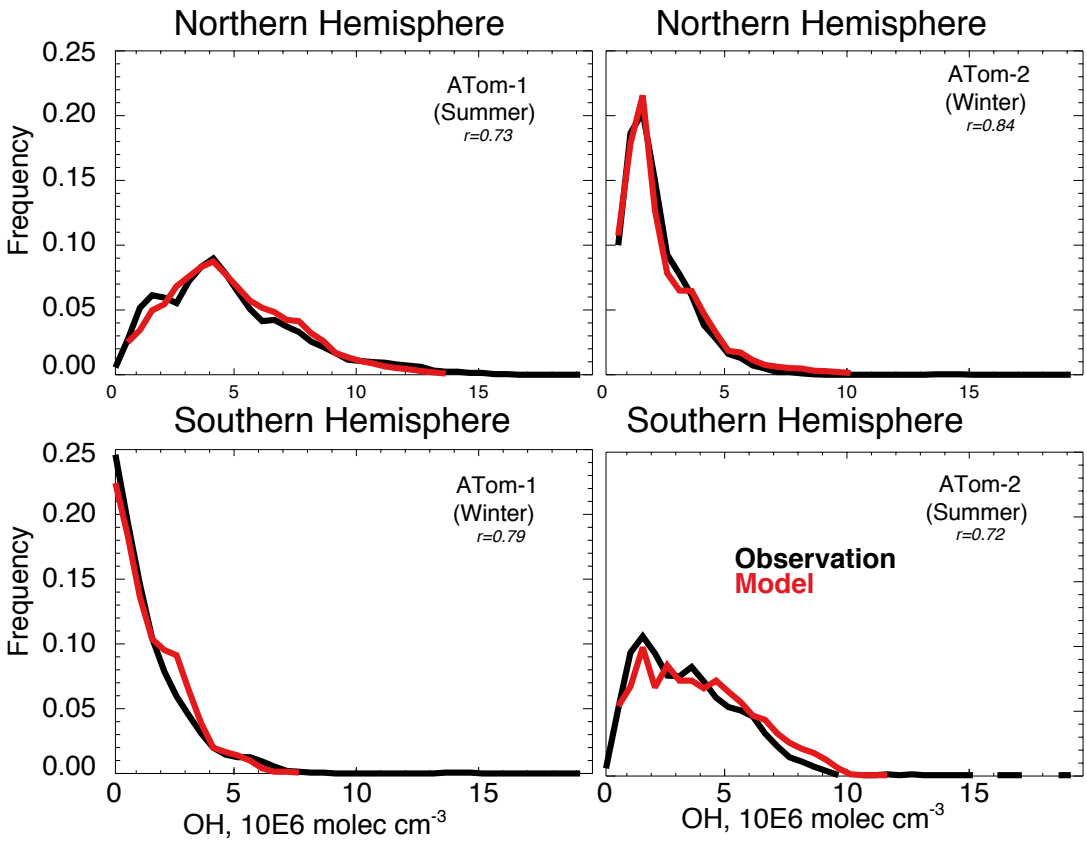

Figure S~~1~~2. Frequency distributions of OH from the model and observations filtered as described in Figure 3.

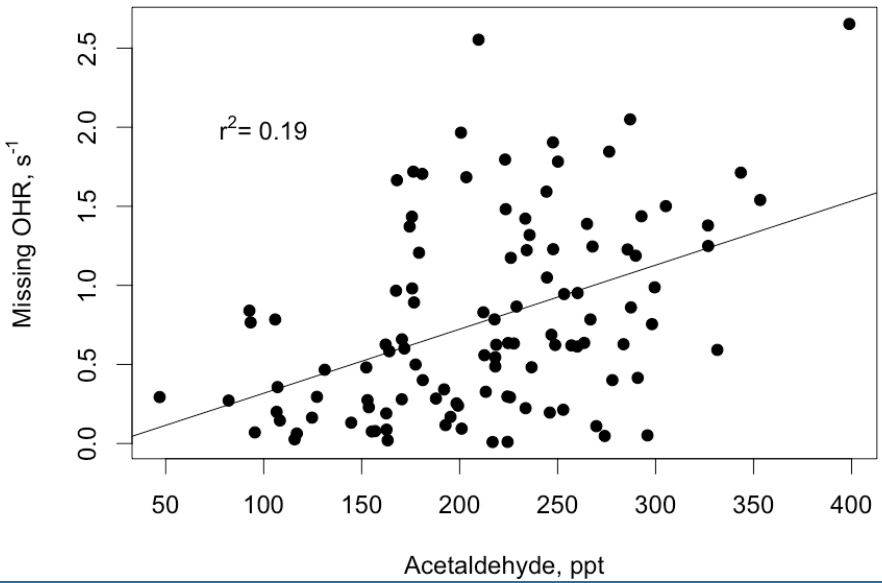

Figure S3. Observations of acetaldehyde and the difference between OHR and $cOHR_{obs}$ below 3 km in the Northern Hemisphere during ATom-1. The data has been filtered to remove biomass burning (acetonitrile >200 ppt) influence.

Section ~~2~~4. Emission factors used to generate Table 4.

Table ~~S2~~S4. Emission factor assumed for each species and the lumping methodology for Table 4.

PTR-TOF-MS	# carbons	Species Identified	Assumed species	GEOS-Chem species	EF[1], production / 10^7 molec. mW^{-1} s^{-1}	EF*1E7*Carbons*12gC $mmol^{-1}$	EF*1E7* molecular weight	Matlab Tool (Tg/yr)
42.034	2	C2H3N (acetonitrile)	Acetonitrile					27.1318
59.047	3	C3H6O (acetone or propanal?)	Acetone	ACET	77.391	2.79E+10	4.49E+10	16.3006
47.048	2	C2H6O (ethanol)	Ethanol	EOH	59.672	1.43E+10	2.75E+10	10.0142
45.032	2	C2H4O (acetaldehyde)	Acetaldehyde	ALD2	26.127	6.27E+09	1.15E+10	4.1974
33.034	1	CH4O (methanol)	Methanol	MOH	16.375	1.97E+09	5.25E+09	1.9302
73.061	4	C4H8O (butanal)	2-methylpropanal	RCHO	4.63	2.22E+09	3.34E+09	1.2067
69.067	5	C5H8 (isoprene)	Isoprene	ISOP	4.788	2.87E+09	3.26E+09	1.1801
57.032	3	C3H4O (acrolein)	Acrolein	RCHO	5.355	1.93E+09	3.00E+09	1.0904
43.054	3	C3H6	Propene	PRPE	6.593	2.37E+09	2.77E+09	1.0121
57.067	4	C4H8 (butene)	Butene	PRPE	4.058	1.95E+09	2.28E+09	0.8265
83.08	6	C6H10 (cyclohexene)	Cyclohexene	PRPE	2.317	1.67E+09	1.90E+09	0.6875
71.045	4	C4H6O (methacrolein)	Methacrolein	MACR	2.397	1.15E+09	1.68E+09	0.6082
127.101	8	C8H14O	2-octenal	PRPE	1.178	1.13E+09	1.49E+09	0.535
85.059	5	C5H8O	2-Methylbut-3-yn-2-ol	RCHO	1.575	9.45E+08	1.32E+09	0.4794
87.075	5	C5H10O	Pentanal	RCHO	1.46	8.76E+08	1.26E+09	0.4535
70.061	4	C4H7N	Butyronitrile	NA	1.7	8.16E+08	1.17E+09	0.4249
41.038	3	C3H4	Cyclopropene	PRPE	2.761	9.94E+08	1.11E+09	0.404
111.104	8	C8H14	Cyclooctene	PRPE	1.01	9.70E+08	1.11E+09	0.4003
97.094	7	C7H12	Cycloheptene	PRPE	1.023	8.59E+08	9.83E+08	0.3533
51.043	1	CH6O2	Methanol-hydrate	MOH	1.895	2.27E+08	9.48E+08	0.3459
113.088	7	C7H12O	2-heptenal	RCHO	0.796	6.69E+08	8.92E+08	0.3227

PTR-TOF-MS	# carbons	Species Identified	Assumed species	GEOS-Chem species	EF[1], production / 10^7 molec. mW^{-1} s^{-1}	EF*1E7*Carbons*12gC $mmol^{-1}$	EF*1E7* molecular weight	Matlab Tool (Tg/yr)
43.017	2	C2H2O (ketene)	NA	NA?	1.904	4.57E+08	8.00E+08	0.2916
71.077	5	C5H10	1-pentene	PRPE	1.041	6.25E+08	7.30E+08	0.2637
129.116	8	C8H16O	3-octanone	RCHO	0.545	5.23E+08	6.98E+08	0.2533
61.026	2	C2H4O2	Acetic acid	ACTA	1.134	2.72E+08	6.81E+08	0.246
109.093	8	C8H12	1,5-cyclooctadiene	PRPE	0.546	5.24E+08	5.90E+08	0.214
143.128	9	C9H18O	5-nonanone	RCHO	0.398	4.30E+08	5.66E+08	0.2042
101.088	6	C6H12O	2-methylpentanal	RCHO	0.564	4.06E+08	5.64E+08	0.2019
63.041	2	C2H6O2	Ethylene glycol	RCHO	0.884	2.12E+08	5.48E+08	0.1979
107.042	7	C7H6O	Benzaldehyde	RCHO	0.514	4.32E+08	5.45E+08	0.1947
121.056	8	C8H8O	2-methylbenzaldehyde	RCHO	0.431	4.14E+08	5.17E+08	0.1857
87.039	4	C4H6O2	1,4-dihydroxy-2-butyne	RCHO	0.593	2.85E+08	5.10E+08	0.1832
141.112	9	C9H16O	trans-2-nonenal	RCHO	0.359	3.88E+08	5.03E+08	0.1812
95.079	7	C7H10	Cyclopentylacetylene	PRPE	0.532	4.47E+08	5.01E+08	0.1798
111.072	7	C7H10O	Dicyclopropylmethanone	RCHO	0.445	3.74E+08	4.90E+08	0.1783
101.052	5	C5H8O2	Acetylacetone	RCHO	0.461	2.77E+08	4.61E+08	0.1658
139.108	9	C9H14O	Isophorone	RCHO	0.332	3.59E+08	4.59E+08	0.1638
153.114	1	C10H16O	α-pinene oxide	RCHO	0.281	3.37E+07	4.27E+08	0.1529
99.074	6	C6H10O	2-hexenal	RCHO	0.405	2.92E+08	3.97E+08	0.1449
123.106	9	C9H14	Cyclohexylallene	PRPE	0.311	3.36E+08	3.80E+08	0.1361
77.055	3	C3H8O2	2-methoxyethanol	RCHO	0.445	1.60E+08	3.38E+08	0.1237
81.065	6	C6H8	1,3-cyclohexadiene	PRPE	0.355	2.56E+08	2.84E+08	0.1041
125.087	8	C8H12O	4-Acetylcyclohexene	RCHO	0.218	2.09E+08	2.71E+08	0.0982
84.082	5	C5H9N	Pentanenitrile	NA	0.271	1.63E+08	2.25E+08	0.081
115.102	7	C7H14O	2-heptanone	RCHO	0.191	1.60E+08	2.18E+08	0.078

PTR-TOF-MS	# carbons	Species Identified	Assumed species	GEOS-Chem species	EF[1], production / 10^7 molec. mW^{-1} s^{-1}	EF*1E7*Carbons*12gC $mmol^{-1}$	EF*1E7* molecular weight	Matlab Tool (Tg/yr)
31.019	1	CH2O (formaldehyde)	Formaldehyde	CH2O	0.704	8.45E+07	2.11E+08	0.0775
67.051	5	C5H6 (cyclopentadiene)	1,3-cyclopentadiene	PRPE	0.291	1.75E+08	1.92E+08	0.0694
121.085	5	C5H12O3	2-(hydroxymethyl)-2-methyl-1,3-propanediol	NA	0.154	9.24E+07	1.85E+08	0.0648
68.048	4	C4H5N	pyrrole	NA	0.247	1.19E+08	1.66E+08	0.0607
58.036		NA	NA	NA	0.289	0.00E+00	1.65E+08	0.06
107.077	8	C8H10	Xylenes	XYLE	0.149	1.43E+08	1.58E+08	0.0573
72.046	3	C3H5NO	NA	NA	0.206	7.42E+07	1.46E+08	0.054
56.054	3	C3H5N	NA	NA	0.226	8.14E+07	1.24E+08	0.046
83.044	5	C5H6O	NA	NA	0.15	9.00E+07	1.23E+08	0.0444
49.01	1	CH4S	NA	NA	0.235	2.82E+07	1.13E+08	0.042
60.079	3	C3H9N	NA	NA	0.187	6.73E+07	1.10E+08	0.0407
93.063	7	C7H8	Toluene	TOLU	0.116	9.74E+07	1.07E+08	0.0398
151.099	1	C10H14O	NA	NA	0.07	8.40E+06	1.05E+08	0.0377
141.079	8	C8H12O2	NA	NA	0.067	6.43E+07	9.39E+07	0.0352
73.024	3	C3H4O2	NA	NA	0.125	4.50E+07	9.00E+07	0.0339
135.075	9	C9H10O	NA	NA	0.067	7.24E+07	8.98E+07	0.0337
97.059	6	C6H8O	NA	NA	0.092	6.62E+07	8.84E+07	0.0312
79.05	6	C6H6 (benzene)	Benzene	BENZ	0.092	6.62E+07	7.18E+07	0.0254
44.022	2	C2H3O	NA	NA	0.136	3.26E+07	5.85E+07	0.022
108.043	6	C6H5NO	NA	NA	0.045	3.24E+07	4.82E+07	0.0193
58.065	3	C3H7N	NA	NA	0.084	3.02E+07	4.79E+07	0.0166
137.084	9	C9H12O	NA	NA	0.017	1.84E+07	2.31E+07	0.0098

[1]Emission factor from (Brüggemann et al., 2017) Table S2 for biofilms on day 6.

Section ~~5~~5. Incremental impact of additional ocean emissions over the baseline model simulation.

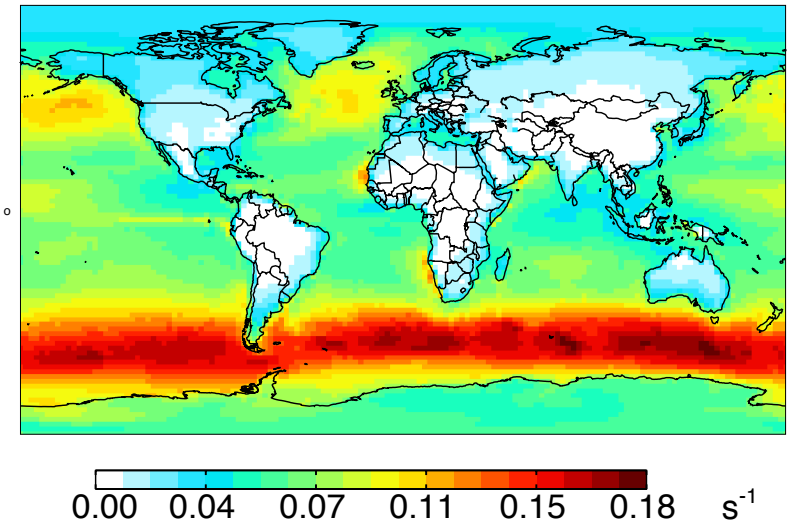

Figure ~~S3~~S4. Impact of additional ocean emissions (Tables 3 and 4) over the baseline model (which includes methanol, acetone, and acetaldehyde) on annual simulated 2016 surface cOHR as described in the text.

Section 6. Description of MHP Interference

Recent laboratory work has shown methanediol (HOCH2OH, hydrated formaldehyde) is detected efficiently in the Caltech CIMS instruments at the same signals used to quantify MHP. Under high water vapor mixing ratios, as found in the lower atmosphere, HOCH2OH is likely detected in the Caltech CIMS with substantially greater efficiency than MHP on a molar basis, thus potentially amplifying the interference. Work is ongoing to better understand and quantify this issue.

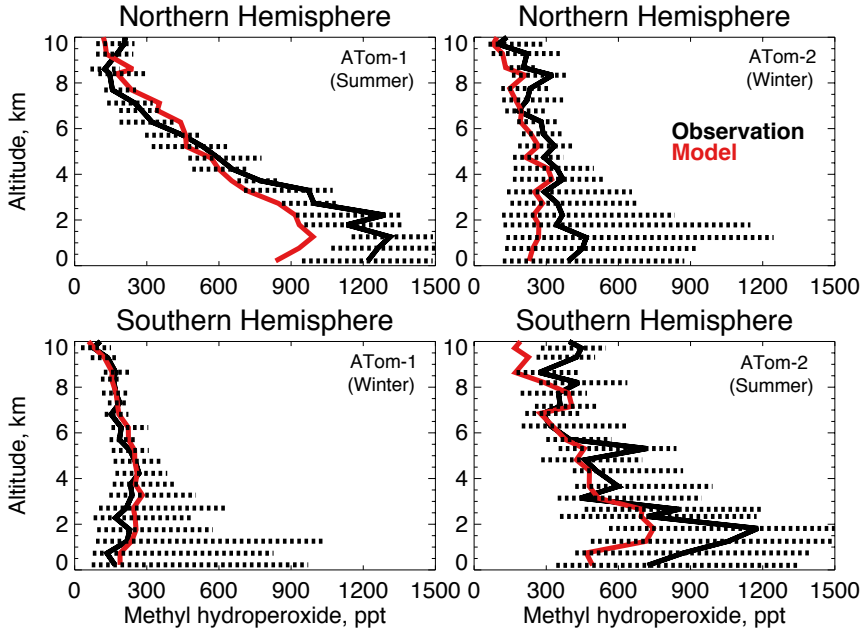

Figure S5. The same as Figure 3 for median methyl hydroperoxide profiles. Methyl hydroperoxide is measured by the Caltech CIMS instrument as described in Table 2.

Section ~~6~~7. Zonal average plots of acetaldehyde for each deployment.

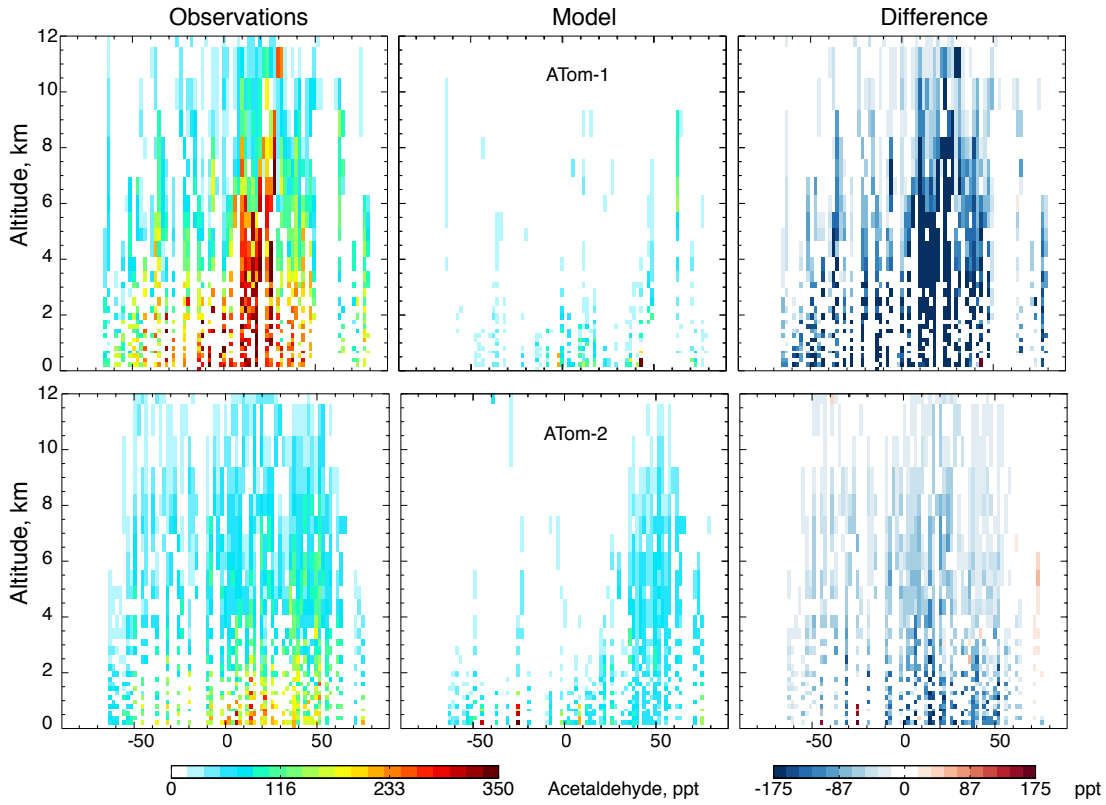

Figure S6. Zonal mean acetaldehyde gridded to the model resolution along the flight tracks over the ocean. Acetaldehyde is measured by the TOGA instrument as described in Table 2.

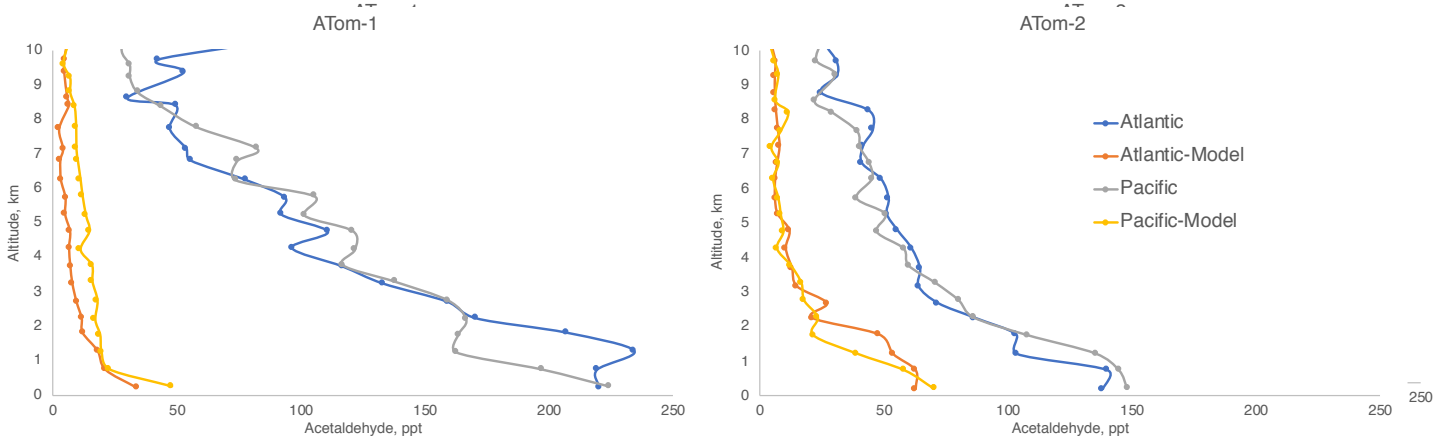

Figure ~~S5~~S7. Acetaldehyde comparison split at 70ºW to represent the Pacific and Atlantic oceans, respectively. Acetaldehyde is measured by the TOGA instrument as described in Table 2.

Section ~~7~~8. Model comparison with observed ethane and propane.

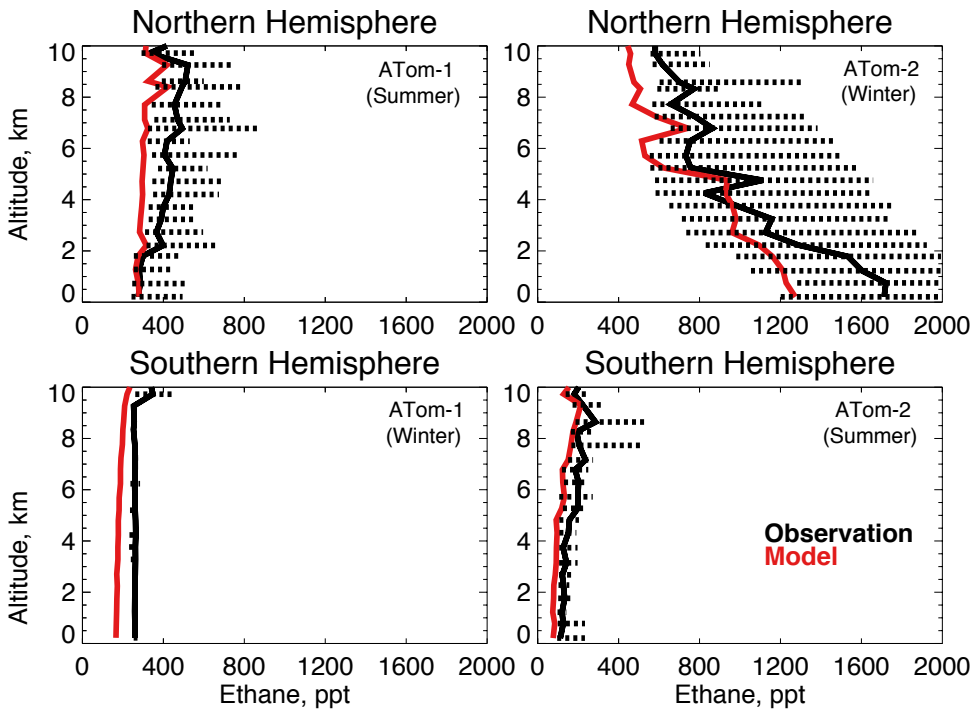

Figure ~~S6~~S8. The same as Figure 3 for median ethane profiles. Ethane is measured by the UCI Whole Air Sampler (WAS) instrument as described in Table 2.

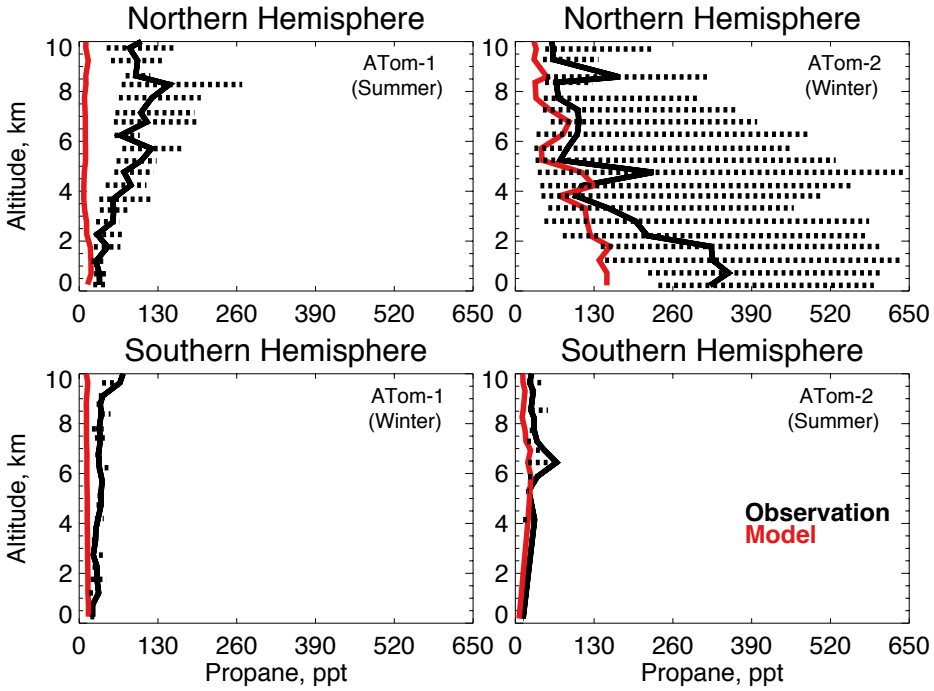

Figure S~~7~~8. The same as Figure 3 for median propane profiles. Propane is measured by the Trace Organic Gas Analyzer (TOGA) instrument as described in Table 2.

Table ~~S3~~S5. GEOS-Chem Ethane and Propane Chemistry (Adapted from Safieddine et al., 2017)

Reaction	Rate
C2H6	
C2H6 +OH→ETO2 +H2O	7.66E-12 exp(-1020/T)
C2H6 +NO3→ETO2 +HNO3	1.4E-18
ETO2 +NO→ALD2 +NO2 +HO2	2.6E-12 exp(365/T)
ETO2 + HO2→ETP	7.4E-13 exp(700/T)
ETO2 + MO2 →0.75CH2O +0.75ALD2 +HO2 +0.25MOH +0.25EOH	3E-13
ETO2 +ETO2→2ALD2 +2HO2	4.1E-14
ETO2 +ETO2→EOH +ALD2	2.7E-14
ETO2 + MCO3→MO2 +ALD2 +HO2 +{CO2}	1.68E-12 exp(500/T)
ETO2 + MCO3→ACTA +ALD2	1.87E-13 exp(500/T)
ETP+ hν→ OH+ HO2+ ALD2	
ETP +OH→0.64OH +0.36ETO2 +0.64ALD2	5.18E-12 exp(200/T)
C3H8	
C3H8 +OH→B3O2	k1=7.6E-12 exp(-585/T); k2=5.87*(300/T)$^{0.64}$ exp(- 816/T); K=k1 / (1+k2)
C3H8 +OH→A3O2	k1=7.60E-12 exp(-585/T); k2= 0.17*(300/T)$^{-0.64}$ exp(816/T) K=k1 / (1+k2)
A3O2 +NO→NO2 +HO2 +RCHO	2.9E-12 exp(350/T)
A3O2 +HO2→RA3P	2.91E-13exp(1300/T)[1-exp(-0.245*n)], n=3
A3O2 +MO2→HO2 +0.75CH2O +0.75RCHO +0.25MOH+0.25ROH	5.92E-13
A3O2+ MCO3 →MO2 +RCHO +HO2 +{CO2}	1.68E-12 exp(500/T)
A3O2 + MCO3 →ACTA +RCHO	1.87E-13 exp(500/T)
B3O2 +NO→NO2 +HO2 +ACET	2.7E-12 exp(350/T)
B3O2 +HO2→RB3P	2.91E-13exp(1300/T)[1-exp(-0.245*n)],n=3
B3O2 +MO2→0.5HO2 +0.5ACET +0.25ACET+0.75CH2O+0.25MOH +0.25ROH +0.5HO2 +0.021{CO2}	8.37E-14
B3O2 +MCO3→MO2 +HO2 +ACET +{CO2}	1.68E-12 exp(500/T)
B3O2 +MCO3→ACET +ACTA	1.87E-13 exp(500/T)
RA3P +OH→0.64OH +0.36A3O2 +0.64RCHO	5.18E-12 exp(200/T)
RB3P +OH→0.791OH +0.209B3O2 +0.791ACET	8.78E-12 exp(200/T)
RA3P+ hν→ OH+ HO2+ RCHO	
RB3P+ hν→ OH+ HO2+ ACET	